CNWRA 90-01Q

REPORT ON RESEARCH ACTIVITIES FOR THE QUARTER JANUARY 1 THROUGH MARCH 31, 1990

Prepared for

Nuclear Regulatory Commission
Contract NRC-02-88-005

Prepared by

Center for Nuclear Waste Regulatory Analyses
San Antonio, Texas

May 1990

462.2 --- T19910514002 2
Report on Research Activities
for the Quarter January 1
through March 31, 1990

CNWRA 90-01Q

Property of
CNWRA Library

REPORT ON RESEARCH ACTIVITIES FOR THE QUARTER JANUARY 1 THROUGH MARCH 31, 1990

Prepared for

Nuclear Regulatory Commission
Contract NRC-02-88-005

Edited by

Wesley C. Patrick

Center for Nuclear Waste Regulatory Analyses
San Antonio, Texas

May 1990

TABLE OF CONTENTS

Page

LIST OF FIGURES v
LIST OF TABLES viii
ACKNOWLEDGMENTS ix

1. EXECUTIVE SUMMARY 1-1

1.1 INTRODUCTION 1-1
1.2 UNSATURATED MASS TRANSPORT (GEOCHEMISTRY) 1-1

1.2.1 Experimental Studies 1-1
1.2.2 Geochemical Modeling 1-2

1.3 THERMOHYDROLOGY 1-2
1.4 SEISMIC ROCK MECHANICS 1-3
1.5 INTEGRATED WASTE PACKAGE EXPERIMENTS 1-4
1.6 STOCHASTIC ANALYSIS OF FLOW AND TRANSPORT 1-4
1.7 GEOCHEMICAL NATURAL ANALOGS 1-5

2. UNSATURATED MASS TRANSPORT (GEOCHEMISTRY)
by Roberto T. Pabalan and William M. Murphy 2-1

2.1 TECHNICAL OBJECTIVES 2-1
2.2 EXPERIMENTAL STUDIES 2-1

2.2.1 Technical Objectives 2-1
2.2.2 Thermodynamics of Ion Exchange 2-2
2.2.3 Characterization of Zeolite Specimens 2-4
2.2.4 Summary of Results 2-6

2.3 GEOCHEMICAL MODELING 2-23

2.3.1 Technical Objective 2-23
2.3.2 Reaction-Path Model for the Evolution of the Groundwater and Mineral Chemistry at Yucca Mountain, Nevada 2-23
2.3.3 Summary of Results 2-33

2.4 REFERENCES: UNSATURATED MASS TRANSPORT (GEOCHEMISTRY), EXPERIMENTAL STUDIES 2-34
2.5 REFERENCES: UNSATURATED MASS TRANSPORT (GEOCHEMISTRY), GEOCHEMICAL MODELING 2-35

3. THERMOHYDROLOGY *by Ronald T. Green and Steve Svedeman* 3-1

3.1 TECHNICAL OBJECTIVES 3-1
3.2 ASSESSMENT OF THE STATE-OF-KNOWLEDGE OF THERMO-HYDROLOGY IN UNSATURATED MEDIA 3-2

TABLE OF CONTENTS (Cont'd)

Page

3.3 DESIGN AND EXECUTION OF PRELIMINARY SEPARATE EFFECTS EXPERIMENTS 3-2

3.3.1 Simulation Analysis 3-4
3.3.2 Separate Effects Experimental Apparatus 3-4
3.3.3 Separate Effects Experiment Test No. 1 3-7
3.3.4 Separate Effects Experiment Test No. 2 3-8
3.3.5 Separate Effects Experiments Results 3-11

3.4 SUMMARY OF RESULTS 3-15

4. SEISMIC ROCK MECHANICS *by Asadul H. Chowdhury and Simon M. Hsiung* 4-1

4.1 TECHNICAL OBJECTIVES 4-1
4.2 EVALUATION OF ROCK-JOINT MODELS AND COMPUTER CODES 4-1

4.2.1 Cyclic Loading of a Specimen With a Slipping Joint 4-2
4.2.2 Circular Excavation Intersected by a Joint 4-4
4.2.3 Slip in a Jointed Body Induced by a Harmonic Shear Wave 4-4
4.2.4 Line Source in an Elastic Medium with a Slip-Prone Joint 4-4
4.2.5 Summary of Results 4-5

4.3 LABORATORY INVESTIGATION OF ROCK-JOINT BEHAVIOR 4-5

4.3.1 Development of Laboratory Test Apparatus 4-5
4.3.2 Sample Collection and Preparation Activities 4-9

4.4 FIELD SITE EVALUATION AND SELECTION 4-15
4.5 REFERENCES 4-17

5. INTEGRATED WASTE PACKAGE EXPERIMENTS *by Gustavo Cragnolino, Hersh Manaktala, and Narasi Sridhar* 5-1

5.1 TECHNICAL OBJECTIVES 5-1
5.2 COLLECTION AND REVIEW OF INFORMATION ON CORROSION OF WASTE PACKAGE CONTAINERS 5-1
5.3 WASTE PACKAGE EXPERIMENTAL PROGRAMS 5-4

5.3.1 Corrosion of Container Materials in the Tuff Repository Environment 5-3
5.3.2 Metallurgical Stability of Container Materials in Tuff Repository Environment 5-9

5.4 REFERENCES 5-13

6. STOCHASTIC ANALYSIS OF UNSATURATED FLOW AND TRANSPORT *by Rachid Ababou* 6-1

6.1 TECHNICAL OBJECTIVES 6-1

TABLE OF CONTENTS (Cont'd)

Page

6.2 PRELIMINARY RESEARCH AND ACCOMPLISHMENTS 6-1
6.3 REFERENCE 6-5

7. GEOCHEMICAL NATURAL ANALOGS *by English C. Pearcy and William M. Murphy* 7-1

7.1 TECHNICAL OBJECTIVES 7-1
7.2 ASSESSMENT OF THE LITERATURE 7-1

APPENDIX A ASSESSMENT OF THE LITERATURE FOR GEOCHEMICAL NATURAL ANALOGS

LIST OF FIGURES

Figure	Title	Page
2-1	Excess Gibbs energy of clinoptilolite	2-4
2-2	Excess Gibbs energy of (Na-K)-phillipsite	2-5
2-3	X-ray diffraction pattern of the zeolitized tuff sample from Hector, California	2-7
2-4	X-ray diffraction pattern of the zeolitized tuff sample from Buckhorn, Grant County, New Mexico	2-7
2-5	X-ray diffraction pattern of the zeolitized tuff sample from Barstow, California	2-8
2-6	X-ray diffraction pattern of the zeolitized tuff sample from Death Valley Junction, California	2-8
2-7	X-ray diffraction pattern of the zeolitized tuff sample from Tilden, Texas	2-9
2-8	X-ray diffraction pattern of the zeolitized tuff sample from Castle Creek, Idaho	2-9
2-9	Photomicrograph of sample CH	2-16
2-10	Photomicrograph of sample CGC	2-17
2-11	Photomicrograph of sample CB	2-18
2-12	Photomicrograph of sample CDV	2-19
2-13	Scanning electron image of clinoptilolite from sample CH	2-21
2-14	Scanning electron image of clinoptilolite from sample CDV	2-22
2-15	Model major element water chemistry	2-29
2-16	Model pH and log CO_2 fugacity for the water	2-30
2-17	Model (lines) and measured water chemistry (circles) data from Kerrisk (1987) for Yucca Mountain	2-32
3-1	Separate effects experimental apparatus - front view	3-3
3-2	Separate effects experimental apparatus - back view	3-3
3-3	Moisture characteristic curves	3-5
3-4	Configuration of experiment sensors	3-5
3-5	Schematic of the tensiometer	3-6

LIST OF FIGURES (Cont'd)

Figure	Title	Page
3-6	Test 1 sequence of events as measured at densitometer locations (11,9) and (11,12)	3-7
3-7	Ambient temperature and barometric pressure during test no. 1	3-9
3-8	Temperature measured in the test chamber during test no. 1	3-9
3-9	Tensiometer measurements during test no. 1	3-10
3-10	Densitometer measurements at locations (11,3), (11,6), (11,9) and (11,12) during test no. 1	3-10
3-11	Test no. 2 sequence of events as measured at densitometer location (9,9)	3-11
3-12	Ambient temperature and barometric pressure during test no. 2	3-12
3-13	Temperature measured in the test chamber during test no. 2	3-12
3-14	Tensiometer measurements during test no. 2	3-13
3-15	Desitometer measurements at locations (9,3), (9,6) and (9,9) during test no. 2	3-13
3-16	Free surface of infiltrated water during test no. 1	3-14
4-1	Four benchmark analytical problems	4-3
4-2	Assembly and instrumentation of the dynamic shear apparatus	4-6
4-3	Truck-mounted Joy 22 drill rig	4-13
4-4	Location of drilled holes for sample collection at the Apache Leap site	4-14
4-5	An 18-inch diameter core with a smooth joint interface	4-15
5-1a	Microstructure of Incoloy alloy 825, transverse cross-section (50X magnification)	5-6
5-1b	Microstructure of Incoloy alloy 825, transverse cross-section (500X magnification)	5-6
5-2a	Microstructure of 304L stainless steel, transverse cross-section (100X magnification)	5-7
5-2b	Microstructure of 304L stainless steel, transverse cross-section (200X magnification)	5-7
5-3	Microstructure of Hastelloy alloy C-22	5-8

LIST OF FIGURES (Cont'd)

Figure	Title	Page
5-4	Microstructure of OFH copper (CDA-102), longitudinal cross-section	5-8
5-5a	Microstructure of CDA-613 (Aluminum Bronze), transverse cross-section	5-10
5-5b	Microstructure of CDA-613, longitudinal cross-section	5-10
6-1	Front view of three-dimensional moisture plume, from stochastic flow simulations of Ababou (1988)	6-4
6-2	Back view of three-dimensional moisture pattern, with moisture plume visible in purple and blue (simulations from Ababou, 1988)	6-4

LIST OF TABLES

Table	Title	Page
2-1	Petrographic Analysis of Sample CH	2-10
2-2	Petrographic Analysis of Sample CGC	2-11
2-3	Petrographic Analysis of Sample CB	2-12
2-4	Petrographic Analysis of Sample CDV	2-13
2-5	Petrographic Analysis of Sample CT	2-14
2-6	Petrographic Analysis of Sample CCC	2-15
2-7	Mineralogy of Zeolitized Tuff Samples Based on X-Ray Diffraction and Petrographic Analyses	2-20
2-8	Initial Model Water Chemistry	2-25
2-9	Model Mineral Chemistry	2-26
2-10	Kinetic Data	2-27
2-11	Bulk Composition (Weight Percent) of Topopah Springs Tuff (TST) Represented as Feldspar Plus Cristobalite	2-28
4-1	Instrumentation Channel Identification	4-8
5-1	Heat Numbers and Chemical Compositions of the Candidate Container Materials in the IWPE Project	5-5
5-2	Surface and Bulk Analyses of Chromium Containing Alloys by SEM-EDX	5-11

ACKNOWLEDGMENTS

This report was prepared to document work performed by the Center for Nuclear Waste Regulatory Analyses (CNWRA) for the U.S. Nuclear Regulatory Commission under Contract No. NRC-02-88-005. The research activities reported here were performed on behalf of the NRC Office of Regulatory Research, Division of Engineering. The report is an independent product of the CNWRA and does not necessarily reflect the views or regulatory position of the NRC.

Each chapter of this report acknowledges those investigators who, although not specifically involved in writing the report, made significant contributions to the research projects. In addition, the authors gratefully acknowledge the technical support and technical reviews conducted by other members of the CNWRA and Institute staffs. Appreciation is particularly due Yolanda Lozano, who prepared the text of the document, Curtis Gray, who provided graphical assistance, and Dr. Shirley Heller, who provided a full range of expert editorial services in the preparation of the final document.

1. EXECUTIVE SUMMARY

1.1 INTRODUCTION

This is the first in a series of research quarterly reports which will document and make available to the technical community work that has been undertaken by the Center for Nuclear Waste Regulatory Analyses (Center) as part of its contract with the U.S. Nuclear Regulatory Commission (NRC). Reports will be prepared each calendar quarter, with the fourth such report each year constituting the annual progress report.

Each of the six research projects discussed here are being conducted in accordance with approved Research Project Plans. These Plans are the vehicle for establishing the objectives, technical approach, justification, and funding for each of the studies. Because the Plans address primarily planning and management matters, they are not discussed further here (with the exception of objectives).

In reading this report, it is important to realize that several of the projects have just been approved. Consequently, there is relatively little work to report at this time. In such cases, this quarter's report provides basic information on the objectives of the new projects as well as early activities such as literature assessments. Other projects have been in progress long enough that significant technical progress in laboratory, calculational, or field studies can be reported.

This report is organized to provide, first, an Executive Summary that documents in capsule form the progress of each research project over the past quarter. The Executive Summary is followed by Chapters 2 through 7 representing respectively each of the six currently active research projects including the project objectives, research activities, and results (as appropriate) to date.

1.2 UNSATURATED MASS TRANSPORT (GEOCHEMISTRY)

1.2.1 Experimental Studies

A major technical consideration in evaluating Yucca Mountain, Nevada, as a potential repository site for high-level nuclear wastes (HLW) is the presence of thick, laterally-extensive zones of zeolitic tuffs. Because of their sorptive properties, zeolites could provide important geologic barriers to migration of radionuclides from the repository to the accessible environment, in case of loss of containment by the waste canisters. To support the NRC's high-level waste program, the Center is conducting experimental studies on the thermodynamic and ion exchange properties of zeolites under Task 3 of the Geochemistry Research Project. These studies are designed to generate data needed to evaluate the effectiveness of zeolitic tuffs as barriers to radionuclide migration. The initial work in this experimental project is focused on the mineral clinoptilolite, which is the predominant zeolite present at Yucca Mountain.

The theoretical bases for the conduct of this work, as well as a review of published experimental ion exchange data on clinoptilolite, have been discussed in a previous report (Pabalan and Murphy, 1990).

One of the objectives of this study is to develop models that can be used to predict ion exchange behavior in complex systems. Therefore, it is necessary to apply thermodynamic principles to the study of ion exchange phenomena. The thermodynamics of ion exchange is briefly discussed below. The evaluation of ion exchange equilibrium constants and standard Gibbs energies are shown to involve corrections for nonideal behavior in both aqueous solution and zeolite phases. Examples of nonideal behavior in zeolites are given here in terms of excess Gibbs energies (G^{ex}) of the solid phase. Calculations of exchanger phase G^{ex} using two models for aqueous solution

activity coefficients indicate the importance of correctly calculating aqueous solution nonideal behavior for precise description of ion exchange phenomena.

Published experimental data on ion exchange between clinoptilolite and aqueous solutions reviewed previously (Pabalan and Murphy, 1990) showed that ion exchange behavior and the resultant thermodynamic quantities derived from them are sensitive to the nature of the experimental materials and the method of pretreatment used in the experiments. Ion exchange experiments that have been done on clinoptilolite have utilized zeolitized tuff specimens due to the unavailability of sufficient amounts of macroscopic crystals of clinoptilolite. These contained mineral impurities which can influence the results of ion exchange and phase equilibrium studies. Consequently, characterization of clinoptilolite materials that will be used in the experiments is essential. In connection with the Center's experimental studies on clinoptilolite, specimens of zeolitized tuff from several localities in the U.S. were obtained and characterized using X-ray diffraction analysis, petrographic (thin section analysis), and scanning electron microscopy. The results of these studies are given in this report and indicate that the specimens from Death Valley Junction, California, are the most suitable materials for the ion exchange experiments.

1.2.2 Geochemical Modeling

Reaction path modeling aids the interpretation of groundwater and mineral chemistry, and permits identification of the controls on the geochemical evolution of the Yucca Mountain system. Development of validated models for the ambient system are required before predictions of repository induced perturbations are possible. A kinetic reaction path model has been generated for the evolution of groundwater and mineral chemistry at Yucca Mountain, Nevada, using the computer program EQ6. In the model, an initial bicarbonate solution saturated with calcite at pH 7 with 10^{-2} m NaCl was reacted with an alkali feldspar and cristobalite. Secondary minerals generated were smectite solid solution, calcite, clinoptilolite solid solution, K-feldspar, and albite. Calculated water chemistry for dissolution of 0.005 to 0.01 moles of feldspar plus cristobalite per kilogram of water corresponds well to the range of analyzed waters from Yucca Mountain for calcium, sodium, potassium, carbonate and pH. Observed values of silica are poorly represented in the model indicating that aqueous silica concentrations in the groundwater are controlled by volcanic glass dissolution. Ca:Na:K ratios for clinoptilolites in the model correspond well to the calcium rich clinoptilolites observed at Yucca Mountain. The remarkably good correspondence between observed and modeled results indicates that many of the essential processes responsible for the Yucca Mountain geochemistry are adequately represented in the model.

1.3 THERMOHYDROLOGY

Technical issues and uncertainties for the proposed Yucca Mountain HLW potential repository site indicate a need for research on thermohydrological phenomena, i.e., phenomena associated with heat and fluid flow, to provide information relevant to performance assessment siting and design criteria. The class of thermohydrological phenomena examined in this project includes phenomena driven by heat emanating from HLW emplaced in a geologic repository. Information derived principally from research will be used to establish a knowledge base of thermohydrologic phenomena which will be utilized to assess models of processes used in performance assessments.

The specific objectives of the thermohydrology research project are summarized as follows: to perform a critical assessment of the state-of-knowledge of thermohydrology in unsaturated fractured media; to perform a detailed dynamic similarity or similitude analysis on the governing equations relevant to unsaturated flow; to design and perform a series of separate effects experiments in order to identify and understand the role of the coupled processes involved in thermohydrologic phenomena; to develop the laboratory facilities, experimental methods,

measurement techniques, and associated analytic skills to design and perform comprehensive experiments whose results will continue to identify key dependent and independent parameters and their relationships to each other in the context of thermohydrologic issues; to examine and correlate laboratory results with field data; and to aid in the design of future field experiments.

The research project has been delineated into five tasks for the purpose of accomplishing these objectives. Two of these tasks, Task 1, Assessment of the State-of-Knowledge of Thermohydrology in Unsaturated Media; and Task 2, Design and Execution of Preliminary Separate Effects Experiments, are active at this time.

Insights gained from the research project at this intermediate point can be summarized in two categories: conclusions that could help direct future efforts in the technical area of thermohydrology and recommendations for adaptations in experimental procedures. In the former category, the TOUGH code is being adapted to facilitate its use in this project.

Results and experience gained from the experiments performed to date have led to modifications in both the laboratory procedures and experimental apparatus used in the separate effects experiments. A more heterogeneous medium will be used instead of a uniformly- and unimodally-sized medium to avoid the highly-nonlinear difficulties associated with a medium that has a steeply-sloped moisture characteristic curve. A smaller sized test chamber will be used to alleviate problems related to use of the larger sized chamber. The problems included excessive heat loss through the side walls, excessive time required for the experiments to approach steady state, unavoidable settling of the medium in the test chamber during saturation, and the added effort required to set up the experiments in the larger chamber.

1.4 SEISMIC ROCK MECHANICS

A state-of-the-art literature review reveals that the seismic effects calculations performed to date on underground structures have not been subjected to an adequate level of experimental and field investigations. The experimental support for most of the programs has focused on soils rather than on structurally complex rock formations. Computer programs are currently available to model dynamic events of underground structures in rock formations. However, these programs have not been validated with well-planned and rigorous experimental and field protocols. This Seismic Rock Mechanics Research Project is aimed at developing a better understanding of the key parameters affecting the repository under seismic loadings and consequently validation of computer programs for use in seismic assessment of underground structures in tuff media.

During this reporting period, several major activities including computer code qualification studies, laboratory test apparatus development, sample collection, and evaluation and selection of a site for instrumented field studies proceeded simultaneously. Substantial progress for the project has been made, with the last three activities being completed. The computer code qualification studies are currently ongoing. Qualification studies against four benchmark analytical problems were completed on two of the six identified computer codes.

The dynamic direct shear test apparatus developed at Southwest Research Institute includes a 90,000-lb vertical and 50,000-lb horizontal loading capacity and is designed to house a specimen with maximum size of 12 x 8 x 4 in. for the lower specimen and 8 x 8 x 4 in. for the upper specimen. For specimens with dimensions larger than this, a modification of the shear boxes will be needed. This modification will be relatively simple, and the capacity of other design features is not expected to be compromised. Demonstration tests of the apparatus indicates that the apparatus is capable of accomplishing the objectives of the Seismic Rock Mechanics Project. These tests also suggested that some minor adjustments on the instrumentation scheme may be necessary while conducting the experiments.

The Apache Leap site in Arizona was selected for sample collection. The welded tuff at Apache Leap is similar to that at the repository horizon at Yucca Mountain. The site is easily accessible for transportation of heavy sample collection equipment and of collected specimens. The site also has sufficient area for a relatively large number and size sample collection. At the completion of the activity, 50 potentially usable joint specimens were collected. This number is 10% more than the number needed under the current projection. Additional specimens were collected to offset losses during sample preparation.

For qualification studies on the UDEC and HONDO II codes, four benchmark analytical problems were exercised. The results indicate that UDEC performs valid simulations of jointed rock, to the extent that the mechanics of these media may be represented by the conceptual models expressed in the problems, while HONDO II has a limited capability. Some of HONDO II's deficiencies are related to the application of static and dynamic boundary loads in the code.

The Lucky Friday Mine at Mullan, Idaho, has been selected for the instrumented field studies on mechanical and geohydrologic responses. The mine is seismically active with 10-20 seismic events per year with magnitudes greater than Richter 2.0. Other features of the mine are that (1) it is well characterized geologically and structurally, (2) it has a macro-seismic monitoring system with 16 channels in place, (3) extensive rock mechanics studies conducted in the past on the mine are readily available for use, and (4) the mine technical personnel are cooperative and interested in this project.

1.5 INTEGRATED WASTE PACKAGE EXPERIMENTS

The objectives of the Integrated Waste Package Experiments Research Project are to critically evaluate current metal corrosion data and other degradation processes and to determine parameters effecting long-term container-material performance. After extensive peer review, a new plan for this project (IWPE, Revision 2) has been completed and will be sent to NRC staff for review. The plan identifies five areas covering the different degradation processes for container materials: corrosion, stress corrosion cracking, material stability under repository thermal conditions, microbiologically induced corrosion, and other degradation phenomena. Since the new plan is not yet approved, reporting for this period is done in accordance with Revision 1 of the IWPE program plan.

A critical review of localized corrosion experiments conducted in relation to the Yucca Mountain program has been performed and is summarized in Section 5.2.1 of this report. The advantages and limitations of the current experimental approaches are briefly pointed out. A topical report will be issued towards the end of this fiscal year.

The results to date of the initial characterization of the alloys under study are described in Section 5.3.1. The surface analyses showed that some of the high-nickel austenitic materials exhibited significant chromium depletion on the surface. Further studies of their corrosion behavior in standard ASTM solutions are being conducted.

A survey of the current literature on low-temperature sensitization (LTS) of austenitic stainless steels has been conducted. The findings of this survey are described briefly in Section 5.3.2.1. Based on this survey, a lack of similar knowledge of higher-nickel alloys such as Incoloy alloy 825 was identified; and a test matrix has been designed to conduct experimental studies. The long-term oxidation behavior of copper-based alloys is surveyed briefly in Section 5.3.2.2.

1.6 STOCHASTIC ANALYSIS OF FLOW AND TRANSPORT

A quantitative characterization of large-scale flow and radionuclide transport through the heterogeneous unsaturated fractured rock of Yucca Mountain will be necessary to evaluate

compliance with the siting criteria and performance objectives associated with the proposed Yucca Mountain high-level waste (HLW) repository (10 CFR 60.122 and 60.113.). Realistic modeling of the complex, heterogeneous flow and transport processes at Yucca Mountain will require incorporating the effects of relatively small scale space-time variability in modeling large-scale unsaturated flow and radionuclide transport.

The effective starting date of the project was February 2, 1990. The specific objectives of the project are to: perform a review of the literature and assess available models and data relevant to the subject site, select a global approach to model large-scale flow and transport in unsaturated fractured rock, develop submodels for incorporation into the global model, and perform large-scale simulations and participate in the validation of flow/transport models for the Yucca Mountain repository. The project is divided in three tasks. The currently active task is Task 1: "Review, Analysis, and Development of Modeling Approach," including Subtask 1, "Literature Review of Modeling Approaches" (active and ongoing); Subtask 2, "Data Review and Assessment" (activated near end of reporting period); and Subtask 3, "Selection and Initial Development of Global Modeling Approach" (not active during reporting period). The time elapsed since the start of the project is less than a full quarter. Preliminary aspects of the work accomplished during the second quarter of FY90 are described in Section 6; the complete results of literature review, initial data assessment, model selection, and first stages of model development will be integrated into the next quarterly report.

1.7 GEOCHEMICAL NATURAL ANALOGS

The Geochemical Natural Analogs Project is designed to provide a knowledge of the state of the art in natural analog studies applied to contaminant transport. As part of this project, a geochemical natural analog study of contaminant transport relevant to the proposed repository in the unsaturated zone at Yucca Mountain will be designed and undertaken. Fundamental new data will be obtained to improve the understanding of particular processes and events affecting contaminant transport in unsaturated media. This natural analog research will aid validation of predictive models for geochemical transport and will provide data for time and space scales generally inaccessible in laboratory studies.

Activities in the project initiated during the reporting period was a review of pertinent literature (Task 1). The literature is being examined for references on geochemical natural analogs using several criteria (1) What sites have been the subjects of previous study? (2) What methods have been used and with what success? (3) What geochemical processes are amenable to natural analog study and with what degree of resolution? and (4) What sites would constitute good analogs of conditions at Yucca Mountain? Progress in Task 1 includes searches of the electronic databases GEOREF, GEOARCHIVE, GEOBASE, CHEM ABSTRACTS, and NTIS. The bibliographies from volumes of the *CEC Natural Analog Working Group Proceedings* have also provided many pertinent references. In addition, references have been sought from journal articles and books as they have been obtained. More than 200 source references have been identified to date.

2. UNSATURATED MASS TRANSPORT (GEOCHEMISTRY)

by Roberto T. Pabalan and William M. Murphy

Investigators: Roberto T. Pabalan (CNWRA), Paul Bertetti (CNWRA) and William M. Murphy (CNWRA)

2.1 TECHNICAL OBJECTIVES

The purposes and general objectives of the Geochemistry Research Project are:

(1) To understand the ambient geochemical conditions and processes at the proposed HLW repository site. This is necessary to support NRC activities associated with site characterization and establishment of design criteria including identification of potentially favorable and potentially adverse conditions designated in NRC regulation 10 CFR 60.

(2) To understand the geochemical conditions and processes affecting the transport of radionuclides through the geologic setting and the release of radionuclides to the accessible environment.

(3) To understand the geochemical conditions and processes that will affect the performance of the waste packages and engineered barrier system and therefore will affect the radionuclide source term.

(4) To recognize and evaluate issues and uncertainties in predictive geochemical models used in assessment of the performance of the HLW repository candidate site in regard to isolation of the waste.

The goal of the Center's Geochemistry Research Project is to develop the technical knowledge base and to perform geochemical investigations which will give the Center the technical capabilities to support independently NRC's provision of appropriate, timely prelicensing guidance to DOE and to support NRC in evaluation of geochemical information presented in DOE's licensing submittals. These capabilities will enable NRC to regulate and make licensing decisions from an informed technical position concerning the disposal of HLW as dictated by the NWPAA.

To attain the objectives, three specific tasks have been designated.

(1) Task 1 - Geochemistry of Tuff and Fluids in Unsaturated and Saturated Tuff

(2) Task 2 - Geochemical Modeling of Fluid/Rock Interactions

(3) Task 3 - Experimental Studies in Geochemistry

The work completed for this project during the past quarter are presented in the following sections 2.2, "Experimental Studies," and 2.3, "Geochemical Modeling."

2.2 EXPERIMENTAL STUDIES

2.2.1 Technical Objectives

A major technical consideration in evaluating the suitability of Yucca Mountain, Nevada, as a potential repository site for HLWs is the presence of thick, laterally extensive zones of zeolitic tuffs. Because of their sorptive properties, zeolites could provide important geologic barriers to migration of radionuclides from the repository to the accessible environment. To

support the program, the Center is conducting experimental studies on the thermodynamic and ion exchange properties of zeolites under Task 3 of the Geochemistry Research Project. The objective of these studies is to generate data needed to evaluate the effectiveness of zeolitic tuffs as barriers to radionuclide migration. The initial work is focused on the mineral clinoptilolite, which is the predominant zeolite present at Yucca Mountain. The theoretical bases for the conduct of this work have been discussed in a previous report (Pabalan and Murphy, 1990).

2.2.2 Thermodynamics of Ion Exchange

A review of ion exchange thermodynamics has been presented previously (Pabalan and Murphy, 1990). Basically, the condition for equilibrium for the ion exchange reaction, written here for singly charged ions as

$$A^+ + BZ \leftrightarrow B^+ + AZ \tag{2-1}$$

gives the usual thermodynamic equilibrium constant expression

$$K_a = a_{AZ}a_{B^+}/a_{A^+}a_{BZ} \tag{2-2}$$

where a represents activities of the subscripted ion in the aqueous solution or in the zeolite phase.

Equation (2-2) may be expanded to give

$$K_a = A_z f_A m_B \gamma_B / B_z f_B m_A \gamma_A \tag{2-3}$$

or

$$K_a = K_c(f_A/f_B)\ ; \quad K_c = A_z m_B \gamma_B / B_z m_A \gamma_A \tag{2-4}$$

where K_c is the Kielland or corrected selectivity quotient (Laudelout and Thomas, 1965; Barrer and Klinowski, 1974), A_z and B_z are the equivalent mole fractions of ions A^+ and B^+ in the zeolite phase, and m_A and m_B are the molalities of the respective ions in the aqueous phase. The quantities γ_A and γ_B are single-ion activity coefficients of A^+ and B^+, respectively, and f_A and f_B are the activity coefficients of A^+ and B^+ in the solid phase in association with their equivalents of zeolite anionic framework. These last four quantities are correction terms for nonideal behavior in the system.

The evaluation of K_a, f_A, and f_B from experimental data results from an appropriate integration of the Gibbs-Duhem relation (Gaines and Thomas, 1953), which requires the standard states of the various components to be defined. For the aqueous electrolyte solution external to the zeolite phase, the usual standard state of a hypothetical, ideal one-molal solution is used. For the zeolite phase, it has been normal practice to follow Gaines and Thomas (1953) and make the standard state for each exchanging cation the appropriate homo-ionic form of the zeolite in equilibrium with an infinitely dilute solution of the same cation (Sposito, 1981). The Gibbs-Duhem equation, together with Eq. (2-4), gives the following expressions for calculating the zeolite phase activity coefficients and the value of K_a:

$$\ln f_A = -B_z \ln K_c + \int_{A_z}^{1} \ln K_c \, dA_z \tag{2-5}$$

$$\ln f_B = A_z \ln K_c - \int_{0}^{A_z} \ln K_c \, dA_z \tag{2-6}$$

$$\ln K_a = \int_{0}^{1} \ln K_c \, dA_z \ . \tag{2-7}$$

The standard Gibbs energy per equivalent of exchange (ΔG°) for the reaction depicted in Eq. (2-1) can then be calculated from

$$\Delta G^{\ominus} = -RT \ln K_a \ . \tag{2-8}$$

If complete exchange studies are made in pairs on three ions (A^+, B^+, and C^+), the self-consistency of the work can be assessed by the "triangle rule" applied to the standard Gibbs energies of exchange; that is,

$$\Delta G^{\ominus}_{A,B} = \Delta G^{\ominus}_{C,B} - \Delta G^{\ominus}_{C,A} \tag{2-9}$$

where $\Delta G^{\circ}_{A,B}$, $\Delta G^{\circ}_{C,B}$, and $\Delta G^{\circ}_{C,A}$ are the standard Gibbs energies for the exchanges AZ→BZ, CZ→BZ, and CZ→AZ, respectively. In terms of the equilibrium constants, the triangle rule requires that (Barrer and Townsend, 1976)

$$K_a^{A,B} = K_a^{C,B} / K_a^{C,A} \ . \tag{2-10}$$

The nonideal behavior in the zeolite phase is reflected in the activity coefficients f_A and f_B. However, despite years of research, there is still no generally accepted activity coefficient model for exchangeable ions. Until a reliable statistical-mechanical approach is developed, commonly used models are based on general equations for the excess Gibbs energy (G^{ex}) of mixtures (Grant and Sparks, 1989). These models have been applied successfully to binary ion exchange equilibria as well as to some ternary ion exchange equilibria (Elprince and Babcock, 1975; Elprince et al., 1980). It is anticipated that a similar approach will be applied to experimental isotherm data generated by the Center's work.

The molar excess Gibbs energy, G^{ex}, for the binary system represented by the Eq. (2-1) may be defined as

$$G^{ex}/RT = A_z \ln f_A + B_z \ln f_B \tag{2-11}$$

where R is the molar gas constant and T is temperature. For an ideal solid solution, G^{ex} is equal to zero over the whole range of solid solution composition (Figure 2-1). The assumption of ideality in the treatment of solid solutions is commonly used in geochemical codes such as EQ3/6 (Wolery et al., 1990), due mostly to the lack of experimental data for the various systems of interest. However, as shown in Figure 2-1, which is based on ion exchange data from Howery and Thomas (1965), deviations from ideality for the zeolite mineral clinoptilolite can be fairly significant. The implications of nonideal behavior in solid solutions for calculations of water-rock interactions still need to be evaluated.

As is apparent from Eqs. (2-3) and (2-4), an evaluation of K_a involves activity corrections for both aqueous solution and exchanger phases. Although the single ion activity coefficients, γ_A and γ_B, cannot be evaluated separately by experiments due to electroneutrality constraints, the ratio γ_B/γ_A can be evaluated in terms of the mean molal stoichiometric activity coefficients, $\gamma_{\pm AX}$ and $\gamma_{\pm BX}$, where X is the coexisting anion present in the aqueous solution and maintains electroneutrality in that phase.

It is important to recognize that $\gamma_{\pm}$ depends on the ionic strength and composition of the solution. Therefore, the mean activity coefficients used in evaluating K_a should be calculated for the *mixed* electrolyte solution at the experimental ionic strength. For binary mixtures of two electrolytes with a common ion, these values may be calculated using the equation of Glueckauf (1949) (e.g., Ames, 1964a,b). More recent models such as that of Pitzer (1973, 1979) are more

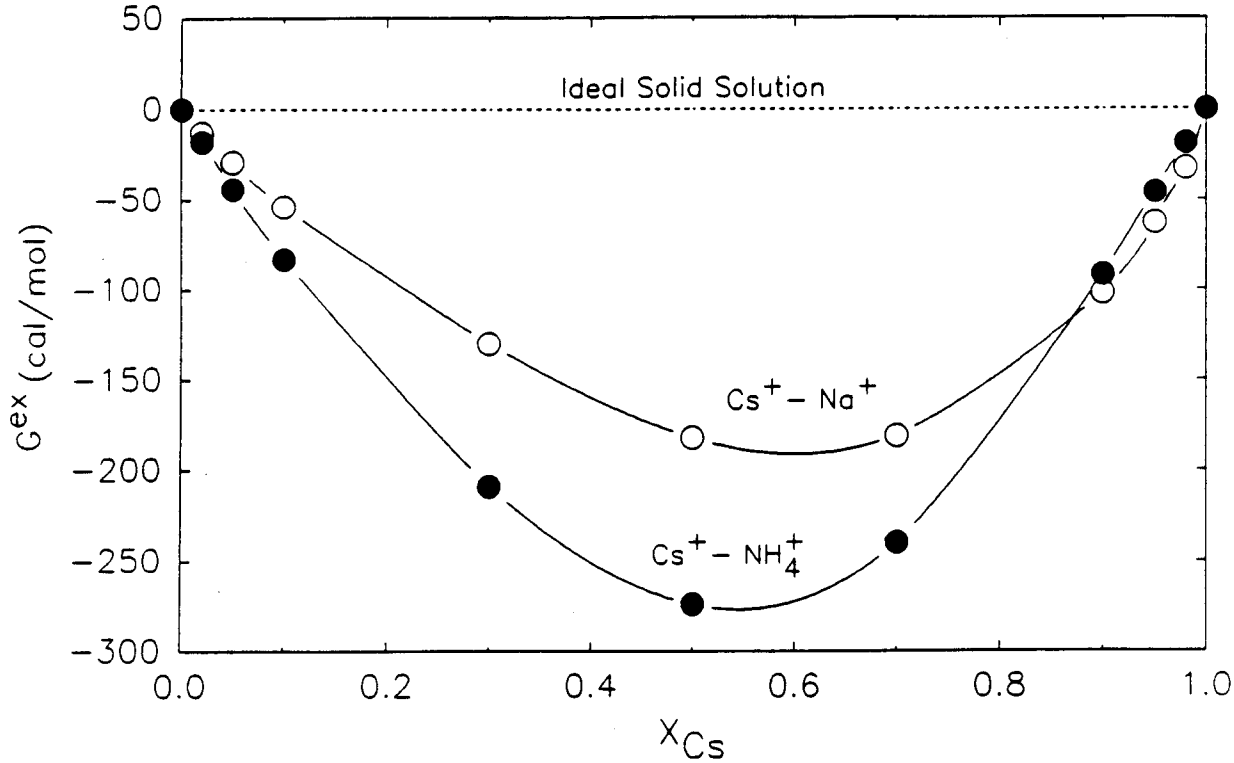

Figure 2-1. Excess Gibbs energy of clinoptilolite (Data from Howery and Thomas, 1965)

useful, however, particularly for systems of complex composition. For these models, parameters are available that were evaluated from more accurate solution thermodynamic data and for a greater number of electrolyte systems.

The exchanger phase activity coefficients as well as the equilibrium constants and Gibbs energies evaluated from isotherm data depend on the $\gamma_{\pm}$ values used in the calculations. To evaluate the magnitude of this dependence, excess Gibbs energies of the zeolite mineral (Na-K)-phillipsite were calculated from the isotherm data of Ames (1964a) and are shown in Figure 2-2. The upper curve was calculated using Ames' tabulated f_K and f_{Na}. Ames (1964a, Table 2) derived these values from his ion exchange data utilizing Glueckauf's (1949) activity coefficient equations for mixed aqueous electrolyte solutions. The bottom curve was calculated from f_K and f_{Na} evaluated from Ames' ion exchange data (which utilized Pitzer's activity coefficient model) using parameters fit to critically evaluated aqueous electrolyte data. The upper curve results in K_a and ΔG° values equal to 0.190 and 985 cal/mole, respectively, while the lower curve gives K_a and ΔG° values of 0.153 and 1,110 cal/mole, respectively. These differences indicate the importance of accurately correcting for aqueous solution nonideality, particularly on systems with mixed background anions (Fletcher and Townsend, 1985) and for calculating or predicting ion exchange behavior in ternary or more complex systems.

2.2.3 Characterization of Zeolite Specimens

Published experimental data on ion exchange between clinoptilolite and aqueous solutions have been reviewed in a previous report (Pabalan and Murphy, 1990). These data showed that ion exchange behavior and the resultant thermodynamic quantities derived from them are sensitive to the nature of the experimental materials as well as to the method of pretreatment used in the experiments. The absence of sufficient amounts of macroscopic crystals of clinoptilolite

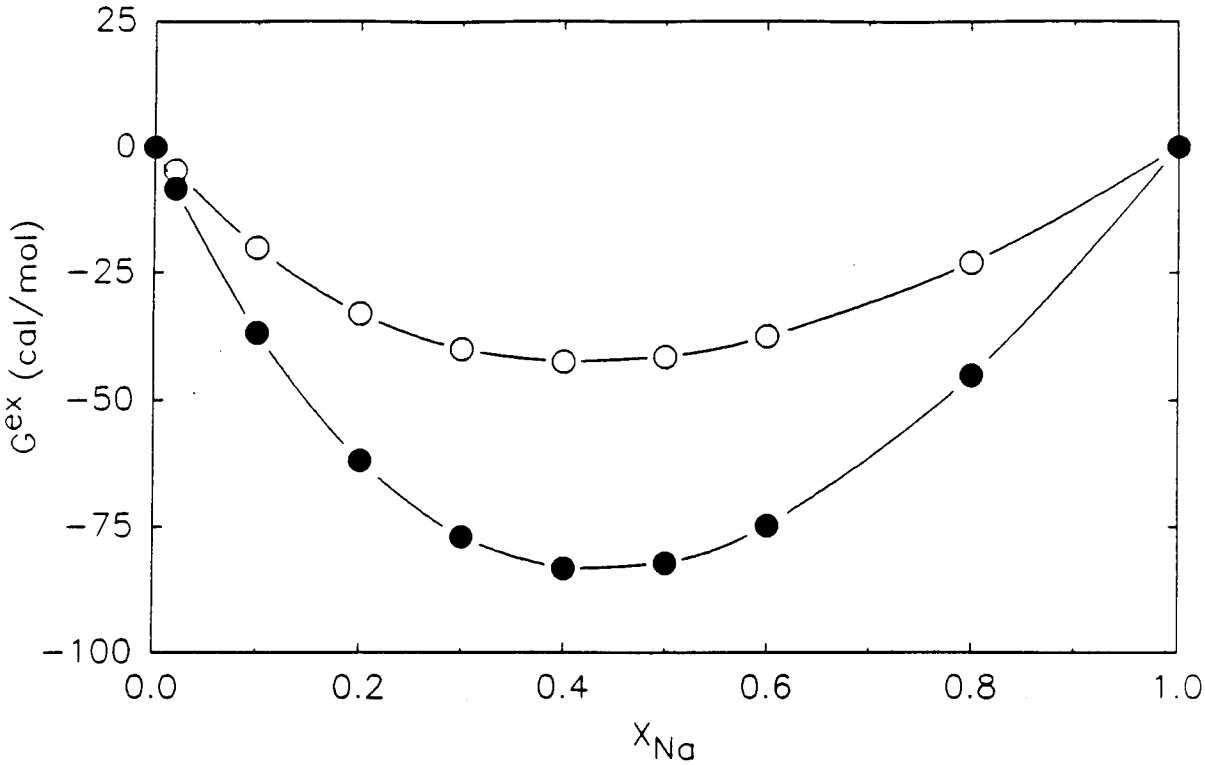

Figure 2-2. Excess Gibbs energy of (Na-K)-phillipsite (Isotherm data from Ames, 1964)

therefore presents special problems in the study of this mineral. Previously published ion exchange studies on clinoptilolite have been done using zeolitized tuff specimens. These commonly contain mineral impurities such as quartz, feldspar, iron oxides, clays, and unaltered glass. The detailed mineralogy of samples from different localities are different, and samples from different outcrops within the same locality may show variations in mineralogical composition. Because mineralogical and chemical composition can influence the results of ion exchange and phase equilibrium studies, the clinoptilolite materials to be used for the experiments must be characterized. Mineralogic characterization of the samples is necessary to (1) identify the best specimens to use, (2) identify procedures that can be used to eliminate mineral impurities, and (3) aid in the interpretation of experimental results.

In connection with the Center's experimental studies on clinoptilolite, specimens of zeolitized tuff from the following localities were obtained: (1) Hector, California (sample CH); (2) Barstow, California (sample CB); (3) Death Valley Junction, California (sample CDV); (4) Castle Creek, Idaho (sample CCC); (5) Buckhorn, Grant County, New Mexico (sample CGC); and (6) Tilden, Texas (sample CT). The samples from the first four localities were obtained from Minerals Research (P.O. Box 591, Clarkson, New York 14430), and the samples from the latter two localities were obtained from Zeotech Corporation (3224 Candelaria N.E., Albuquerque, New Mexico 87107).

Characterization of these samples were done using X-ray diffraction (XRD) analysis, petrographic (thin section) analysis, and scanning electron microscopy coupled with energy-dispersive X-ray spectrometry. The mineralogy of the bulk samples was identified by XRD analysis of finely ground (-325 mesh) material. The XRD pattern for each sample was run over the range 2-65° 2θ at 0.5° 2θ per minute with a Siemens D-500 powder diffractometer using a Cu-

target X-ray tube and a diffracted-beam monochromator. The operating voltage and current of the diffractometer were set at 40kV and 40ma, respectively; and a time constant of 4 seconds was used. The X-ray diffraction pattern for each tuff sample is shown in Figures 2-3 to 2-8. The major diffraction peaks of the minerals are labeled (Cl=clinoptilolite, M=mordenite, Er=erionite, Q=quartz, Sm=smectite, Il=illite, Pl=plagioclase, Kf=K-feldspar, Gyp=gypsum, Dol=dolomite, and Hal=halite). The minerals present in the samples were identified by comparison of the XRD pattern with Joint Committee on Powder Diffraction Standards (JCPDS) powder data files or with previously determined XRD patterns of monomineralic samples.

2.2.4 Summary of Results

The results obtained from the XRD analyses were combined with information obtained from petrographic examination of thin sections to establish the approximate amounts of the major and minor crystalline phases present in the tuff. Details of the petrographic analyses for samples CH, CGC, CB, CDV, CT and CCC are given in Tables 2-1 through 2-6. Photomicrographs of samples CH, CGC, CB, and CDV are shown in Figures 2-9 through 2-12 (the field of view is approximately 2.5 mm; upper photos were taken under plane-polarized transmitted light; lower photos were under crossed-nichols). The estimated percentages of the phases in each sample are tabulated in Table 2-7.

The X-ray diffraction and petrographic analyses indicate that the samples contain mostly well-crystallized clinoptilolite, which has replaced the glass in the poorly welded tuffs. The clinoptilolite, however, is very fine grained; and well-formed crystals occur only in vugs or in voids previously occupied by glass shards. The morphology of crystalline clinoptilolite is exhibited in Figures 2-13 and 2-14, which are scanning electron photomicrographs of samples CH and CDV, respectively. The most common accessory minerals present in the tuff samples are quartz, mordenite, erionite, feldspars, and clay. The results in Table 2-7 indicate that the CDV samples from Death Valley Junction, California, appear to be the most suitable materials for the ion exchange experiments based on their having the least quantities of impurities.

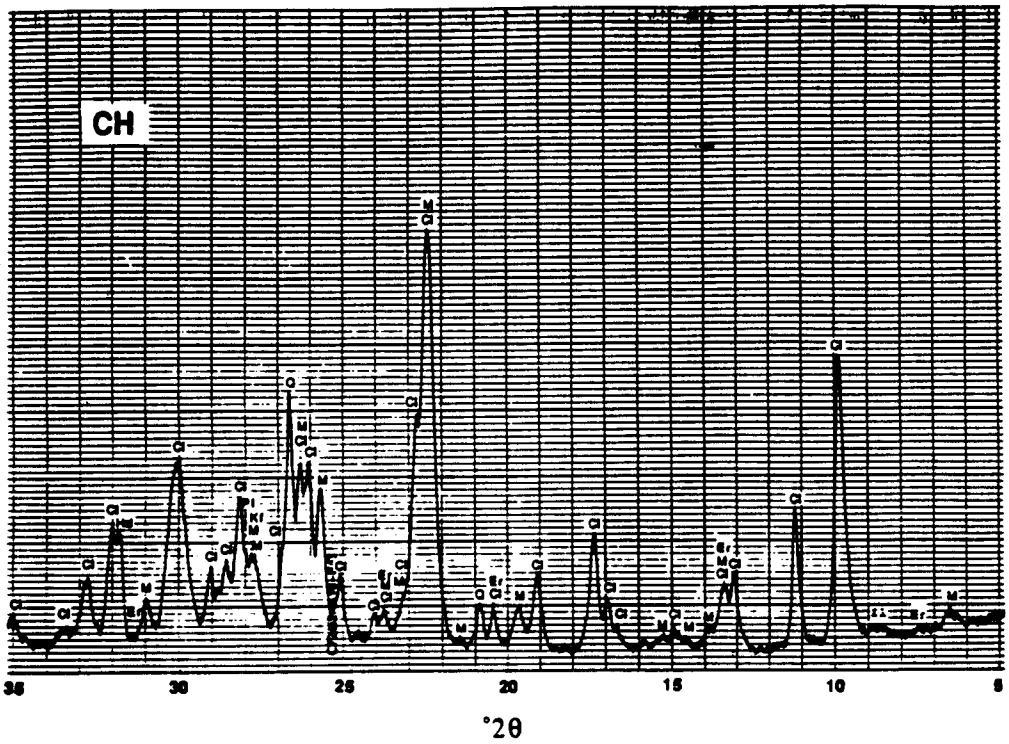

Figure 2-3. X-ray diffraction pattern of the zeolitized tuff sample from Hector, California

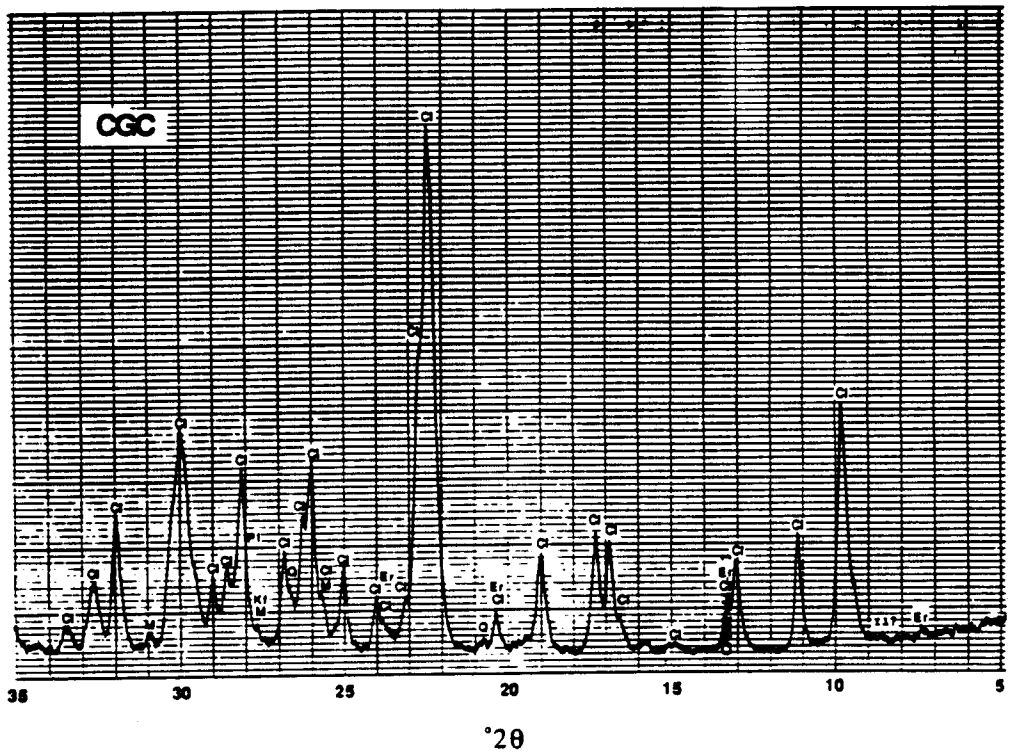

Figure 2-4. X-ray diffraction pattern of the zeolitized tuff sample from Buckhorn, Grant County, New Mexico

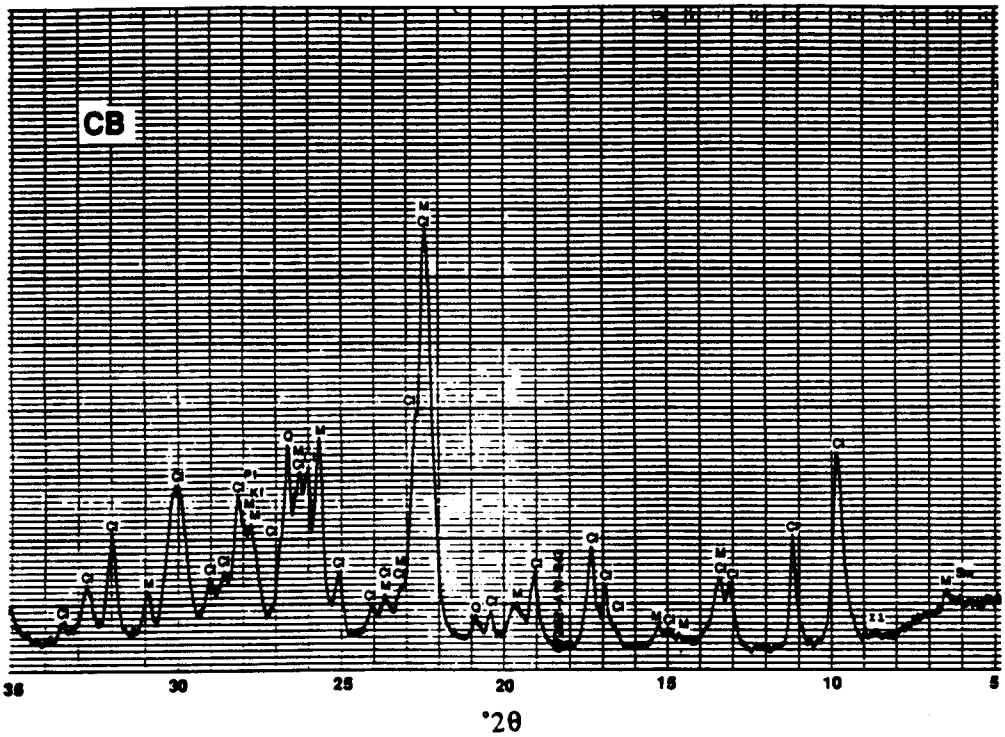

Figure 2-5. X-ray diffraction pattern of the zeolitized tuff sample from Barstow, California

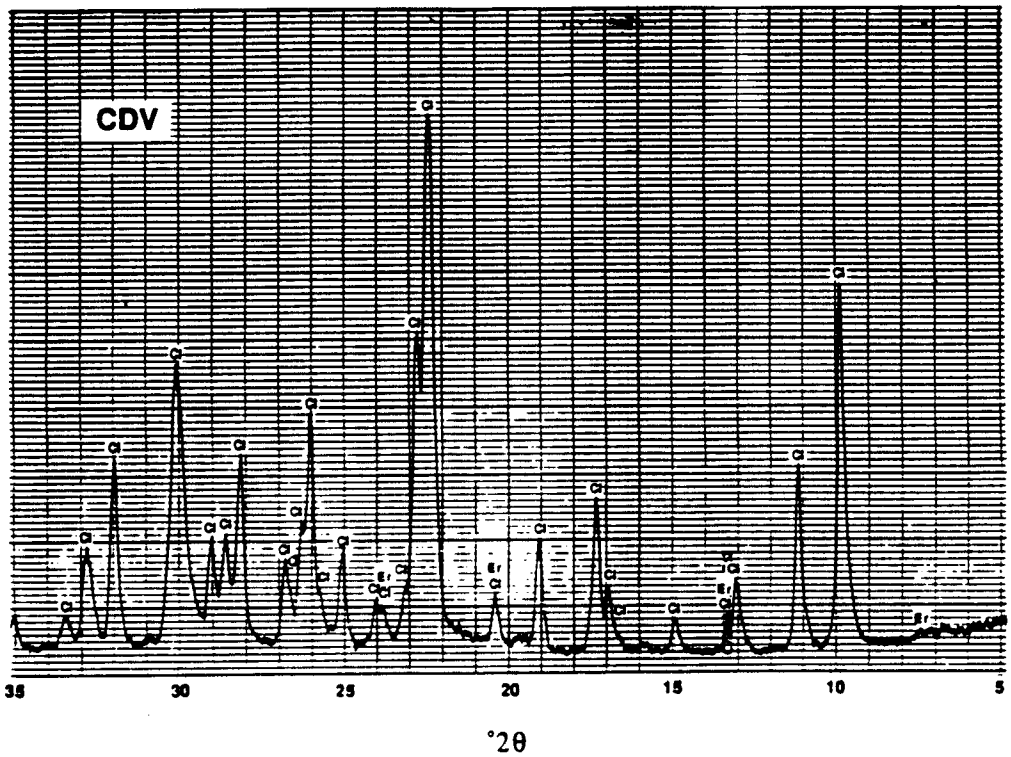

Figure 2-6. X-ray diffraction pattern of the zeolitized tuff sample from Death Valley Junction, California

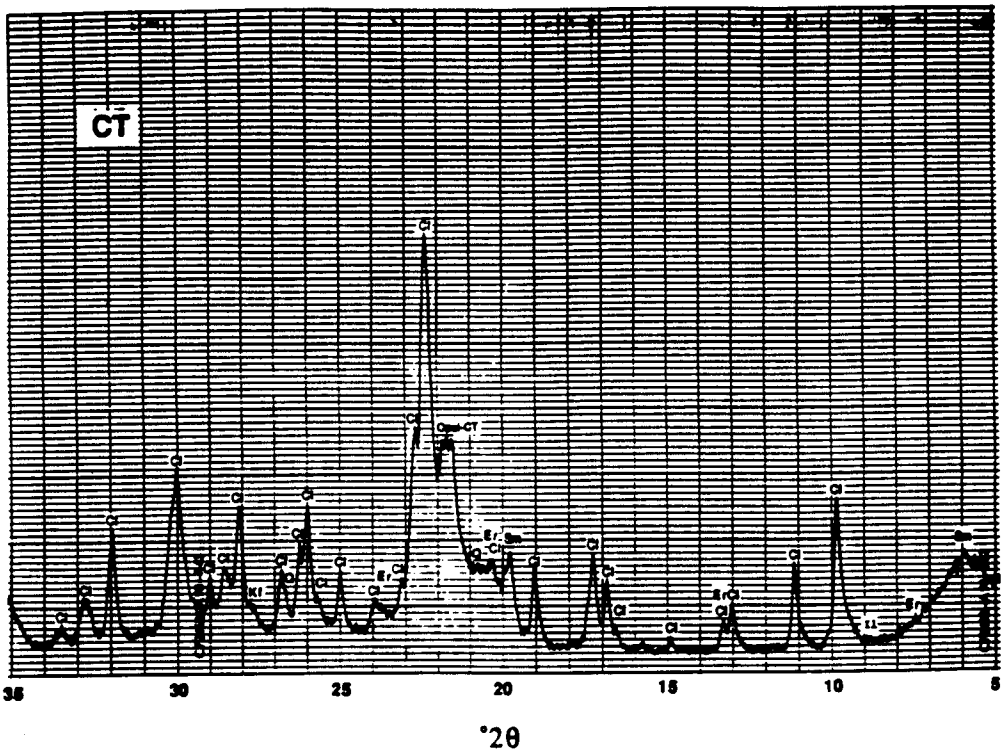

Figure 2-7. X-ray diffraction pattern of the zeolitized tuff sample from Tilden, Texas

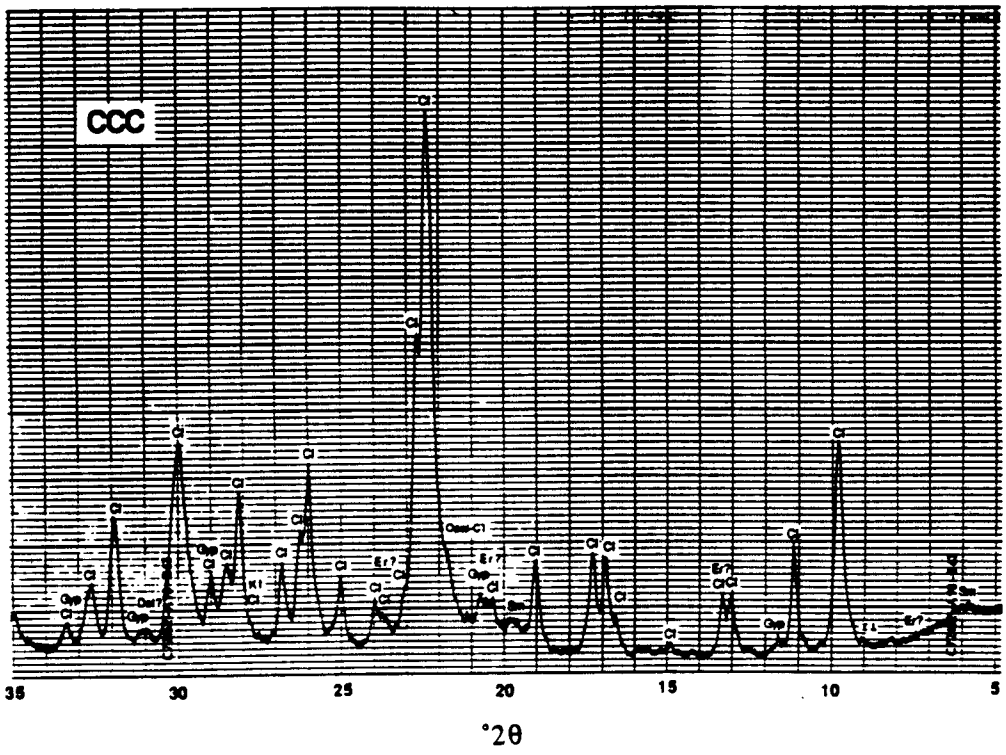

Figure 2-8. X-ray diffraction pattern of the zeolitized tuff sample from Castle Creek, Idaho

TABLE 2-1. PETROGRAPHIC ANALYSIS OF SAMPLE CH

LOCALITY: ***Hector, California***

TYPE OF ROCK: Quartz Latite or Decite Tuff

Matrix: 85-90%

Zeolitized glass with some relicit shards (0 - 40%)

Nondescript opaque (10-20%)

Grains:

Phenocrysts:

Quartz and feldspars (10-15%)

Biotite (1-2%)

Clinopyroxene (trace)

TEXTURE:

Poorly welded, very fine grained, up to 75 microns.

Graded laminations, exhibiting symmetric grading from one lamination, which is entirely without relict shards or phenocrysts.

ALTERATION/MINERALIZATION:

All glass altered to zeolites.

Veins of nondescript opaque; some mineral has also replaced some of the shards. This opaque mineral may be ultra-fine clinoptilolite or an amorphous clay.

DEPOSITIONAL ORIGIN: Fallout tuff or possibly surge deposit.

TABLE 2-2. PETROGRAPHIC ANALYSIS OF SAMPLE CGC

LOCALITY: ***Buckhorn, Grant County, New Mexico***

TYPE OF ROCK: Quartz Latite or Dacite Tuff

Matrix: 90%

Zeolitized glass shards (70-90%)
Some round bubble shards
Brownish opaque around shards

Grains: 10%

Phenocrysts:

Quartz (1-2%)
Feldspars (5-8%)
Biotite (1-2%)
Clinopyroxene (2%)
Hornblende (trace)
Magnetite or ilmenite (trace)

Lithoclasts:

Few glassy lithic fragments with plagioclase microlites
Some detrital iron-titanium oxide

TEXTURE:

Poorly welded, no compaction or deformation of shards, and very little glassy matrix around shards.

Phenocryst fragments are very fine grained about 100 microns in size. Relict shards are slightly larger at about 200 microns in length.

Abundant shards, with many plucked from thin section; rest are bordered with a high birefringent mineral (possibly sericite), and rimmed and replaced with zeolites.

Clinoptilolite appears better crystallized than in other samples.

ALTERATION/MINERALIZATION:

Many of the plagioclase phenocrysts are altered to sericite.

Some of the magnetite is altered to hematite.

Many relict shards appear to be rimmed; perhaps the shards were dissolved out and then infilled with zeolites. Many of the shard borders are outlined with a high birefringent mineral, possibly sericite, although the XRD analysis only indicates 1-2% illite and mica.

Grungy brown opaque that could be an amorphous clay (it does not have the high birefringence or relief of leucoxene/sphene).

DEPOSITIONAL ORIGIN: Fallout tuff.

TABLE 2-3. PETROGRAPHIC ANALYSIS OF SAMPLE CB

LOCALITY: ***Barstow, California***

TYPE OF ROCK: Quartz Latite or Dacite Tuff

Matrix: 75-85%

Zeolitized glass with relict shards (30-60%)
Dendritic manganese-iron oxide (goethite?)
Many round bubble shards

Grains: 15-25%

Phenocrysts:

Quartz and feldspars
Biotite (4%)
Hornblende (1%)

TEXTURE:

Thinly laminated, one lamination of coarser grains, both quartz and relict shards up to 300 microns.

Average grain size about 100 microns.

Poorly welded and some uncompacted relict shards visible, especially in the coarser lamination.

Dendritic manganese-iron oxide extends from the coarser lamination.

ALTERATION/MINERALIZATION:

All glass has altered to zeolites.

Rare detrital ferromagnesian mineral (pyroxene or amphibole) is altered to hematite.

Some plagioclase phenocrysts altered to sericite.

Bubble shards are partially infilled with a brownish-green clay (possibly smectite?).

DEPOSITIONAL ORIGIN: Fallout tuff.

TABLE 2-4. PETROGRAPHIC ANALYSIS OF SAMPLE CDV

LOCALITY: ***Death Valley Junction, California***

TYPE OF ROCK: Quartz Latite or Dacite Tuff

- Matrix: 95%
  - Zeolitized glass shards (50-90%)
  - Nondescript opaque (5-10%)
  - Many round bubble shards
  - Brownish opaque around shards
- Grains: 5%
  - Phenocrysts:
    - Quartz and feldspars (2-5%)
    - Biotite (1-2%)
    - Clinopyroxene (trace)
  - Lithoclasts:
    - A few glassy lithic fragments with plagioclase microlites
    - Some detrital iron-titanium oxide

TEXTURE:

Poorly welded and no compaction or deformation of shards.

Abundant shards, bordered with a high birefringent mineral (possibly sericite) and rimmed and replaced with zeolites.

Both shards and phenocrysts are very large grained, many around 500 microns or larger.

ALTERATION/MINERALIZATION:

Many of the plagioclase phenocrysts are altered to sericite.

Many of relict shards appear to be rimmed; perhaps the shards were dissolved out and then infilled with zeolites. Many of the shard borders are outlined with a high birefringent mineral.

DEPOSITIONAL ORIGIN: Fallout tuff or possibly surge deposit.

TABLE 2-5. PETROGRAPHIC ANALYSIS OF SAMPLE CT

LOCALITY: ***Tilden, Texas***

TYPE OF ROCK: Quartz Latite or Dacite Tuff

Matrix: 95%

Glass altered to a mixture of zeolites, smectite, and opal-CT

Grains: 5%

Phenocrysts:

Quartz and feldspars (3%)

Biotite (2%)

TEXTURE:

Poorly welded with little or no recognizable shard texture (may be obscured by zeolites and clays).

Very fine-grained phenocrysts; average size of the biotite grains is about 30 microns; several are up to 100 microns in length.

ALTERATION/MINERALIZATION:

Smectite and clinoptilolite almost completely obscure the very fine phenocrysts; hence the phenocryst content listed above may be an underestimate. Some are rounded to elongated clumps of opal (up to a millimeter in size) without smectite, which may have been larger shards in the generally shard-poor ash flow tuff. The fine ash groundmass is completely altered to clinoptilolite, smectite, and iron oxides.

DEPOSITIONAL ORIGIN: Fallout tuff

TABLE 2-6. PETROGRAPHIC ANALYSIS OF SAMPLE CCC

LOCALITY: *Castle Creek, Idaho*

TYPE OF ROCK: Quartz Latite or Dacite Tuff

Matrix 96%

- Zeolitized glass shards
- Brownish-green smectite (3 to 15%)
- Reddish-brown iron oxide (<1%)

Grains 4%

- Phenocrysts:
  - Quartz (1%)
  - Feldspar (mostly sanidine) (2%)
  - Biotite (2%), some altered
  - Hornblende (trace)
  - Magnetite (trace-1%)

TEXTURE:

Poorly welded with well-preserved shard texture. Most of the shards are thin and long and average about 200 microns in length. These shards may be Pele's hair (although this term implies a more basaltic composition). Other shards are more Y-shaped.

This sample is finely laminated; most of the rounded and abraded phenocrysts are in one slightly coarser grained lamination. The grains of quartz, feldspar, and biotite are smaller in size (100 to 200 microns) than the shards. The phenocrysts and the smectite are concentrated along the base of the graded lamination.

Grains of magnetite are very irregular in shape.

ALTERATION/MINERALIZATION:

Zeolites have replaced nearly all the glass; only about 1% of the more blocky (Y-shaped) shards are still glassy.

Most of the smectite is present in altered lithic fragments; from their elongate shape, these may have been biotites. Some of the more rounded patches of smectite may have filled pores (dissolved-out shards or the interior of bubble shards?) in the tuff.

Nodules of iron-oxide (hematite) are located along the periphery of the thin section. They may present surficial weathering (desert varnish).

The gypsum and anhydrite indicated in the XRD analysis of this sample are not evident in this thin section. Perhaps these minerals represent irregularly distributed fracture-filling or weathering phases not present in the sample prepared for petrographic analysis.

DEPOSITIONAL ORIGIN: Fallout tuff

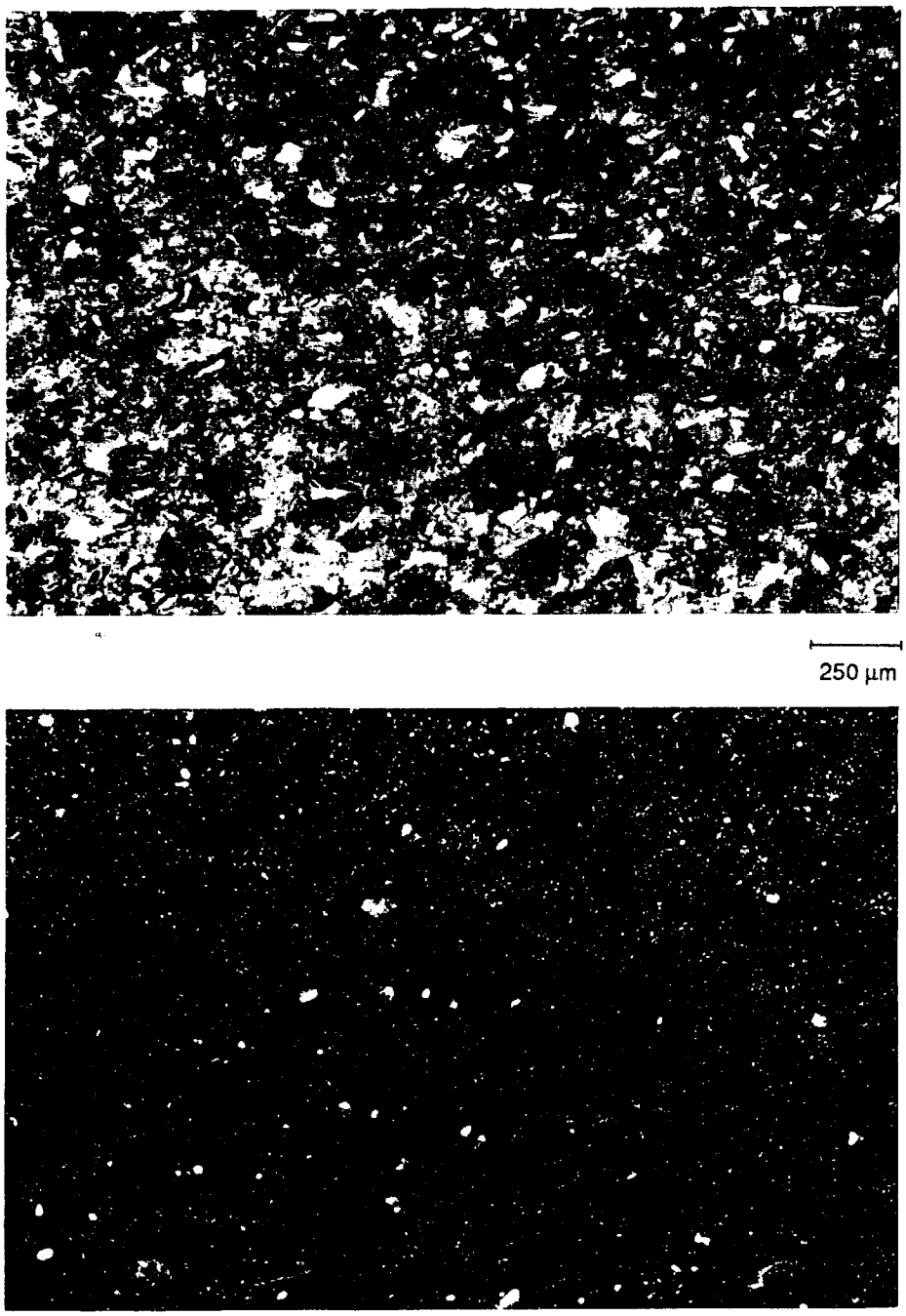

Figure 2-9. Photomicrograph of sample CH. The upper photo was taken under plane-polarized transmitted light; the lower photo was taken under crossed-nichols. Field of view is approximately 2.5 mm.

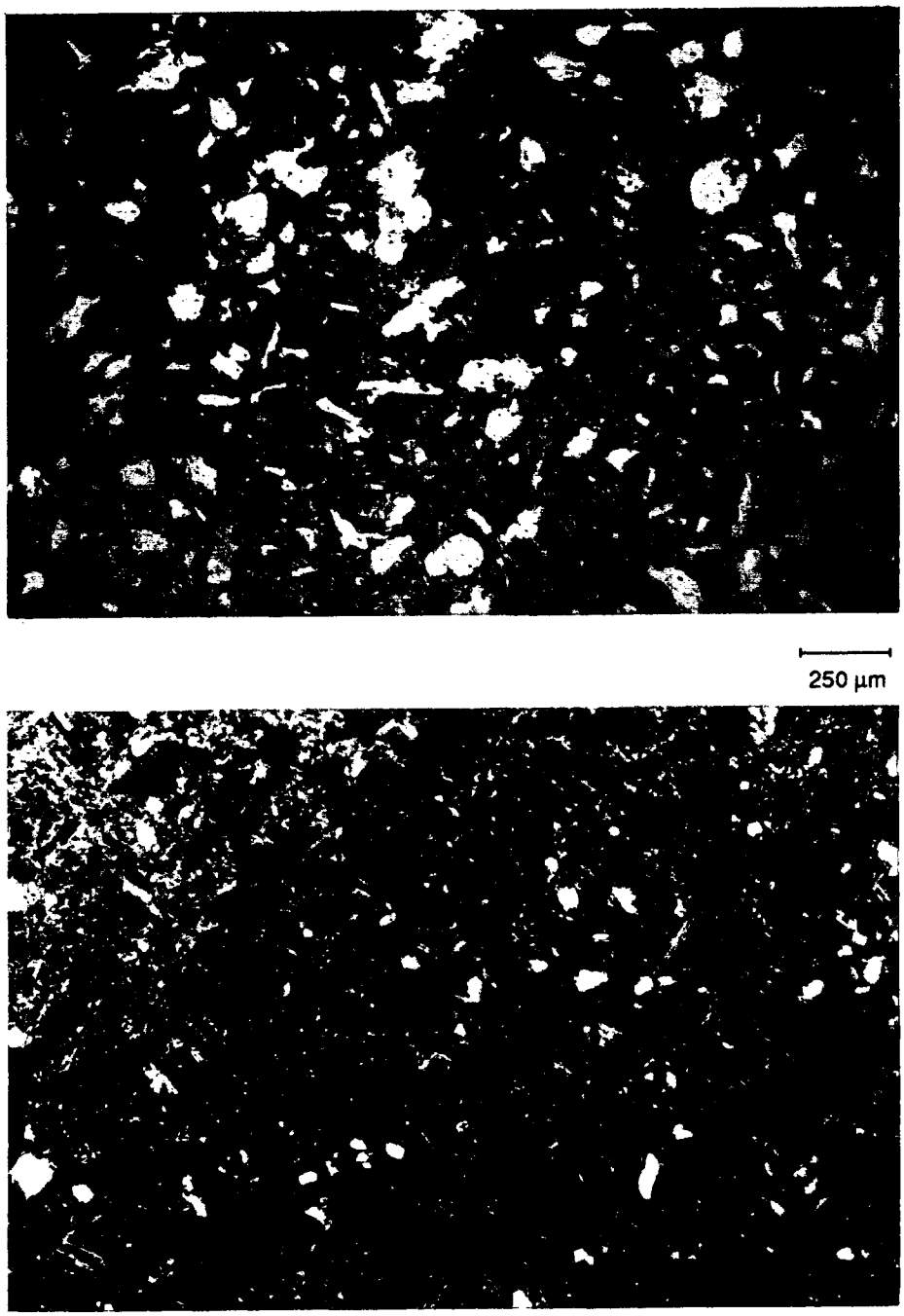

Figure 2-10. Photomicrograph of sample CGC

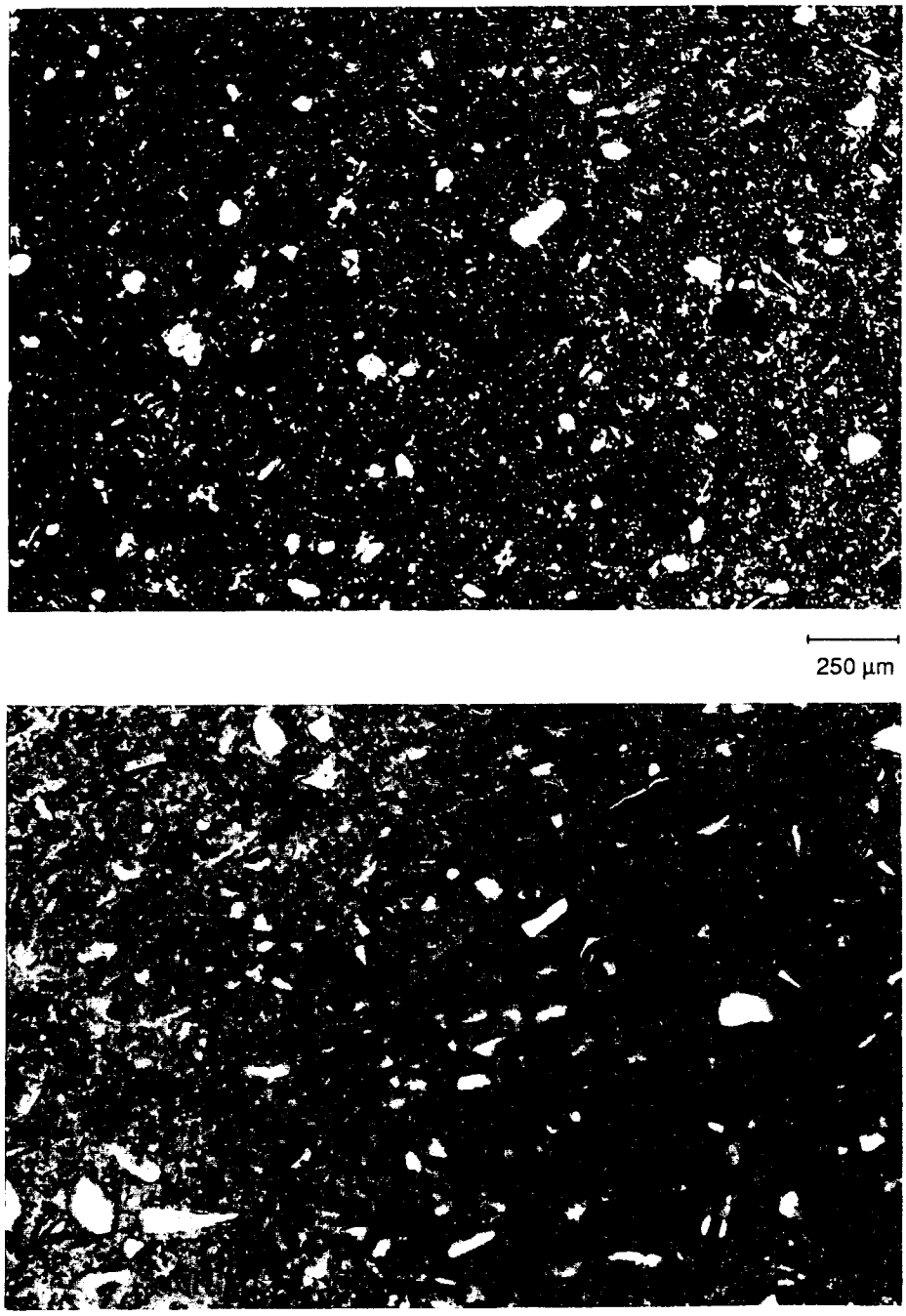

Figure 2-11. Photomicrograph of sample CB

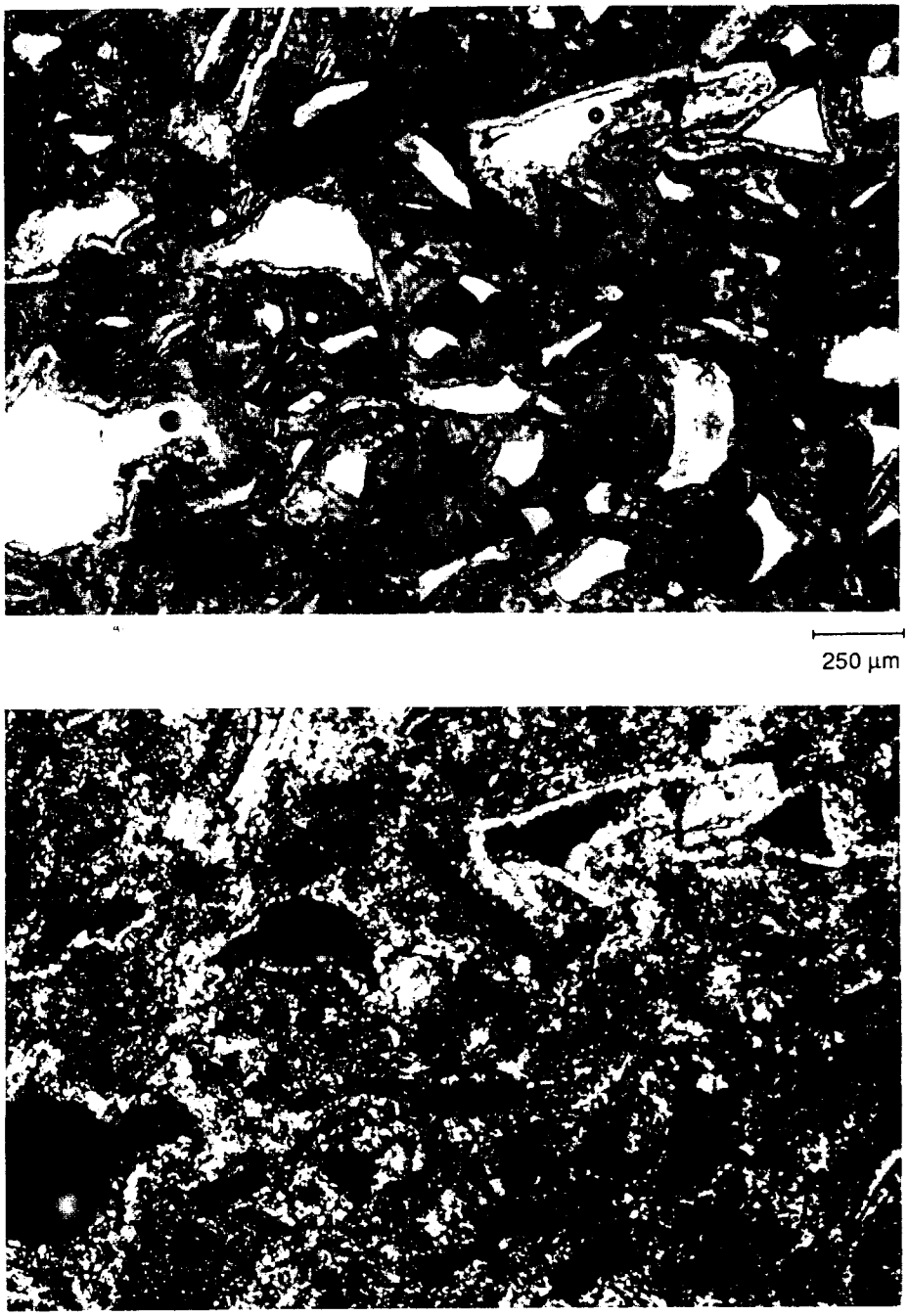

Figure 2-12. Photomicrograph of sample CDV

TABLE 2-7. MINERALOGY OF ZEOLITIZED TUFF SAMPLES BASED ON X-RAY DIFFRACTION AND PETROGRAPHIC ANALYSES

ZEOLITIZED TUFFS	MINERALOGY, APPROXIMATE WT. %																
BULK XRD SAMPLE NO.	OPAL - CT	QUARTZ	PLAGIOCLASE	K - FELDSPAR	GEOTHITE	HEMATITE	AMPHIBOLE	GYPSUM	ANHYDRITE	ILLITE (±10Å MICA)	SMECTITE	CLINOPTILOLITE	MORDENITE	ERIONITE	HALITE	AMORPHOUS/ BELOW DETECTION	
CT	25	1	TR?	2						2	33	35		2		-	
CDV		1	1	1	TR		TR			TR	2	86	TR?	1		6	
CCC	5	1	TR	2	TR		TR	5	1	2	16	65		2		-	Tr DOLOMITE?
CB		6	9	8	3?	TR	TR			4		58	9	TR?		2	
CH		6	6	5			TR			4		61	11	2	4	-	
CGC		2	3	2		4				2		72	3	2		10	
																	From thin-sections:
																	Illite + Mica is biotite.
																	Amphibole is hornblende.

Tr = TRACE ? = TENTATIVE IDENTIFICATION

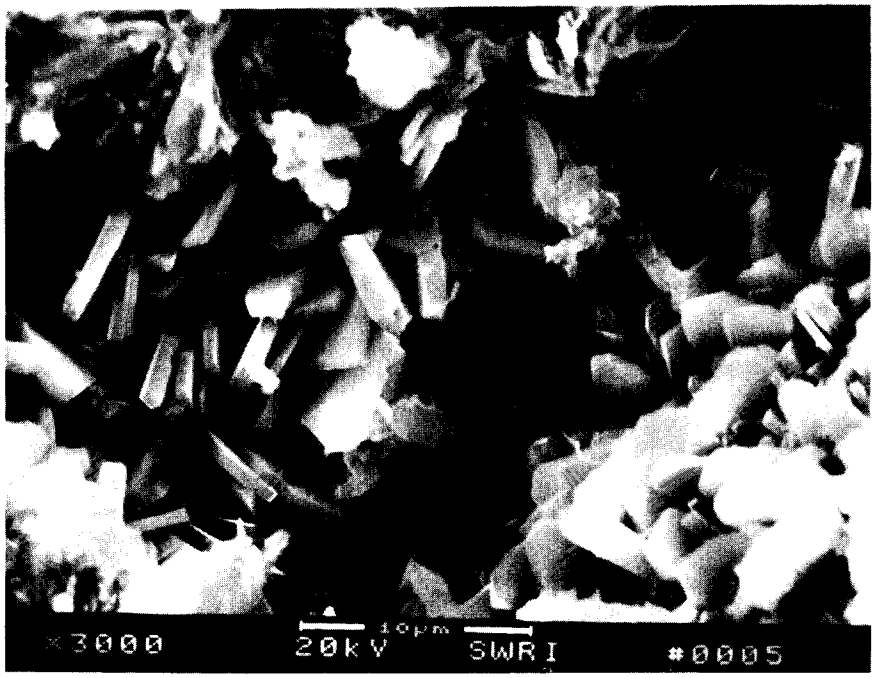

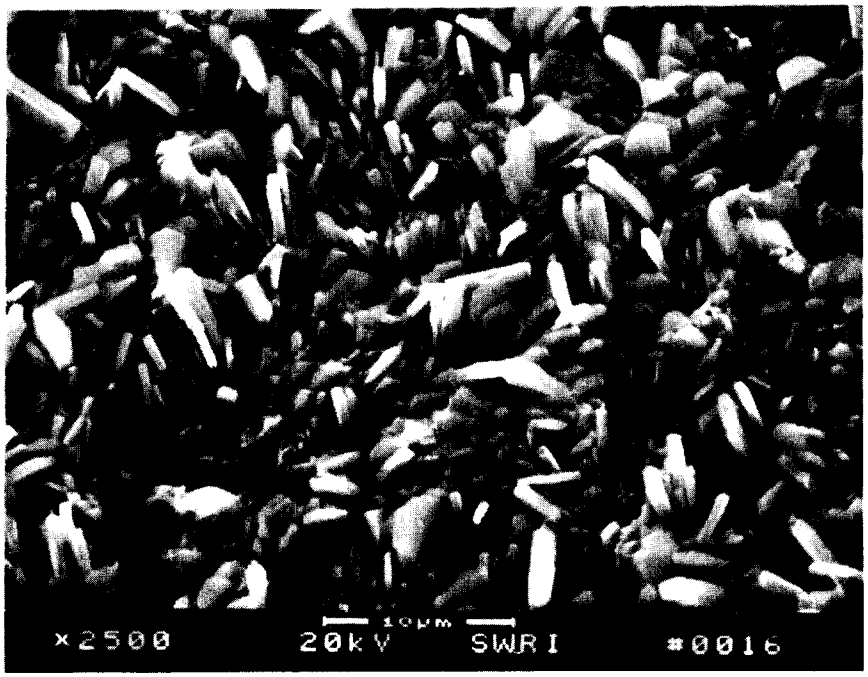

Figure 2-13. Scanning electron image of clinoptilolite from sample CH

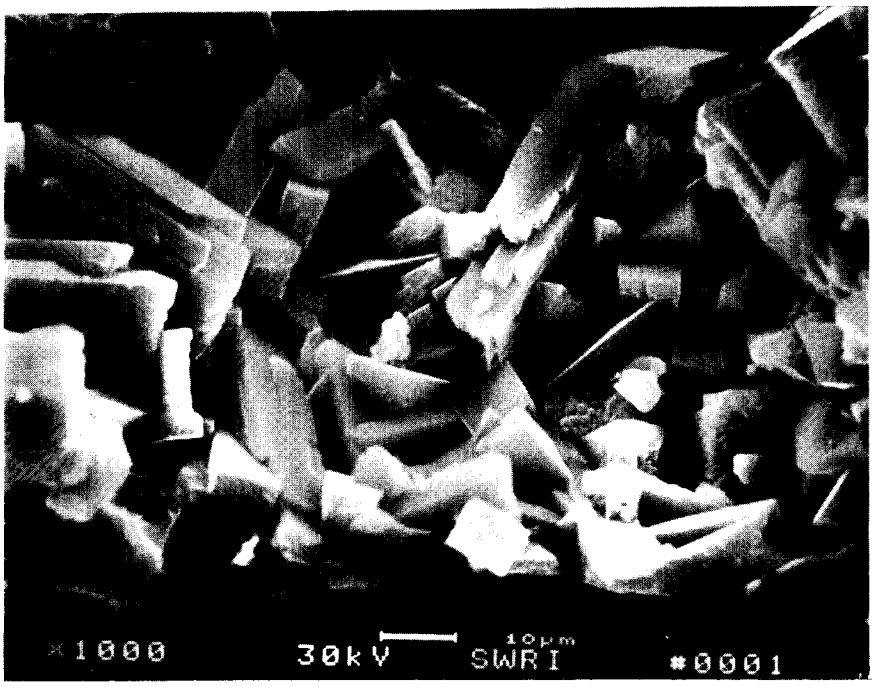

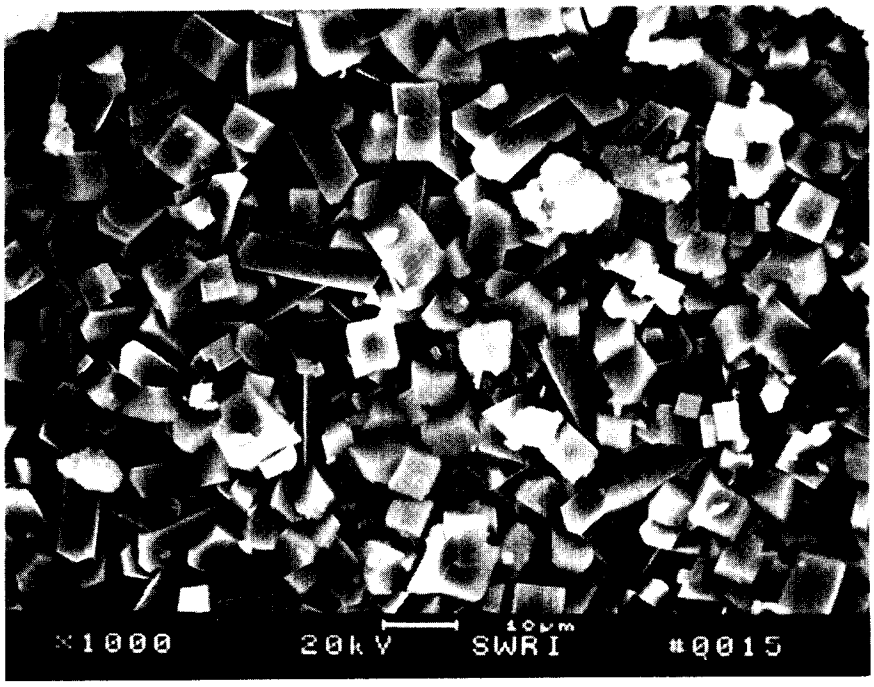

Figure 2-14. Scanning electron image of clinoptilolite from sample CDV

2.3 GEOCHEMICAL MODELING

2.3.1 Technical Objective

The technical objective for geochemical modeling during the second quarter of fiscal year 1990 was to develop a model for the groundwater and mineral chemistry at Yucca Mountain using the EQ6 reaction path code.

2.3.2 Reaction-Path Model for the Evolution of the Groundwater and Mineral Chemistry at Yucca Mountain, Nevada

The groundwater at Yucca Mountain is derived from meteoric water that has migrated downward; reacted with soil, air, rock, and vadose zone gases; and has been affected by biological activity. Reaction-path modeling of these processes aids the interpretation of the groundwater chemistry and alteration mineralogy, and permits identification of the controls on the geochemical evolution of the system. Development of models for the geochemistry of the ambient system is required before predictions of repository-induced perturbations are possible. The object of this report is to present one reaction-path simulation of the evolution of the groundwater and mineral chemistry at Yucca Mountain, Nevada. Validity of the model is evaluated by comparison of predictions with observations of groundwater and mineral chemistry at Yucca Mountain.

Site-specific characteristics were used to condition the model. The composition of the initial aqueous phase is based on a model for the reaction of rain water with soil-zone carbon dioxide gas, calcite, and halite. The primary solid-phase assemblage of feldspar and cristobalite is based on the primary mineralogy and bulk chemistry of the devitrified Topopah Springs tuff. A set of secondary minerals comprising smectite, clinoptilolite, and calcite corresponds to common alteration products at Yucca Mountain (e.g., Bish and Chipera, 1989). Authigenic K-feldspar and albite occur at Yucca Mountain (e.g., Broxton et al., 1986) and are also included as secondary species in the model. The initial water chemistry and all solids are described in Tables 2-8 and 2-9.

The model is generated using the computer programs EQ3NR to speciate the initial aqueous solution and EQ6 to simulate the reaction path (e.g., Wolery, 1979, 1983, 1986). Thermodynamic and kinetic relations represent partial equilibrium among the aqueous species and secondary mineral phases coupled to irreversible dissolution of the primary mineral assemblage. The system is assumed to be isothermal at 25°C and closed. Thermodynamic data are taken from the EQ3/6 data base 3245R54. Unevaluated uncertainties exist in these data, particularly for smectite, clinoptilolite, and the solid solution relations. (All solid solutions were assumed to be represented by ideal mixing of molecular endmembers.) Data for the dissolution rates of feldspar and cristobalite are given in Table 2-10.

2.3.2.1 Initial Water Chemistry

The dominant components of groundwaters from tuffaceous aquifers in the vicinity of Yucca Mountain are sodium, silica, calcium, potassium, magnesium, iron, aluminum, manganese, bicarbonate, chloride, and fluoride. Magnesium, iron, manganese, and fluoride will be neglected in the model, which is designed to simulate the behavior of major elements and the genesis of the most abundant secondary phases. Geologic and geochemical data suggest that calcium, bicarbonate, and chloride in the Yucca Mountain groundwaters are derived partially or dominantly from a source other than the tuffs. Unaltered Paintbrush Tuff from Yucca Mountain generally contains less than 1% CaO by weight. In contrast, rocks that have been partially altered to zeolites and/or clays typically contain CaO at 3 to 4% (Broxton et al., 1986). Although the altered rocks may have silica depletion of 10 to 20% and alumina enrichment up to 30%, the large difference in calcium suggests that it is added to the altered rocks from an external

source. The near surface at Yucca Mountain is generally characterized by caliche composed dominantly of calcite. The likely origin of much of the $CaCO_3$ near the surface is the widespread exposures of Paleozoic carbonate rocks in the region. These rocks are subject to mechanical weathering by wind-blown particles leading to aeolean deposition of carbonate dust. Calcite in the soil zone, whether as dust or caliche, would rapidly dissolve in slightly acidic meteoric water. The initial water in the model is taken to be saturated with calcite.

Rainwater is saturated with respect to atmospheric CO_2 at a partial pressure of $10^{-3.5}$ bar, which leads to bicarbonate contents of approximately 10^{-5} molal and a pH of approximately 5. Groundwaters from tuffaceous aquifers in the vicinity of Yucca Mountain have excess CO_2 relative to atmospheric CO_2 pressures (e.g., Kerrisk, 1987). This is probably derived by oxidation of organic matter in root respiration and in soils in the recharge zone. Relatively sparse vegetation and thin soils on Yucca Mountain may lead to lower CO_2 contents for unsaturated zone water than for saturated zone waters with recharge areas of thicker soil (e.g., Ogard and Kerrisk, 1984), which is consistent with analyses of the CO_2 content of vadose zone gases at Yucca Mountain (Yang et al., 1989). A chemical potential gradient in CO_2 exists between relatively high levels in the saturated zone groundwater and relatively low levels in the unsaturated zone. Consequently, CO_2 in the unsaturated-zone gas and pore water may also be derived in part by exsolution from the lower saturated-zone waters. The fugacity of CO_2 and the pH in the model are initially constrained at levels consistent with significant input of CO_2 from the soil zone (Table 2-8).

The chlorine content of the tuffs is low (approximately 500 ppm), and the molar fluorine to chlorine ratio in the unaltered tuffs is approximately 10 (e.g., Warren and Broxton, 1986, cited in Kerrisk, 1987). In contrast, chloride is the second most abundant anion in groundwaters from the tuffaceous aquifer where its molality usually exceeds the fluoride molality. This difference suggests an external source of chlorine, although it may also be due to incorporation of fluoride in secondary minerals such as zeolites, clays, and apatite. An external source of chloride could be aerosol or dust halite derived from the numerous playas in the region and deposited at the surface of the mountain. The initial solution in the model is set to contain $2x10^{-4}$ m NaCl to yield a chloride content typical of Yucca Mountain groundwaters (e.g., Kerrisk, 1987).

2.3.2.2 *Primary and Secondary Mineral Assemblages*

The dominant primary solid phases at Yucca Mountain are alkali feldspar, cristobalite, quartz, tridymite, and glass (e.g., Bish and Chipera, 1989). The devitrified tuff at the repository horizon is composed almost completely of alkali feldspar and cristobalite. The major element chemistry of cryptocrystalline Topopah Springs rhyolite is represented almost identically by alkali feldspar with minor calcium plus silica, e.g., cristobalite (Table 2-11). These two minerals are taken as the primary solids in the model.

Dominant secondary minerals in the upper sections of Yucca Mountain are clinoptilolite, mordenite, and smectite. In the lower sections, analcime and kaolinite occur instead of clinoptilolite and mordenite. Calcite and secondary quartz occur in many horizons. For the model, solid solutions of smectite and clinoptilolite (Table 2-9) are permitted to form at equilibrium with the aqueous solution, which is assumed to become supersaturated with respect to kaolinite and quartz. Calcite, K-feldspar, and albite are also permitted to precipitate in partial equilibrium with the aqueous and secondary mineral phases.

TABLE 2-8. INITIAL MODEL WATER CHEMISTRY

Major Component	Total Molality	Dominant Species	Species Molality	Basis/Notes
Ca	2.04×10^{-3}	Ca^{2+}	1.94×10^{-3}	1
CO_2	4.92×10^{-3}	HCO_3^- $CO_{2(aq)}$	3.97×10^{-3} 8.5×10^{-4}	2
Na	2.0×10^{-4}	Na^+	2.0×10^{-4}	3
Cl	2.0×10^{-4}	Cl^-	1.99×10^{-4}	3

TRACE COMPONENTS: K, $SiO_{2(aq)}$, Al

OTHER PARAMETERS:

pH = 7	4
O_2 fugacity = $10^{-0.7}$ bar	5
CO_2 fugacity = $10^{-1.62}$ bar	6

1. Calculated values based on equilibrium with calcite (together with constraints on bicarbonate and pH)
2. HCO_3^- species calculated by its adjustment to achieve charge neutrality in the solution
3. Fixed value based on the typical chloride content of tuffaceous aquifer water at Yucca Mountain
4. Fixed value based on the typical pH of tuffaceous aquifer water at Yucca Mountain
5. Calculated value based on equilibrium with air (Note: there are no redox reactions in the model.)
6. Calculated value based on charge balance, pH, and carbonate equilibria

TABLE 2-9. MODEL MINERAL CHEMISTRY

Mineral	Components
Cristobalite	SiO_2
Feldspar	0.53 $KAlSi_3O_3$ (sanidine)
	0.45 $NaAlSi_3O_8$ (high albite)
	0.02 $CaAl_2Si_2O_8$ (anorthite)
Calcite	$CaCO_3$
Smectite	$Na_{.33}Al_{2.33}Si_{3.67}O_{10}(OH)_2$ (Na beidellite)
	$K_{.33}Al_{2.33}Si_{3.67}O_{10}(OH)_2$ (K beidellite)
	$Ca_{.165}Al_{2.33}Si_{3.67}O_{10}(OH)_2$ (Ca beidellite)
Clinoptilolite	$CaAl_2Si_{10}O_{24}.8H_2O$
	$Na_2Al_2Si_{10}O_{24}.8H_2O$
	$K_2Al_2Si_{10}O_{24}.8H_2O$
K-feldspar	$KAlSi_3O_8$ (microcline)
Albite	$NaAlSi_3O_8$ (low albite)

TABLE 2-10. KINETIC DATA

RATE EXPRESSION:

$$\frac{d\xi}{dt} = k\ s\ a_{H^+}^{n}\ (1-\exp(\frac{-A}{R\ T}))$$

ξ: reaction progress variable for the individual dissolution reaction (xi = the sum of ξ for all dissolution reactions)

t: time

k: rate constant

s: surface area

a_{H^+}: activity of the hydrogen ion

n: order of the dissolution reaction with respect to the hydrogen ion

A: chemical affinity for the dissolution reaction

R: ideal gas constant

T: temperature

reactant*	s (cm^2)	k (moles/cm^2/sec)	n
feldspar	2000	$3x10^{-16}$	0
	2000	2.5×10^{-19}	-0.4
cristobalite	1000	$1.6x10^{-18}$	0
	1000	$5x10^{-21}$	-0.5

*There are two parallel reactions for each reactant. Feldspar rate parameters are based on data from Helgeson et al. (1984) for albite. Cristobalite rate parameters are based on data for quartz from Murphy and Helgeson (1989) and Knauss and Wolery (1988).

TABLE 2-11. BULK COMPOSITION (WEIGHT PERCENT) OF TOPOPAH SPRINGS TUFF (TST) REPRESENTED AS FELDSPAR PLUS CRISTOBALITE

Oxide	TST*	Feldspar plus Cristobalite**
SiO_2	77	77.04
Al_2O_3	12.5	12.97
CaO	0.25	0.28
Na_2O	3.5	3.48
K_2O	6.5	6.23

*Typical values extracted from data reported by Byers (1985)

**0.25 moles of feldspar with the composition given in Table 2-9 plus 0.54 moles of cristobalite

2.3.2.3 *Results of the Model*

The evolution of major components of the aqueous phase as a function of reaction progress is represented in Figures 2-15 and 2-16. Reaction progress, represented by xi, corresponds to the sum of the number of moles of feldspar and cristobalite dissolved per kilogram of water. A calcium-rich smectite and calcite begin to precipitate almost immediately, which causes the calcium and bicarbonate concentrations to drop. Sodium, silica, and potassium increase rapidly as the feldspar and cristobalite dissolve. Silica concentrations rapidly exceed quartz saturation (10^{-4} m). A potassium- and calcium-bearing clinoptilolite begins to precipitate at xi = 1.85×10^{-5}. The high silica content of clinoptilolite leads to a subsequent decrease in the aqueous silica concentration. As potassium increases, the K content of the clinoptilolite and smectite increase; and the solution becomes saturated with K-feldspar at xi = 2.16×10^{-3}. The K^+ content of the solution decreases sharply thereafter, and the calcium content of the smectite and clinoptilolite increases relative to potassium. As the sodium concentration reaches 4×10^{-3} m, albite begins to precipitate at xi = 9.65×10^{-3}. Calcite precipitates to xi = 7×10^{-3}, and then slowly redissolves as the solution becomes depleted in Ca^{2+}. The logarithm of the CO_2 fugacity continuously decreases, and the pH continuously increases in a complementary fashion. At the end of this simulation, the overall reaction leads to a nearly isochemical transformation of the primary feldspar and cristobalite to the secondary phase assemblage and to an approximately steady-state solution composition.

The rates of dissolution of cristobalite and feldspar vary as a function of the degree of disequilibrium and pH (represented by A and a_{H^+} in Table 2-10). The solution continuously approaches equilibrium with the feldspar. However, even when it is saturated with K-feldspar and albite at the end of the simulation, an affinity remains of nearly 6 kJ/mole for

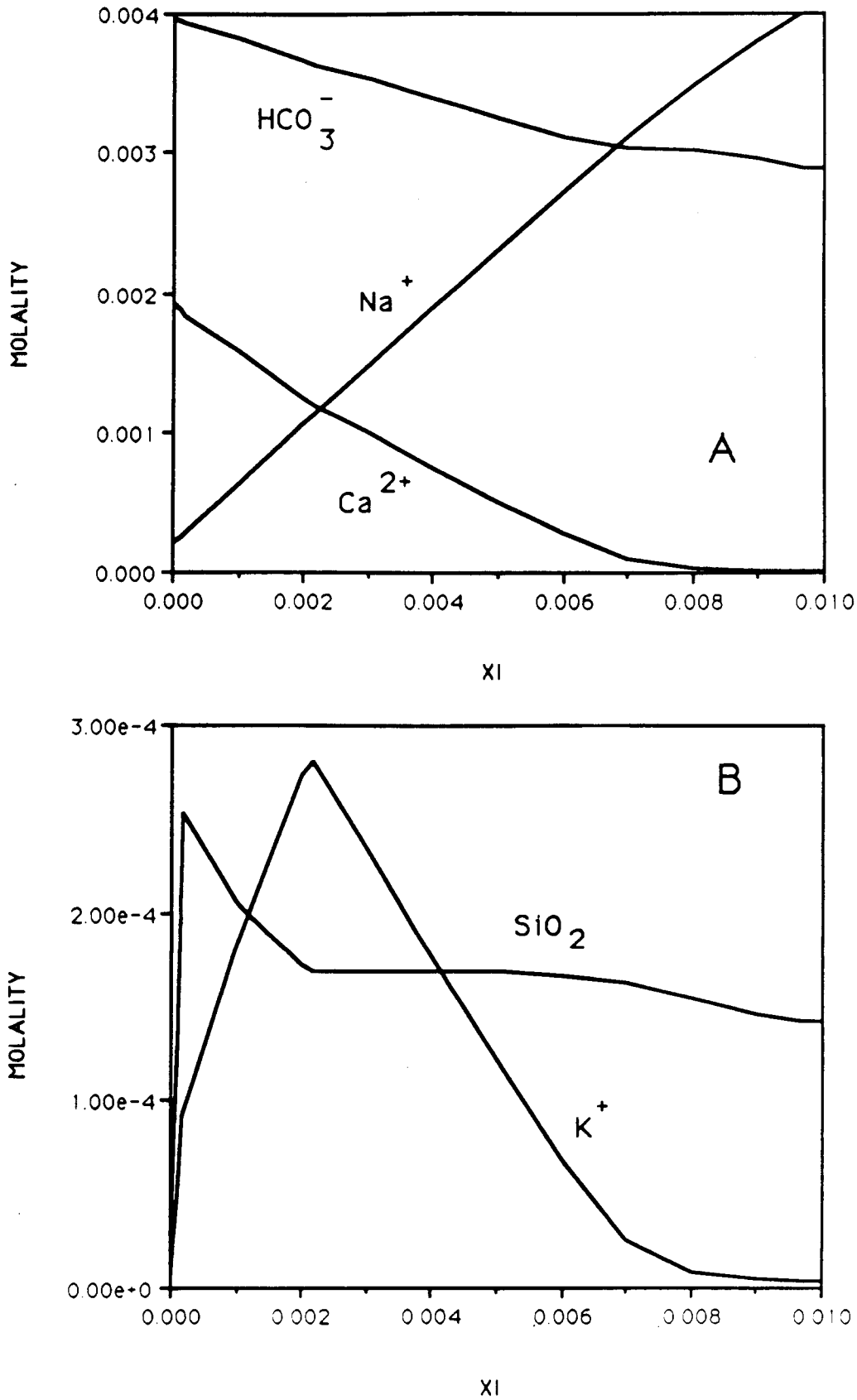

Figure 2-15. Model major element water chemistry

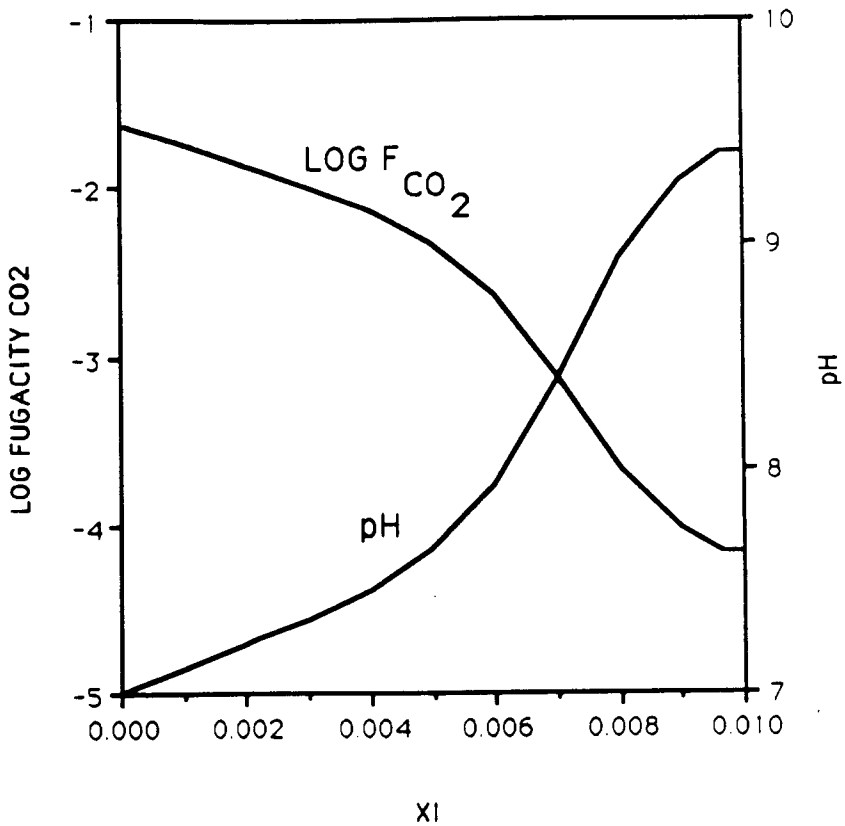

Figure 2-16. Model pH and log CO_2 fugacity for the water

dissolution of the feldspar solid solution, which is assumed to have thermodynamic properties consistent with the mixing of components with high-temperature structures. The solution remains undersaturated with respect to cristobalite; but the degree of undersaturation varies as the total silica content goes up and then down, and as the $H_3SiO_4^-$ species becomes important at high pH. The increase in reaction rate with increasing pH above approximately pH 8 for both reactants has a larger effect than the decrease in rate due to the approach to equilibrium. Hence, the overall reaction rate increases slightly with time and reaction progress. The time calculated to reach saturation with K-feldspar is 71 years; and for saturation with albite, it is 232 years. The absolute time is calculated on the basis of surface area to mass ratios of 1000 and 2000 $cm^2/kg\ H_2O$ for cristobalite and feldspar, respectively. The total surface area to water mass ratio corresponds to the surface area of a 7-mm wide fluid-filled fissure. Because the surface area is a constant that can be incorporated in the rate constants, larger or smaller surface-area to mass ratios would correspond proportionately to shorter or longer times, respectively. The reaction paths would be unaffected.

2.3.2.4 *Validity of the Model*

The validity of the model can be evaluated by comparing the computed results with empirical data from Yucca Mountain and by judging the reasonableness of variations and magnitudes of model-dependent variables. An examination of each component and phase reveals aspects of the model that correspond reasonably to observations and other aspects that are deficient, indicating areas for improvement. Because the water chemistry in the unsaturated zone at Yucca Mountain is essentially unknown, calculated water compositions are compared with those of waters from fourteen wells at Yucca Mountain and vicinity. Water chemistry data are taken from the compilation by Kerrisk (1987) for Yucca Mountain and vicinity samples excluding those from well UE-25p#1, which taps the carbonate aquifer.

pH, CO_2, and carbonate. The modeled pH and logarithm of the CO_2 fugacity (Figure 2-16) correspond well to measured pH and calculated fugacities for groundwaters at Yucca Mountain and vicinity reported by Kerrisk (1987), at least up to xi = $7x10^{-3}$. The modeled inverse relation between these variables matches almost identically the relation shown in Figure 8 of Kerrisk (1987) between empirical pH and calculated log fugacity. The match occurs, in part, because Kerrisk calculated CO_2 fugacities using the same equilibria used in the model. Nevertheless, this agreement suggests that the variety of groundwaters in the vicinity of Yucca Mountain represents varying degrees of progress along a reaction path such as that of the model. These data may therefore be used to test other aspects of the model. CO_2 fugacity drops below the atmospheric level of $10^{-3.5}$ bar at xi > $7x10^{-3}$. This calculation appears to be unrealistic for the unsaturated zone at Yucca Mountain because air is expected to circulate in the mountain and because CO_2 gas concentrations measured in the unsaturated zone at Yucca Mountain do not fall below this level (Yang et al., 1988). Conditioning the model to buffer the CO_2 pressure within the range of values observed for the unsaturated zone at Yucca Mountain would be an improvement.

Nevertheless, Kerrisk (1987) reports one pH at 9.2 and calculates a corresponding CO_2 fugacity of $10^{-3.8}$ bar for the USW H-3 well water at Yucca Mountain. These values correspond almost exactly to corresponding values from the model shown in Figure 2-16. The initial total carbonate in the model system was $5x10^{-3}$ molal, which was fixed by the charge balance constraint together with calcite equilibrium and the fixed pH. This value corresponds to the maximum total carbonate in Yucca Mountain vicinity groundwaters from tuff reported by Kerrisk (1987). Total carbonate decreases into the middle range of observed values ($4.1x10^{-3}$ m) as calcite precipitates. Lower initial total carbonate values could reasonably be achieved in the model by adding the fluoride anion to the charge balance or by increasing the initial pH to decrease calcite solubility.

Na^+, Ca^{2+}, and K^+. A dominant trend in the data of Figure 2-15 is the increase in Na^+ and decrease in Ca^{2+}. The Na^+ increases because it is a major species released from the feldspar, its initial concentration is low, and the secondary phases are sodium poor. The Ca^{2+} decreases because it is initially high at equilibrium with calcite; it is an important component of the three dominant secondary minerals--smectite, clinoptilolite, and calcite; and the dissolving rock is poor in calcium. This inverse relation between Na^+ and Ca^{2+} is reflected roughly in the data from Yucca Mountain vicinity groundwaters, as illustrated in Figure 2-17(a). The curve in this figure represents corresponding values of total aqueous calcium and sodium calculated in the model for values of xi from 0.005 to 0.01. The good correspondence in magnitude and trend between the groundwater data and the model is a remarkable indication of the validity of the model.

The K^+ content of groundwater from the vicinity of Yucca Mountain ranges generally from $3x10^{-5}$ to $1.4x10^{-4}$ molal. In the model, the K^+ concentration increases to nearly $3x10^{-4}$ molal before K-feldspar begins to precipitate. It then declines to the range observed at Yucca Mountain. The modeled and observed relations between Ca^{2+} and K^+ concentrations are illustrated in Figure 2-17(b) for the same range of reaction progress shown in Figure 2-17(a). It is remarkable that the model potassium concentrations correspond well to the Yucca Mountain groundwater data at the values of xi for which the model also correctly predicts sodium and calcium concentrations.

The question could be asked as to why the natural system should evolve only to the levels of reaction progress indicated by the correspondence between model and observation shown in Figure 2-17. A possible explanation is that as the solutions become saturated with respect to K-feldspar, the product phase nucleates and grows preferentially using the primary alkali feldspar surface as a template. This process, analogous to asymmetric irreversible dissolution of solid solutions described by Murphy and Smith (1988), would tend to isolate the primary feldspar

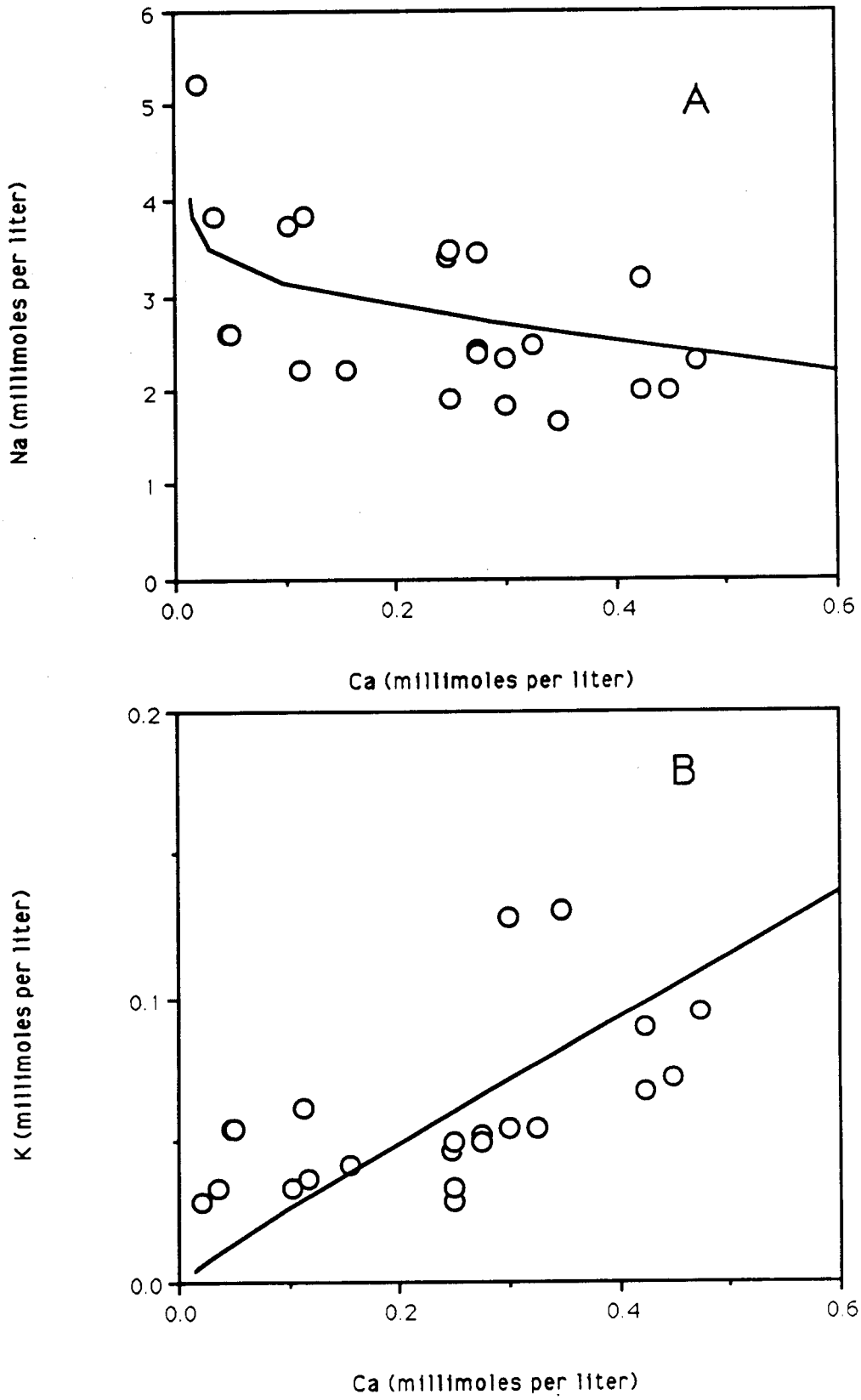

Figure 2-17. Model (lines) and measured water chemistry (circles) data from Kerrisk (1987) for Yucca Mountain. Note: for the model calcium decreases as reaction progress increases.

from further reaction [Figure 2-17(a) and Figure 2-17(b)] by stabilizing its surface. Detailed surface chemical analyses of the alkali feldspars, for instance, by auger electron spectroscopy (e.g., Hochella et al., 1988), could permit an evaluation of the significance of this mechanism.

Silica. Analyzed groundwaters at Yucca Mountain generally have silica contents in excess of saturation with cristobalite and below saturation with amorphous silica (Kerrisk, 1987). This is not reflected in the model, in which silica concentrations remain below cristobalite saturation. Generation of aqueous silica concentrations in excess of cristobalite saturation requires dissolution of other silica-bearing phases such as feldspars or glass. With conservation of aluminum among solid phases, dissolution of alkali feldspar and growth of clay minerals result in increasing aqueous silica concentrations. However, in the model this increase also leads to saturation of the solution with clinoptilolite and its growth. Alteration of feldspars to clinoptilolite with aluminum conservation results in a decrease in aqueous silica. This reaction can not produce the elevated silica concentrations observed in the Yucca Mountain area.

The silicon:aluminum ratio in rhyolite glass (or bulk Topopah Springs tuff) exceeds that in clinoptilolite. Alteration of glass is the most likely mechanism for generation of secondary clinoptilolite and elevated aqueous silica activities. This conclusion is supported by petrographic evidence, which indicates that clinoptilolite forms predominantly by alteration of rhyolitic glass at Yucca Mountain. The low silica concentrations predicted in the model may also be a consequence of uncertainties in the thermodynamic and kinetic properties of clinoptilolite. Clinoptilolites in the unsaturated zone at Yucca Mountain tend to be heulanditic, with lower silica contents than the idealized stoichiometries employed in the model (Table 2-9). However, the Si:Al ratio of heulandite also exceeds that of alkali feldspar. Slow nucleation and grow kinetics resulting in clinoptilolite supersaturation or incorrect, standard free energies for clinoptilolite could also lead to higher silica contents than indicated by the model.

Mineral chemistry. The Ca:Na:K ratios calculated for clinoptilolites correspond well with measured values for the eastern calcic group and the calcium-rich subset of the transitional group of clinoptilolites as given in Broxton et al. (1986). Clinoptilolites rich in both Na and K characteristic of the western alkalic group and the transitional group are not generated in the model. Compositions of smectites from Yucca Mountain are poorly known, which restrict comparisons to the model.

2.3.3 Summary of Results

A reaction-path model for the evolution of the solid- and liquid-phase chemistry at Yucca Mountain corresponds remarkably well with the observed ranges of water and mineral compositions. Conditioning the model with geological and geochemical data from the site is essential. Field data appear to support a source for calcium and carbonate other than the tuff such as the near-surface source offered in the model. Nearly quantitative correspondence occurs between modeled and empirical relations among calcium, sodium, and potassium in Yucca Mountain groundwaters. The pH and carbonate contents are also well represented. Groundwater compositions observed at Yucca Mountain appear to reflect varying degrees of evolution along reaction paths similar to the model. Variations of modeled clinoptilolite compositions correspond to those observed for calcium-rich clinoptilolites at Yucca Mountain, indicating that they also are a consequence of variations in water chemistry along reaction paths such as that in the model. In addition, the modeling results indicate that silica concentrations in excess of cristobalite saturation, commonly observed at Yucca Mountain, are due to alteration of volcanic glass.

2.4 REFERENCES: UNSATURATED MASS TRANSPORT (GEOCHEMISTRY), EXPERIMENTAL STUDIES

Ames, L. L., Jr. 1964a. Some zeolite equilibria with alkali metal cations. *Amer. Mineral* 49:127-145.

Ames, L. L., Jr. 1964b. Some zeolite equilibria with alkaline earth metal cations. *Amer. Mineral* 49:1099-1110.

Barrer, R. M., and J. Klinowski. 1974. Ion exchange selectivity and electrolyte concentration. *J. Chem. Soc., Faraday Trans. 1* 70:2080-2091.

Elprince, A. M., and K. L. Babcock. 1975. Prediction of ion-exchange equilibria in aqueous systems with more than two counter-ions. *Soil Science* 120:332-338.

Elprince, A. M., A. P. Vanselow, and G. Sposito. 1980. Heterovalent, ternary cation exchange equilibria: NH_4^+-Ba^{2+}-La^{3+} exchange on montmorillonite. *J. Soil Sci. Soc. Am.* 44:964-968.

Fletcher, P., and R. P. Townsend. 1985. Ion exchange in zeolites. The exchange of cadmium and calcium in sodium X using different anionic backgrounds. *J. Chem. Soc., Faraday Trans. 1* 81:1731-1744.

Gaines, G. L., Jr., and H. C. Thomas. 1953. Adsorption studies on clay minerals: II. A formulation of the thermodynamics of exchange adsorption. *J. Phys. Chem.* 21:714-718.

Howery, D. G., and H. C. Thomas. 1965. Ion exchange on the mineral clinoptilolite. *J. Phys. Chem.* 69:531-537.

Landelout, H., and H. C. Thomas. 1965. The effect of water activity on ion exchange selectivity. *J. Phys. Chem.* 69:339-341.

Pabalan, R. T., and W. M. Murphy. 1990. Progress in experimental studies on the thermodynamic and ion exchange properties of clinoptilolite. Report No. 89-006. San Antonio, Texas: Center for Nuclear Waste Regulatory Analyses:91.

Pitzer, K. S. 1973. Thermodynamics of electrolytes: Theoretical basis and general equations. *J. Phys. Chem.* 77:268-277.

Pitzer, K. S. 1979. Theory: ion interaction approach. *Activity Coefficients in Electrolyte Solutions*. Pytkowicz, R., ed. Boca Raton, Florida: CRC Press:157-208.

Sposito, G. 1981. *The Thermodynamics of Soil Solutions*. New York: Oxford Univ. Press.

Wolery, T. J., K. J. Jackson, W. L. Bourcier, C. J. Bruton, B. E. Viani, K. G. Knauss, and J. M. Delany. 1990. Current status of the EQ3/6 software package for geochemical modeling. *Chemical Modeling of Aqueous Systems II*. Melchior, D. C., and R. L. Bassett, eds. ACS Symposium Series 416, Washington, D.C.: American Chemical Society:104-116.8.1.

2.5 REFERENCES: UNSATURATED MASS TRANSPORT (GEOCHEMISTRY), GEOCHEMICAL MODELING

Bish, D. L., and S. J. Chipera. 1989. *Revised Mineralogic Summary of Yucca Mountain, Nevada*. Los Alamos National Laboratory (LANL) LA-11497-MS. Los Alamos, New Mexico: LANL.

Broxton, D. E., R. G. Warren, R. C. Hagan, and G. Luedemann. 1986. *Chemistry of Diagenetically Altered Tuffs at a Potential Nuclear Waste Repository, Yucca Mountain, Nye County, Nevada*. LANL LA-10802-MS. Los Alamos, New Mexico: LANL.

Byers, F. M., Jr. 1985. *Petrochemical Variation of Topopah Springs Tuff Matrix with Depth (Stratigraphic Level), Drill Hole USW G-4, Yucca Mountain, Nevada*. LANL LA-10561-MS. Los Alamos, New Mexico: LANL.

Helgeson, H. C., W. M. Murphy, and P. Aagaard. 1984. Thermodynamic and kinetic constraints on reaction rates among minerals and aqueous solutions: II. Rate constants, effective surface area, and the hydrolysis of feldspar. *Geochim. Cosmochim. Acta* 48:2405-2432.

Hochella, M. F., Jr. 1988. Auger electron and x-ray photoelectron spectroscopies. *Spectroscopic Methods in Mineralogy and Geology: Reviews in Mineralogy*, Hawthorne, F. C., ed. 18:573-637.

Kerrisk, J. F. 1987. *Groundwater Chemistry at Yucca Mountain, Nevada, and Vicinity*. LANL LA-10929-MS. Los Alamos, New Mexico: LANL.

Knauss, K. G., and T. J. Wolery. 1988. The dissolution of quartz as a function of pH and time at 70°C. *Geochim. Cosmochim. Acta* 52:43-53.

Murphy, W. M., and H. C. Helgeson. 1989. Thermodynamic and kinetic constraints on reaction rates among minerals and aqueous solutions: IV. Retrieval of rate constraints and activation parameters for the hydrolysis of pyroxene, wollastonite, olivine, andalusite, quartz, and nepheline. *Amer. Jour. Sci.* 289:17-101.

Murphy, W. M., and R. W. Smith. 1988. Irreversible dissolution of solid solutions: A kinetic and stoichiometric model. *Radiochim. Acta* 44/45:395-401.

Ogard, A. E., and J. K. Kerrisk. 1984. *Groundwater Chemistry Along Flow Paths Between a Proposed Repository Site and the Accessible Environment*. LANL LA-10188-MS. Los Alamos, New Mexico: LANL.

Wolery, T. J. 1979. *Calculation of Chemical Equilibrium Between Aqueous Solution and Minerals: The EQ3/6 Software Package*. Lawrence Livermore National Laboratory (LLNL) UCRL-52658. Livermore, California: LLNL.

Wolery, T. J. 1983. *EQ3NR, a Computer Program for Geochemical Aqueous Speciation-Solubility Calculations: User's Guide and Documentation*. LLNL UCRL-53414. Livermore, California: LLNL.

Wolery, T. J. 1986. EQ3/6: Status and Future Development. *Proceedings of the Workshop on Geochemical Modeling*. LLNL CONF-8609134. Livermore, California: LLNL:10-19.

Yang, I. C., H. H. Haas, E. P. Weeks, and D. C. Thorstenson. 1989. Analysis of gaseous-phase stable and radioactive isotopes in the unsaturated zone, Yucca Mountain, Nevada. In preparation at U.S. Geological Survey, Denver, Colorado.

3. THERMOHYDROLOGY

by Ronald T. Green and Steve Svedeman

Investigator: Ronald H. Martin

3.1 TECHNICAL OBJECTIVES

Technical issues and uncertainties for the proposed Yucca Mountain HLW repository site indicate a need for research on thermohydrological phenomena, i.e., phenomena associated with heat and fluid flow, to provide information relevant to performance assessment and design criteria. The class of thermohydrological phenomena examined in this project includes phenomena driven by heat emanating from HLW emplaced in a geologic repository. Information derived principally from research is used to establish a knowledge base of thermohydrologic phenomena; the base will be used to assess models of processes used in performance assessments. The specific objectives of the thermohydrology research project are summarized as follows:

(1) To perform a critical assessment of the state-of-knowledge of thermohydrology in unsaturated fractured media, in the context of present HLW-NRC program activities. This assessment will require an in-depth review of existing literature and on-going programs. The assessment will focus on flow processes, heat transfer mechanisms, and the state-of-knowledge experimental methods in porous media.

(2) To perform a detailed dynamic similarity or similitude analysis on the complete set of governing equations relevant to unsaturated flow and to determine the set of dimensionless parameters required to conduct appropriate laboratory simulations. In this analysis of modeling parameters, the range of parameter applicability and limitation on the magnitude of these parameters, as constrained by the principles of dynamic similarity, will be determined.

(3) To identify potential problems associated with the design and performance of laboratory simulations with scaled geometry, fluid, media, and other relevant properties subject to modeling distortion.

(4) To perform a series of separate effects experiments in order to identify and understand the role of each effect in the overall, coupled processes involved in thermohydrologic phenomena.

(5) To design and perform comprehensive experiments whose results will continue to identify key dependent and independent parameters and their relationships to each other in the context of thermohydrologic issues.

(6) To develop the laboratory facilities, experimental methods, measurement techniques, and associated analytic skills to evaluate and validate other program results and to provide a high quality of technical assistance and research in support of NRC's licensing of a HLW repository.

(7) To examine and correlate laboratory results with field data that will aid in the design of future field experiments.

The research project has been delineated into five tasks for accomplishing these objectives.

(1) Task 1 - Assessment of the State-of-Knowledge of Thermohydrology in Unsaturated Media

(2) Task 2 - Design and Execution of Preliminary Separate Effects Experiments

(3) Task 3 - Design of Unsaturated Zone Thermohydrological Experiments

(4) Task 4 - Thermohydrologic Phenomena Induced by the Aggregate of Emplaced HLW in Unsaturated Geologic Media

(5) Task 5 - Unsaturated Zone Thermohydrologic Phenomena Induced by Multiple Packages of HLW

Tasks 1 and 2 are active at this time and are discussed in the following two subsections 3.2 and 3.3.

3.2 ASSESSMENT OF THE STATE-OF-KNOWLEDGE OF THERMOHYDROLOGY IN UNSATURATED MEDIA

Review of the state-of-knowledge in the area of thermohydrology continued during this reporting period. Documents relevant for the HLW program have been summarized and are being incorporated into the Technical Document Index (TDI) maintained at the Center for use by the staff at both NRC and the Center for future review and reference.

In thermohydrology, an unsaturated media poses significant challenges in modeling and phenomelogical interpretations of its thermohydrologic behavior. While technology has been developed under saturated conditions, the knowledge base for unsaturated media is limited. As part of a strategy to develop the knowledge base, participation in technical exchange meetings and focused workshops has been a key element for this task.

A technical interchange among researchers associated with DOE and representatives from NRC (Messrs. Tim Margulies and Paul Prestholt) and the Center (Messrs. Frank Dodge, Ron Green, and Steve Svedeman) was held at Lawrence Berkeley Laboratory on March 12, 1990. Experiments with relevancy to thermohydrology were observed and discussed.

3.3 DESIGN AND EXECUTION OF PRELIMINARY SEPARATE EFFECTS EXPERIMENTS

Two separate effects experiments (test Nos. 1 and 2) were performed during this reporting period. The experiments were designed to measure temperature, suction pressure, and moisture content within a test chamber containing glass beads. These three physical parameters were measured using thermistors, tensiometers, and a gamma-ray densitometer, respectively. Two photographs of the separate effects experiments are included as Figures 3-1 and 3-2.

The goal or purpose of the separate effects experiments is to identify, individually, the key phenomena that affect unsaturated fluid transport and the magnitude of their influence for use in similar studies and future experimental design. The effects to be investigated in the experiments include the following:

- Liquid infiltration and distribution
- Local heating of pore liquid
- Gas and liquid convection
- Transient heating
- Forced vs. free convection

Because of the need to study the influence of certain phenomena without coupled interactions from other "effects," the first two experiments were performed on a uniform medium under near-isothermal conditions. The experiments investigated the processes affecting liquid infiltration and distribution.

Figure 3-1. Separate effects experimental apparatus - front view

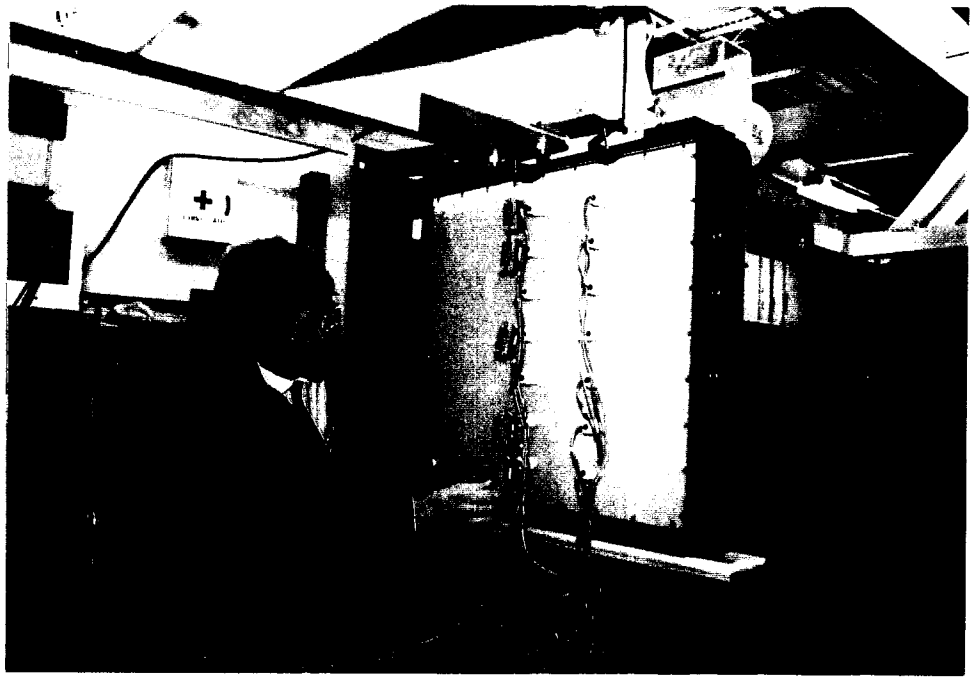

Figure 3-2. Separate effects experimental apparatus - back view

3.3.1 Simulation Analysis

The computer code TOUGH was acquired to assist in the evaluation of the separate effects experiments, in particular, the nonisothermal, two-phase flow experiments to be completed as part of this task. During this fiscal quarter, the version of TOUGH modified by NRC-RES, called MCTUFF, has been adapted to run on the VAX 8700 at Southwest Research Institute (SwRI). Further modifications will be required prior to using the code for evaluation of the separate effects experiments.

3.3.2 Separate Effects Experimental Apparatus

The two separate effects experiments were performed using a 23.8 x 26.0 x 3.0-in. (60.5 x 66.0 x 7.6-cm) test chamber. The two side walls of the chamber were constructed of 3/4-in. (1.9-cm) thick acrylic. The four ends of the chamber were constructed of anodized aluminum. The completed test chamber was sealed (with the exception of a small vent at the top of a side wall of the chamber to maintain atmospheric pressure) so as to prevent the loss of water or water vapor during the experiments. The small vent is presumed to not affect the balance of mass in light of the relatively short duration of the experiments.

The two opposing ends of the chamber contain manifolds for the purpose of permitting fluid circulation. Fluid circulating at a specified temperature through the manifolds maintains the end plates at the temperature of the circulating fluid. Although these two experiments were conducted under approximately isothermal conditions, the inclusion of the manifolds will permit future experiments to be conducted under controlled, nonisothermal conditions.

The interior of the chamber was filled with uniformly sized glass beads. Water was added at specific times during each experiment so that measurements could be made at different levels of water saturation. Test No. 1 was conducted using No. 812 sieve-size glass beads, and test No. 2 was conducted using No. 2740 sieve-size glass beads. The No. 812 beads were factory-sieved between 125 and 177 microns, and the No. 2740 beads were factory-sieved between 28 and 53 microns.

Moisture characteristic curves were measured for the media used in experiments test Nos. 1 and 2. The relationship between suction pressure and moisture content for the two media was determined using the technique specified in ASTM D 2325. A positive-pressure, porous-plate apparatus was used to incrementally increase pressure on the coarse- or medium-textured medium and measure the amount of water retained in the pores of the medium at those pressures. The resulting moisture characteristic curves for these media are illustrated in Figure 3-3.

The porosity of the bead media was calculated by subtracting a known volume of dry beads from the same volume of fully saturated beads. This calculated porosity (37 percent) was used in the analysis of the first two separate effects experiments.

A series of five tensiometers and seven thermistors was installed into the side of the test chamber for the purpose of monitoring the suction pressure and the temperature, respectively, during the experiment. The configuration of the sensor array is illustrated in Figure 3-4.

The tensiometers are constructed of 3/8-in. (0.95-cm) ceramic porous cups connected using 3/8-in. (0.95-cm) outside diameter (OD) PVC tubing to 0-5 psig (vacuum) pressure sensors (Figure 3-5). The 140PC series pressure sensors are equipped with an amplifier and were manufactured by Micro Switch. The ceramic porous cups are one-bar, high-flow cups and are manufactured by Soil Moisture Equipment Corporation. The ceramic porous cups are documented

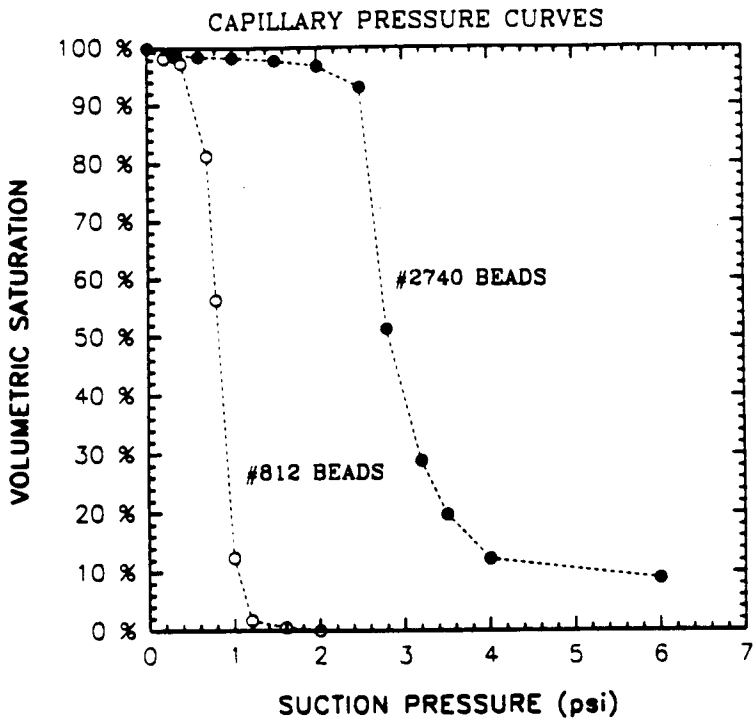

Figure 3-3. Moisture characteristic curves

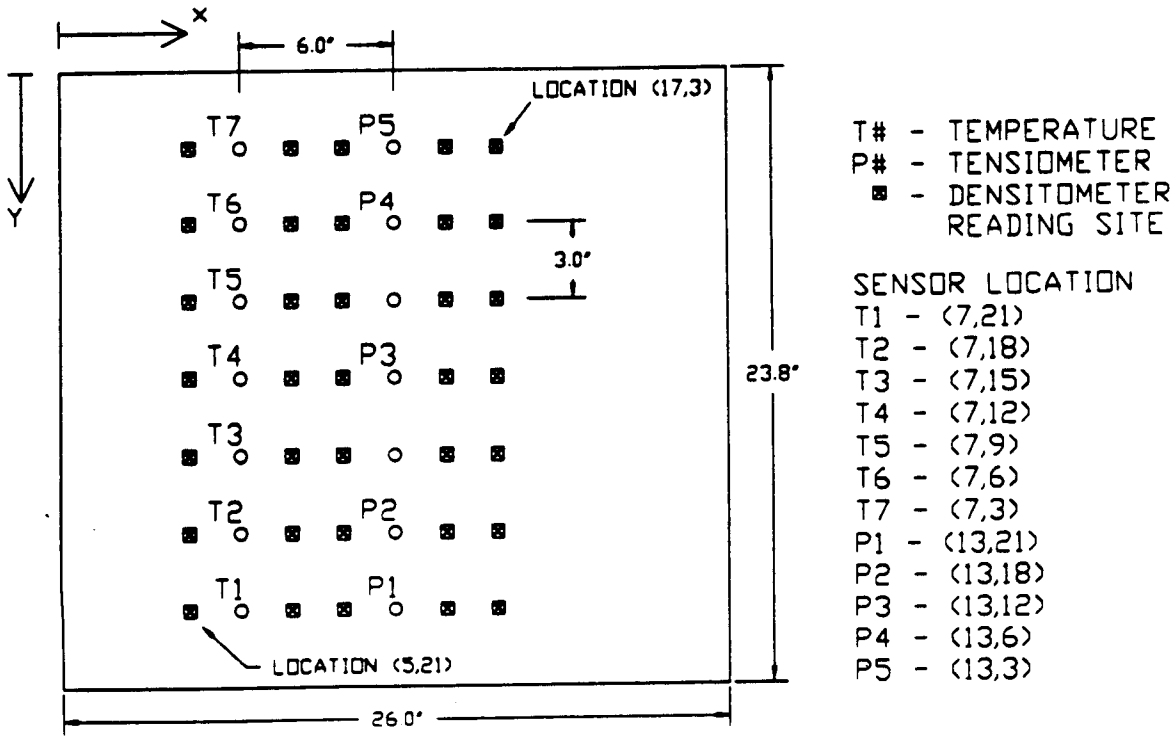

Figure 3-4. Configuration of experiment sensors

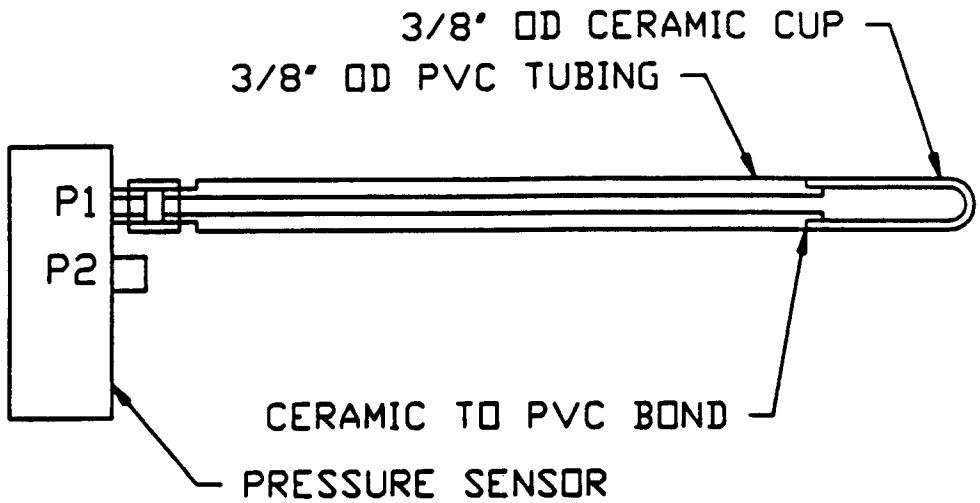

Figure 3-5. Schematic of the tensiometer

to have a pore size of 2.5 microns and a saturated hydraulic conductivity of 8.6 E-6 cm/s. The thermistors are of the 46000 series manufactured by Yellow Spring Instruments and are specified to be accurate to within 0.51°C over the range of interest (0-100°C).

A Texas Nuclear gamma-ray densitometer Model 9700D was used to measure the moisture content of the test chamber at preselected locations. The gamma-ray source is 500 millicuries of cesium-137. The densitometer was initially assembled for measurement of fluid flow in pipelines. It was modified for use in this experiment by constricting the detector aperture with lead such that the resultant detection aperture was approximately 1.9 sq. in. (12.3 sq. cm). A total of 1.5 in. (3.8 cm) of lead was attached to the front face of the detector to mask out the gamma-rays that were more broadly emitted toward the detector than the desirable solid angle of 1.9 sq. in. (12.3 sq. cm). If it is assumed that a 0.25-in. (0.64-cm) thick slab of lead will absorb 50 percent of the gamma-ray particles passing into the lead, then the 1.5-in. (3.8-cm) thick slab absorbed approximately 98 percent of the gamma-ray particles impinging upon the detector face.

The gamma-ray densitometer was attached to a planar tracking table for scanning of the entire test chamber, thus leaving the test chamber stationary during the experiment. The densitometer began and terminated each scanning sequence by recording the number of gamma-ray counts that penetrated through an aluminum mass at the edge of the chamber. The detection counts recorded prior to and subsequent to each scanning sequence were compared to detect instrument drift that may have occurred during the course of the scanning sequence.

The data produced by the experiment were collected using a data acquisition system (DAS). Additional operational tasks were also conducted by the DAS. The tasks performed by the DAS included automatic data sampling; conversion of raw data to engineering units; control of the densitometer traversing system; and data logging, display, and plotting. The operation of the DAS was controlled by an IBM PS 2/80. Also included in the DAS were a multiplexer (HP3458A), multimeter (HP3488A), and the traversing system controller (VELMEX 28351).

3.3.3 Separate Effects Experiment Test No. 1

Test No. 1 was performed over an 11-day period to observe water movement through the No. 812 sieve-size glass beads at isothermal conditions. The test sequence is illustrated in Figure 3-6 and is summarized as follows:

- The densitometer scanned the glass beads within the test chamber prior to the introduction of water into the chamber. The purpose of this measurement was to record the attenuation of the gamma-ray beam by the test chamber and the glass beads without the influence of water and to provide a baseline for subsequent measurements.

- A total of 3875 ml of deionized water was injected during the initial injection through the port of tensiometer No. 3 located in the middle of the test chamber. The 3875 ml of water filled 37 percent of the void space of the medium in the test chamber.

- The temperature, suction pressure, and moisture content of the test chamber were monitored for a total of eight days.

- Additional deionized water (7600 ml) was added to the test chamber during the second injection to bring the level of saturation to 100 percent. The gamma-ray attenuation of the saturated chamber was measured to determine the level of attenuation attributed to combined effect of the test chamber, glass beads, and saturated pore space.

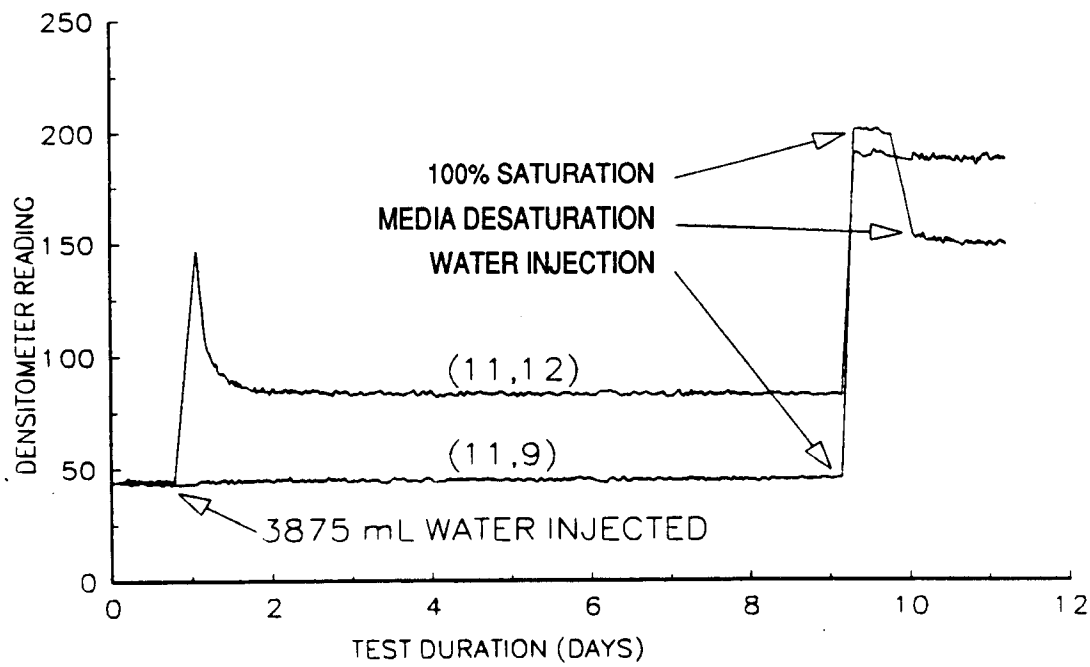

Figure 3-6. Test 1 sequence of events as measured at densitometer locations (11,9) and (11,12)

- A vacuum pump was connected to tensiometer ports 1 and 2 and operated at a negative pressure of about 10 psig during day ten to partially desaturate void spaces within the glass beads. A total of 3065 ml of water was removed in this fashion. The resulting moisture content distribution within the test chamber was measured at selected locations using the densitometer.

The ambient temperature and barometric pressure recorded during the experiment are presented in Figure 3-7. The temperature recorded at the seven sensors within the test chamber are illustrated in Figure 3-8. The suction pressures measured relative to the barometric pressure using the five tensiometers during the experiment are illustrated in Figure 3-9. The densitometer readings for test No. 1 at selected locations are illustrated in Figure 3-10. The densitometer measurements are expressed in terms of relative counts.

3.3.4 Separate Effects Experiment Test No. 2

Test No. 2 was performed over a 13-day period to observe water movement through the No. 2740 sieve-size glass beads. The test sequence is illustrated in Figure 3-11 and is summarized as follows:

- The densitometer scanned the glass beads within the test chamber prior to the introduction of water into the chamber. The purpose of this measurement was to record the attenuation of the gamma-ray beam by the test chamber and the glass beads without the influence of water.

- A total of 1100 ml of deionized water was injected during the initial injection through a port located between tensiometer ports 3 and 4 on the back side of the test chamber. The 1100 ml of water filled 11 percent of the void space of the medium in the test chamber.

- The temperature, suction pressure, and moisture content of the test chamber were monitored for a total of three days.

- A total of 5870 ml of water was added to the test chamber during the second injection to increase the level of saturation to 68 percent.

- The temperature, suction pressure and moisture content of the test chamber were monitored for a total of five and one half days.

- Additional deionized water was added to the test chamber during the third injection to bring the level of saturation to 100 percent. The gamma-ray attenuation of the saturated chamber was measured to determine the level of attenuation attributed to combined effect of the test chamber, glass beads, and saturated pore spaces.

- The temperature, suction pressure, and moisture content of the test chamber were monitored for one additional day.

- A vacuum pump was connected to tensiometer ports 1 and 2 and operated to partially desaturate void spaces within the medium during the removal portion of the test sequence. A total of 220 ml of water was removed under a vacuum of 3 psig. The resulting moisture content distribution of the test chamber was measured using the densitometer.

- The temperature, suction pressure, and moisture content of the test chamber were monitored for one-half day.

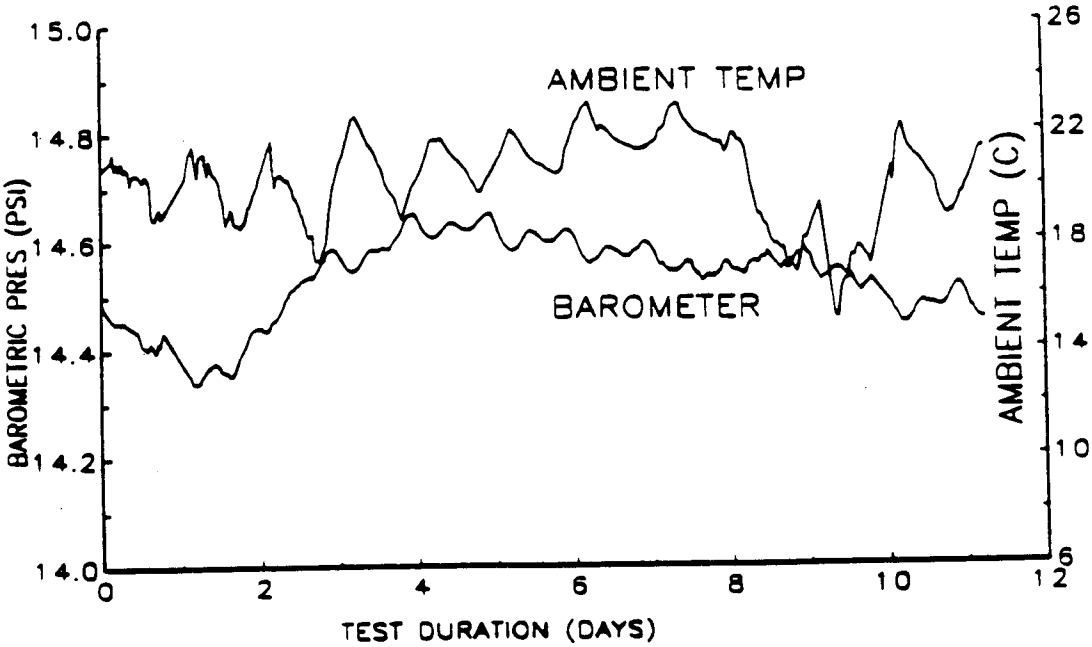

Figure 3-7. Ambient temperature and barometric pressure during test no. 1

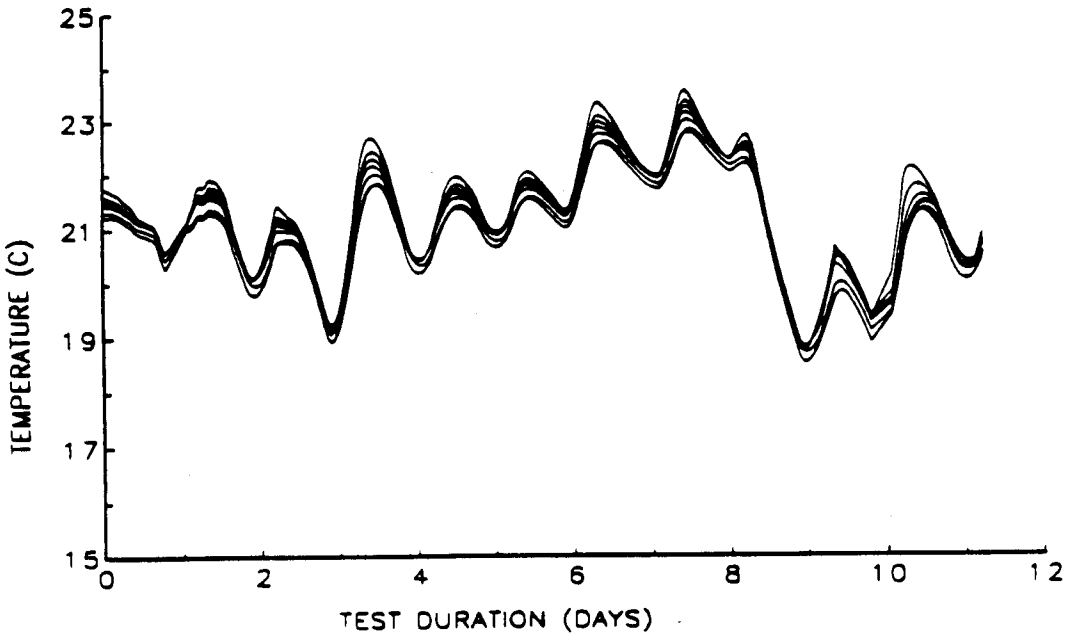

Figure 3-8. Temperature measured in the test chamber during test no. 1. Because the measured temperatures were similar, the individual sensor measurements are not identified.

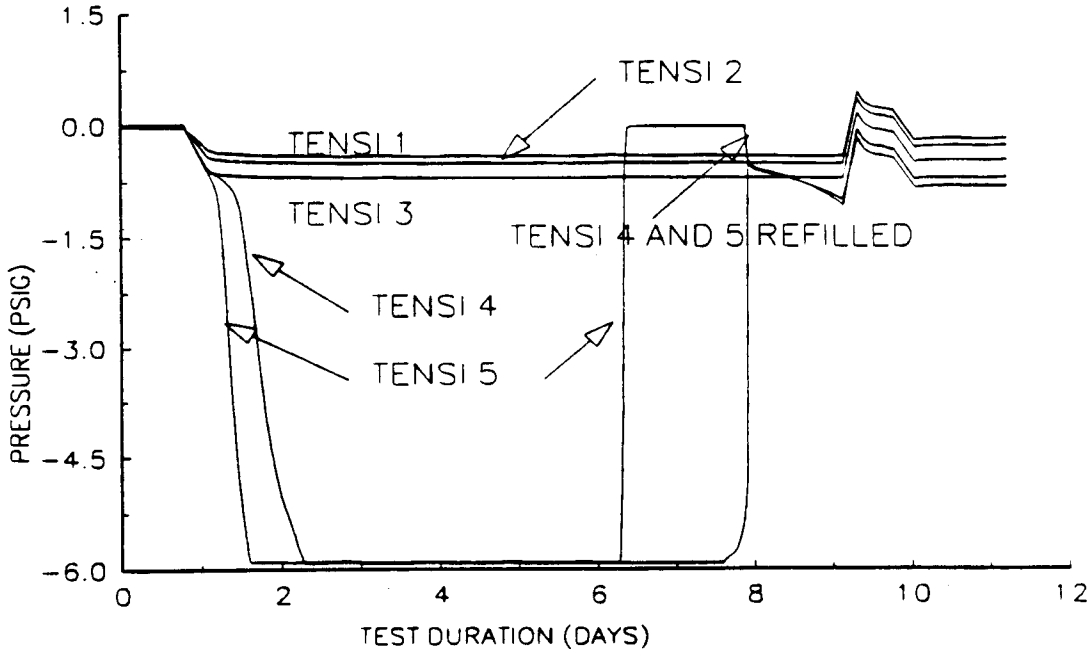

Figure 3-9. Tensiometer measurements during test no. 1. Pressure is measured relative to barametric pressure.

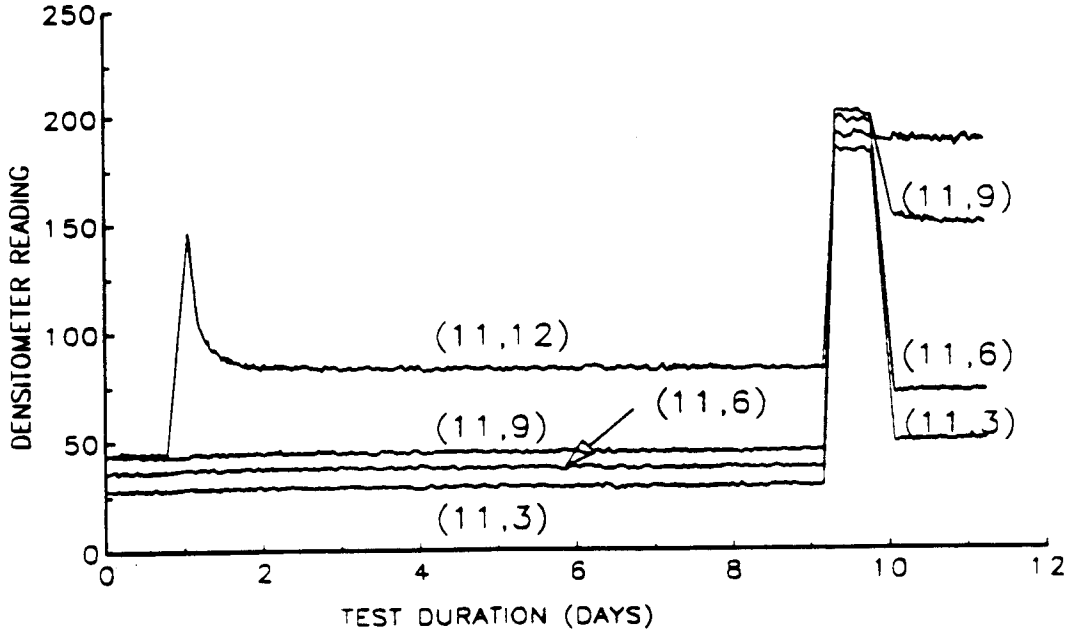

Figure 3-10. Densitometer measurements at locations (11,3), (11,6), (11,9) and (11,12) during test no. 1

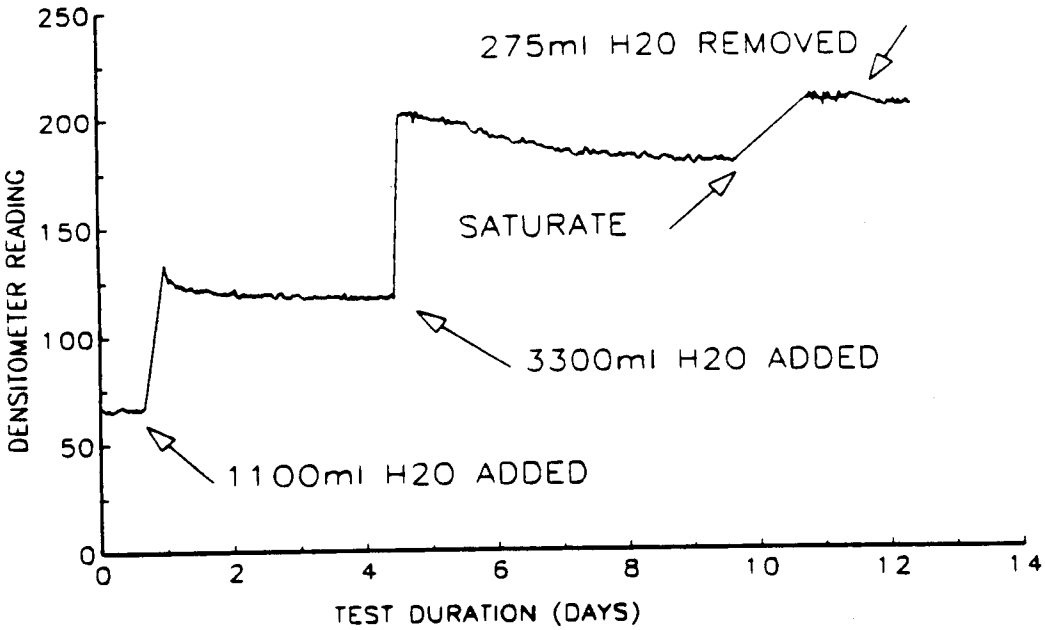

Figure 3-11. Test no. 2 sequence of events as measured at densitometer location (9,9)

The ambient temperature and barometric pressure recorded during the experiment are presented in Figure 3-12. The temperature recorded within the test chamber are illustrated in Figure 3-13. The suction pressures measured relative to barometric pressure using the tensiometers during the experiment are illustrated in Figure 3-14. The densitometer readings for test No. 2 at selected locations are illustrated in Figure 3-15. The densitometer measurements are expressed in terms of relative counts.

3.3.5 Separate Effects Experiments Results

The results of separate effects experiments test Nos. 1 and 2 are presented in this section.

3.3.5.1 Results of Test No. 1

For the preliminary tests, the experiment was assembled in a laboratory that does not have a controlled environment. Consequently fluctuations in the ambient temperature and barometric pressure occurred through out the test. Temperature fluctuation of 7 degrees Celsius and barometric pressure fluctuation of about 0.3 psig were recorded. The fluctuations in the ambient temperature were directly reflected in the temperatures recorded in the test chamber, although the temperatures recorded in the chamber demonstrated slightly smaller fluctuations (approximately 5 degrees Celsius).

During the initial water injection event, the injected water spread in a circular pattern away from the point of injection until it reached a diameter of about 6 inches. The water then flowed downward until it reached the bottom of the test chamber where it spread laterally toward the edges of the test chamber. The water in the initial 6-inch diameter region visually appeared to become redistributed slightly over the next few days by migrating toward the bottom of the test chamber. The upper free surfaces of the injected water for the two observations are illustrated on Figure 3-16. These observations correlated positively with the measurements recorded with the densitometer.

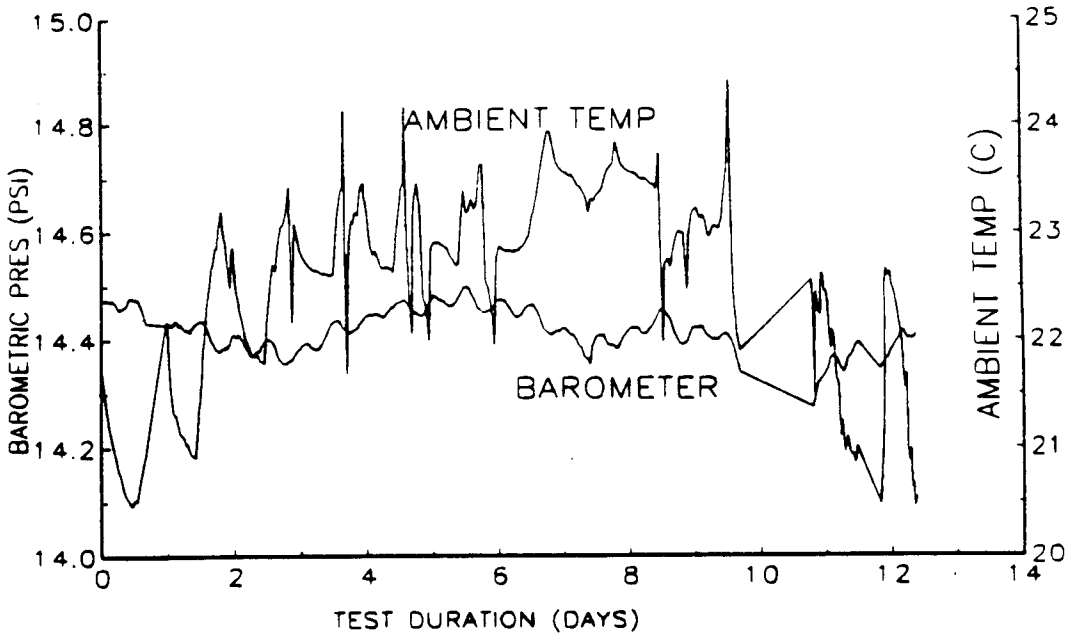

Figure 3-12. Ambient temperature and barometric pressure during test no. 2

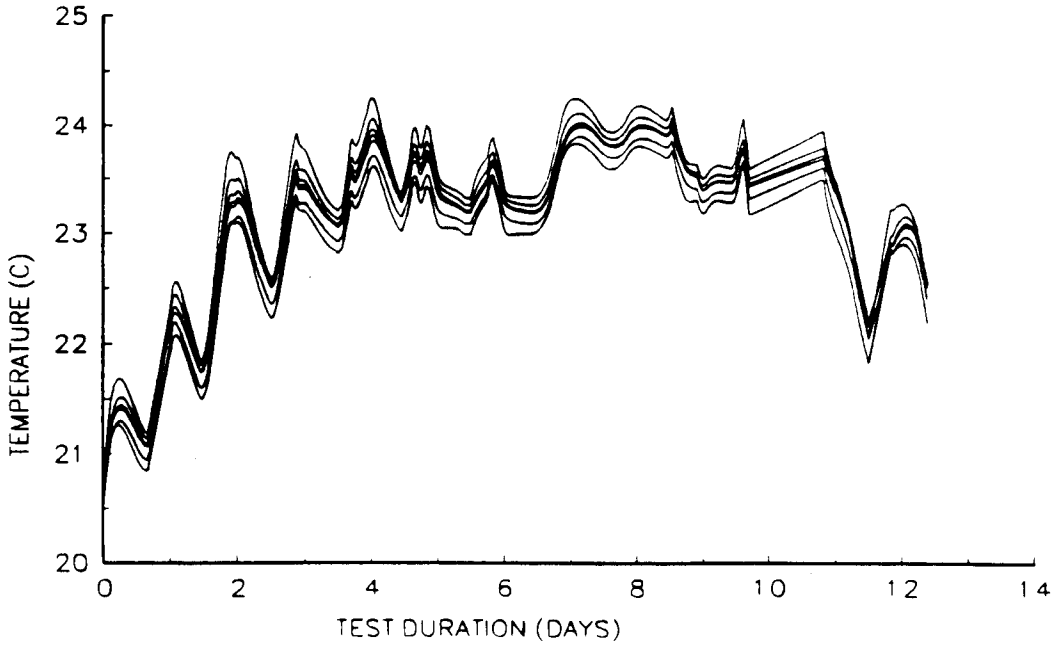

Figure 3-13. Temperature measured in the test chamber during test no. 2. Because the measured temperatures were similar, the individual sensor measurements are not identified.

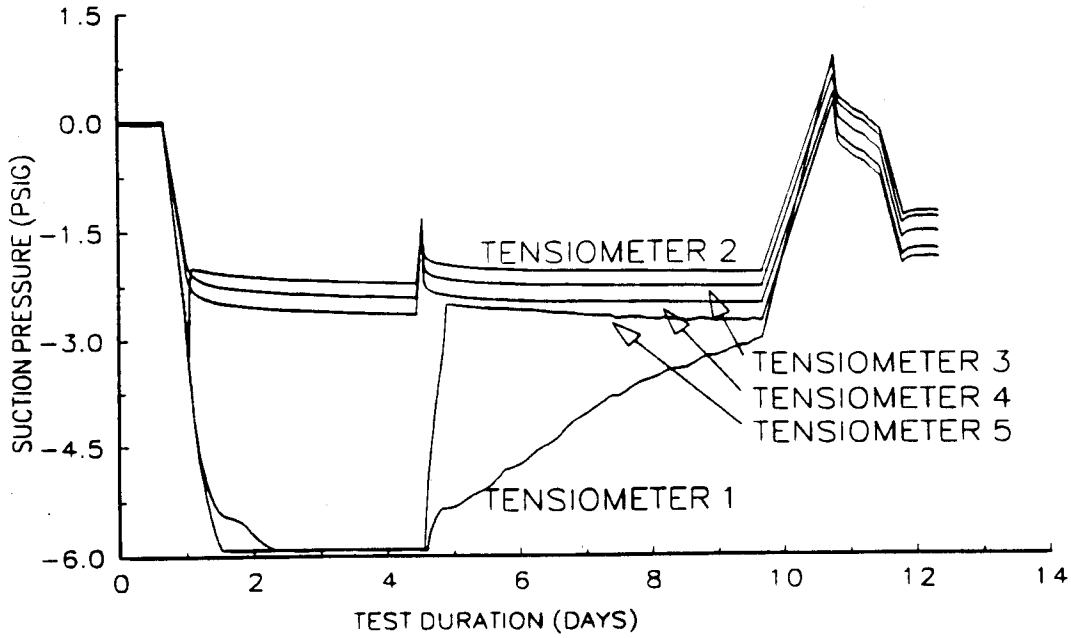

Figure 3-14. Tensiometer measurements during test no. 2. Pressure is measured relative to barometric pressure.

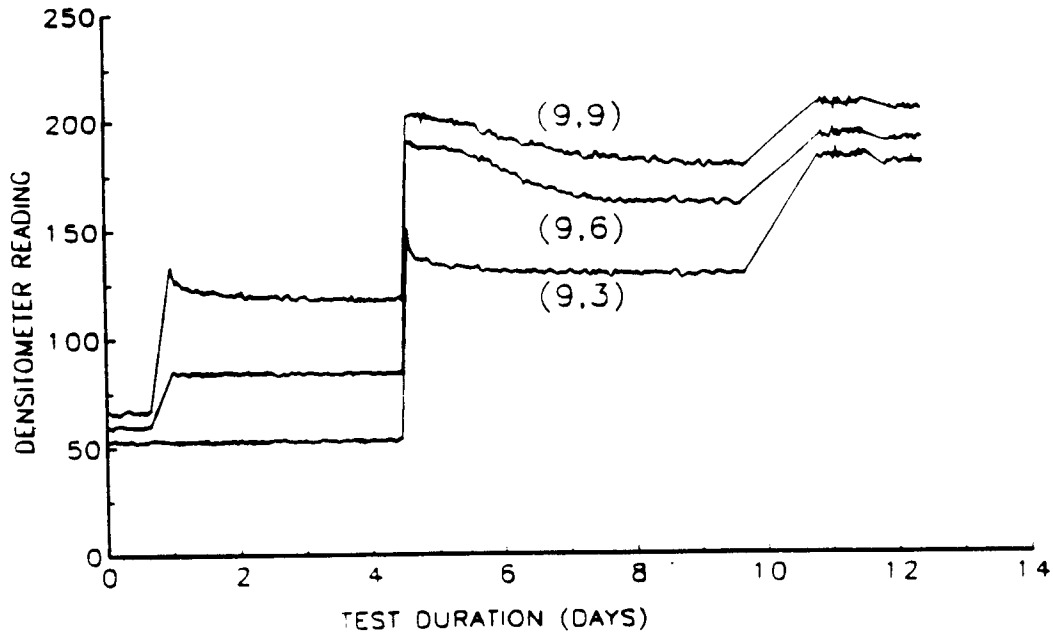

Figure 3-15. Desitometer measurements at locations (9,3), (9,6) and (9,9) during test no. 2

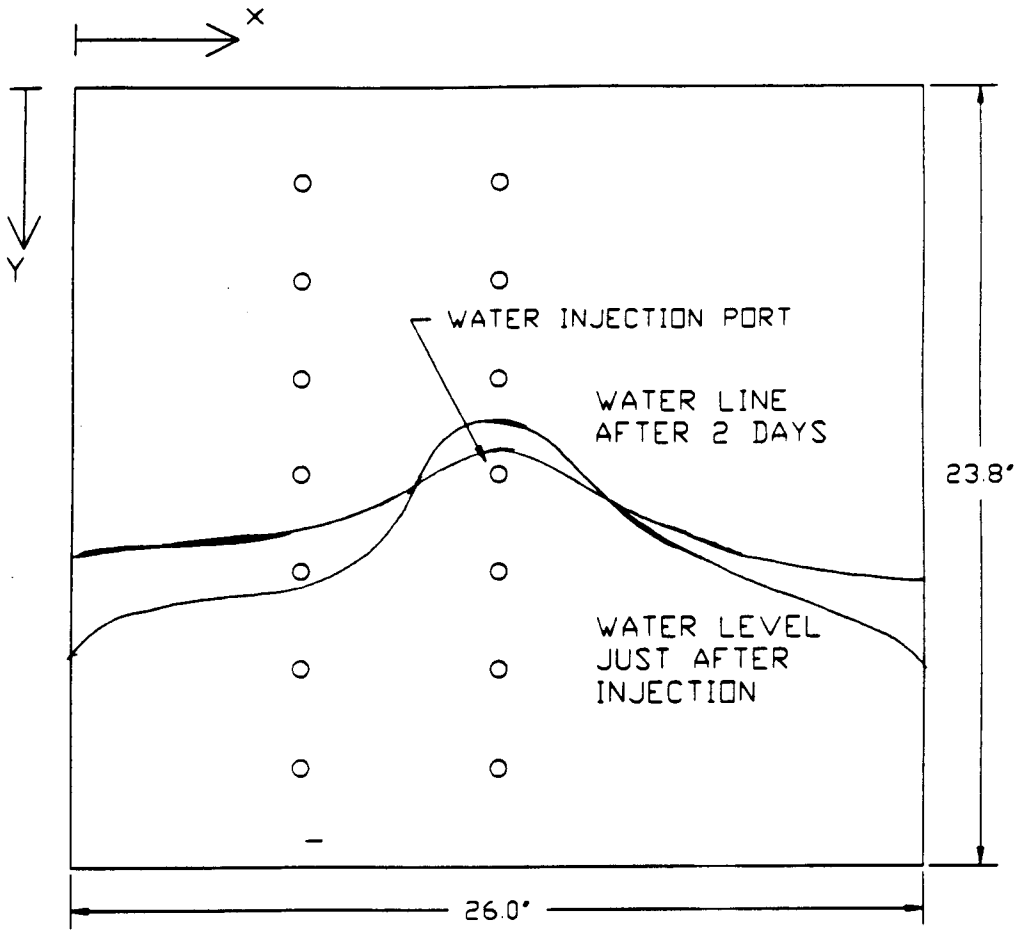

Figure 3-16. Free surface of infiltrated water during test no. 1

During desaturation at day ten in the test, the free surface of the water was observed to drop as the water was removed. Measurements made with the densitometer indicated that in regions above the observed free surface, the pore space in the medium was unsaturated (with a relatively low level of moisture content) and the pores below the free surface were close to full saturation.

Tensiometers 4 and 5 dried out during the eighth day of the test and had to be refilled with water. Tensiometers 1, 2, and 3 were located in the saturated portion of the media and recorded suction pressures of about -0.5 psig. Tensiometers 4 and 5 were initially in the dry region, and suction pressures of -5.0 psig were recorded at both locations. Full scale for the sensors is -5.0 psig; therefore, negative pressures less than -5.0 psig may have been present but were not detected by these sensors.

The tensiometer readings reflected the vertical difference in their positions with an approximate 0.1 psig difference for each 3-in. change in elevation. Measurements from tensiometers 4 and 5 did not indicate that the pores in the upper portion of the test chamber became desaturated during the removal of water in day ten of the experiment.

3.3.5.2 *Results of Test No. 2*

The ambient temperature fluctuated about 4 degrees C during test No. 2. Temperatures recorded in the medium had fluctuations that were slightly less, or about 3 degrees.

The initial injection of water was not readily accepted by the medium even though there was a positive head of 3 feet of water in the infiltration water column. This slow acceptance of water was attributed to the high air-entry pressure of the medium. The initial water injection uniformly infiltrated the medium in a radial pattern relative to the point of injection.

The second injection of water was more readily accepted by the medium. A downward component in water movement became apparent as the moisture content of the medium was increased. A slight settling of the medium was noticed during the second injection. This settling was manifested by a vertically oriented, fault-like offset approximately 4 inches from the side of the chamber. The offset occurred in a region that had not yet been wetted by the infiltrating water. The offset acted as a barrier to water flow. Water did not infiltrate into media on the dry side of the offset until the water had advanced to the lower plate, moved laterally past the offset, and then moved upward into the dry portion.

When water was initially injected into the medium, the tensiometers were filled with water. The tensiometers that were located in the dry portions of the test chamber (tensiometers 4 and 5) remained at -5.0 psig (the full-scale negative output of the sensor) until the upper portion of the chamber became saturated, at which time the pressure increased to -2.0 psig. The response of tensiometer 1 (Figure 3-14) illustrated that the bottom area was initially dry (suction pressure was -5.0 psig) but gradually increased to -3.0 psig as water infiltrated into this region. Tensiometers 2, 3 and 4 were initially located in a wet region with suction pressures of about -2.0 psig. After the medium was fully saturated on day ten, the suction pressure decreased at these three locations to a point that even positive pressures were recorded for a brief period. A slow leak in a thermistor connection allowed some water to escape, with the result that pressure in the chamber decreased over the course of the day.

3.4 SUMMARY OF RESULTS

Insights gained from the research project at this intermediate point can be summarized in two categories: (1) insights that could help direct future efforts in the technical area of thermohydrology and (2) recommendations for modifications in experimental procedures. In the former category, the TOUGH code is being modified to facilitate its application to usage in this project. The matrix solver in the code may be replaced with a more efficient one. This would permit the calculation of problems with greater nonlinearity in the soil moisture characteristics, with larger grid sizes, or for longer durations of simulated experimentation.

Results and experience gained from the experiments performed to date have led to modifications in laboratory procedures and in the experimental apparatus. The media used in the first two experiments were uniformly sized glass beads. The moisture-release characteristics for each of the two bead sizes are graphically illustrated in Figure 3-3. Because the beads are unimodally and uniformly sized, the moisture characteristic curves are relatively steep. The steepness in the curve implies that large changes in moisture content can occur from small changes in suction pressure. A limited transition zone between saturation and desaturation in the moisture-release curve enhances the nonlinearity of the relationships used to describe unsaturated flow. Highly nonlinear media are not desirable for use in the experiments for two reasons: (1) media more representative of porous rock would tend to be less nonlinear than the uniformly sized beads (e.g., media with less steep soil-moisture curves) and (2) analytical methods are more applicable to less nonlinear representations.

A bead-size mixture will be used in future experiments to alleviate the limited moisture-release transition zone. A medium composed of a mixture of bead sizes will have a broader distribution of pore sizes and a less steep moisture-release curve.

The test chamber used in the first two experiments measured 23.8 x 26.0 x 3.0 inch. A chamber of this relatively large size was selected for the separate effects experiments for several reasons. First, since the area of resolution of the densitometer was 1.9 sq. in., the size of the chamber had to be sufficiently large to accommodate a detector of this resolution size. Second, it was presumed that greater flow detail could be visualized with a larger test chamber. Finally, either more or larger features (such as fractures) could be incorporated into a larger test chamber.

Several problems resulted from using the larger test chamber. One problem is the shifting of the bead material when saturated during test No. 2, which is partially attributed to the large size of the chamber or with problems associated with filling the large chamber with beads. It appears that the bead shifting and the associated offset were caused by either a slight outward bowing of the over-sized side walls or to settling of the beads during saturation.

A second problem associated with the large chamber size is the time required for the experiment to approach either a quasi-steady state or an equilibrium. This problem is exacerbated by the relatively slow response of flow under partially saturated conditions. Related to this problem is the anticipated problem of heat loss through the large side walls during the nonisothermal experiments.

It appears that the advantages of a larger size test chamber in the separate effects experiments are out-weighed by the disadvantages. A densitometer detector with a significantly smaller detection cross-sectional area has been ordered to permit the use of a smaller test chamber. Prior to receipt of the new detector, the larger test chamber will be adapted for additional experiments. A bolt will be installed midpoint between the two side walls to prohibit the walls from bowing outward as the beads are saturated. Additionally, the side walls will be insulated to diminish the effects of the ambient fluctuations in temperature and the diminish the rate of heat loss through the side walls, which is particularly important during the nonisothermal experiments.

The importance of minor heterogeneities in test media was illustrated with the offset observed during test No. 2. The moderate increase in pore size associated with the offset was large enough to prohibit water flow across the offset until the suction pressure was small enough to permit the larger pores to become saturated. Water then traversed the offset and infiltrated the dry media across the offset.

4. SEISMIC ROCK MECHANICS

by Asadul H. Chowdhury and Simon M. Hsiung

4.1 TECHNICAL OBJECTIVES

Six specific objectives have been identified for the Seismic Rock Mechanics Research Project. These are:

(1) To develop a good understanding of the information currently available of seismic effects on underground structures.

(2) To assess, by conceptual models and experimental studies, the capabilities and limitations of rock-joint models and computer codes currently in use.

(3) To demonstrate by laboratory model studies and instrumented field studies the degree of accuracy (validation) for the rock-joint models and computer codes used for seismic analysis in a tuff medium.

(4) To assess by instrumented field studies the significance of seismic pumping and to demonstrate the degree of validation for the rock-joint models and computer codes for simulation of seismic effects on groundwater hydrology.

(5) To identify and assess the key seismic-related parameters that are applicable to the Yucca Mountain site.

(6) To generate technical data for preparing licensing-related positions as they relate to the effect of seismic action on the underground repository in a tuff medium.

The objectives are to be addressed in the following eight tasks.

(1) Task 1 - Focused Literature Search

(2) Task 2 - Laboratory Characterization of Jointed Rock

(3) Task 3 - Assessment of Analytical Models/Computer Codes

(4) Task 4 - Rock Dynamics Laboratory and Field Studies and Code Validation

(5) Task 5 - Groundwater Hydrology Field Studies and Code Validation

(6) Task 6 - Yucca Mountain Scoping Analysis

(7) Task 7 - Technical Report

(8) Task 8 - Quarterly Research Report

The second, third, and fourth objectives are currently being worked on. Results to date are reported in this quarterly report.

4.2 EVALUATION OF ROCK-JOINT MODELS AND COMPUTER CODES

The evaluation of rock-joint models and associated computer codes consists of two studies: qualification (Task 3) and validation (Tasks 4 and 5). At the present, the qualification studies are

in progress, and they will be reported in this section. The objective of Task 3 is to identify and qualify (against benchmark problems and laboratory test results) analytical models (rock-joint) and associated computer codes which may be useful in explaining and understanding the behavior of excavations in brittle, jointed, partially saturated rock when the host formations are subjected to displacements, velocities, and accelerations imparted by earthquake or groundshock motions.

Several codes that may be applicable were identified as current candidates for assessment. These include the distinct element codes UDEC and 3DEC (Cundall, 1988), the discrete element code DECICE (Williams et al., 1985), the finite-element codes HONDO II and SPECTROM-331 (Key, 1986), and the boundary element code BEST3D (Banerjee et al., 1985). These codes may model the dynamic performance of jointed rock masses. The particular feature of each code which qualifies it for consideration in the qualification studies is the formulation of an interface element on which rigid-body slip or separation can occur under static or dynamic loading. Whether the interface meets the requirements for satisfactory simulation of discontinuous deformation of jointed rock is the concern of these studies.

Two types of qualification studies are being performed. The first is to confirm that a code can reproduce the response of four well-established conceptual models (benchmark analytical problems) of the performance of a jointed rock mass. Codes with acceptable performance will be candidates for the second type of qualification studies on single rock-joint performance. Each candidate code will be used in the second type of study to analyze the dynamic response of a well-designed and executed laboratory experiment on a single rock joint. Assessment will be made of the ability of the rock-joint models to handle accumulation of permanent shear displacement induced by groundshocks and earthquakes.

Currently, qualification studies on the HONDO II and UDEC codes against the four benchmark analytical problems have been completed, and reports were prepared by Brady et al. (1990) and Brandshaug et al. (1990). A brief discussion on these two reports is presented in this quarterly report; for detail technical results and discussions, readers should refer to those two documents.

Figure 4-1 shows the four benchmark problems, which represent discontinuous rock masses considered in the current study. The first two problems are static, and the other two are dynamic. The Mohr-Coulomb joint model was used in the analysis of all four benchmark problems.

4.2.1 Cyclic Loading of a Specimen With a Slipping Joint

An elastic block with an inclined internal closed joint is shown in Figure 4-1a(i). When a constant axial displacement u_a is applied to one end of the block and the other end is fixed, the resulting load causes inelastic slip on the joint. If the sense of displacement on the end of the block is reversed, the original unloaded condition may be re-established; the load-displacement paths for loading and unloading, however, are quite different. As shown by Olsson (1982), the stress-displacement relation for the loaded specimen illustrated in Fig. 1a(ii) consists of three components. The subtle hysteresis response in a load-unload cycle is a result of joint slip and frictional locking at various stages of block deformation. A closed-form solution for the determination of the three slopes in Figure 4-1a(ii) were provided by Brady et al. (1985).

The results for the UDEC analysis with the standard Mohr-Coulomb rock joint for the stiffnesses (slopes) in loading and unloading were virtually identical with the independent closed-form solution. The HONDO II analysis of a jointed block did not, however, reproduce the expected hysteric response. This suggested the joint formulation in HONDO II is not sufficiently rigorous to express the mechanics of joint deformation in terms of a Mohr-Coulomb joint. The source of the problem for inability to reproduce the expected response was not identified.

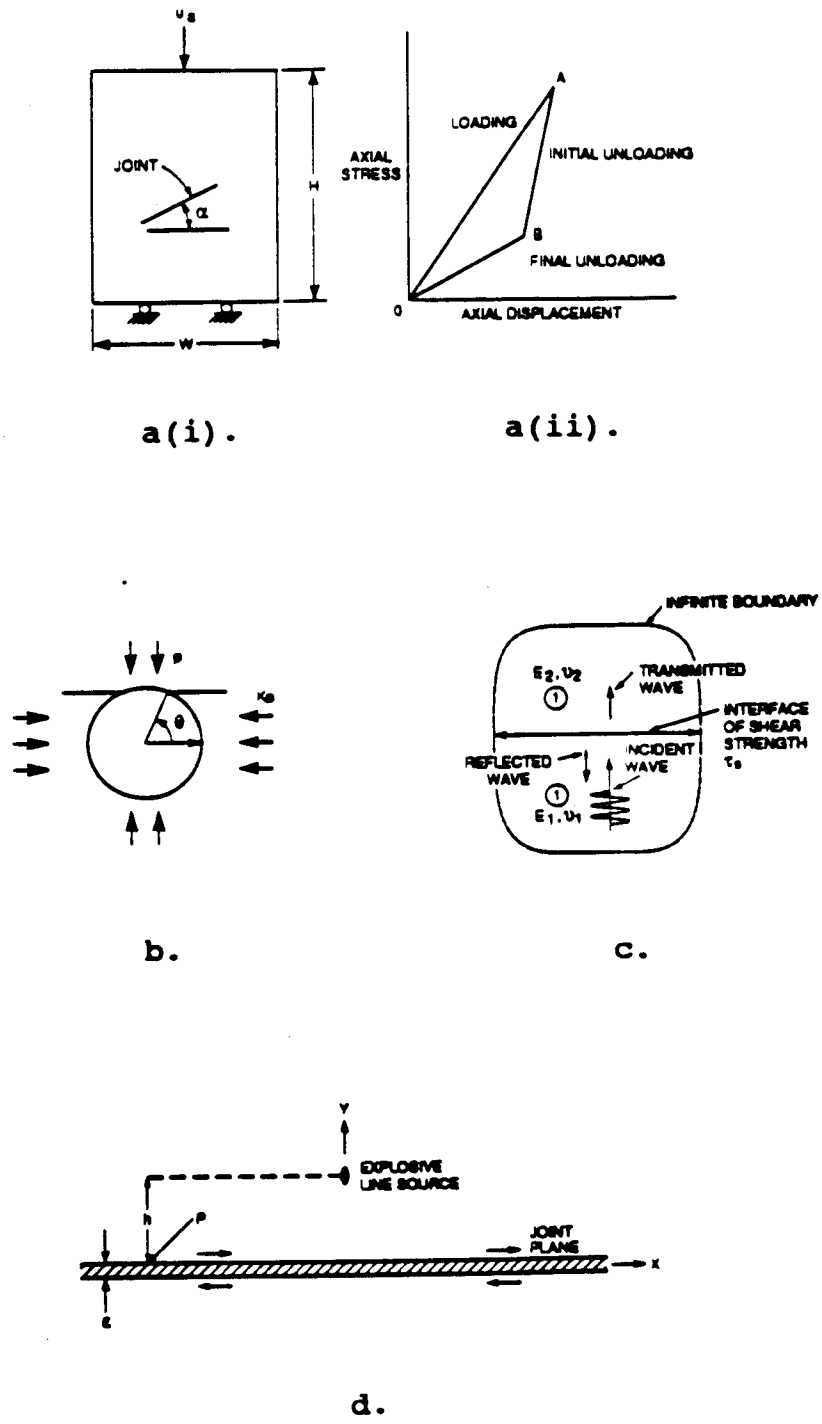

Figure 4-1. Four benchmark analytical problems: (a) Cyclic loading of a specimen with a slipping joint, (b) joint intersecting a circular excavation, (c) slip in a jointed body induced by a harmonic shear wave, and (d) line source in an elastic medium with a slip-prone joint.

4.2.2 Circular Excavation Intersected by a Joint

The circular excavation intersected by a joint presents a problem of joint slip in the zone of a relatively high stress gradient generated near a circular excavation, as illustrated in Figure 4-1b. Consideration of the state of stress on the plane of weakness shows that, at its intersection with the excavation, slip occurs when the angular coordinate of the joint intersection is greater than the angle of friction of the joint (Brady and Brown, 1985). Once slip occurs, static equilibrium can only be achieved when the tangential stress is zero at the boundary-joint intersection. This implies that substantial redistribution of stress may occur.

The results of the UDEC analysis indicated that, despite the very high boundary stress gradient near the intersection of the plane of weakness and the excavation, the stress magnitude calculated with UDEC converges on the results predicted analytically. Compared with the elastic solution, the boundary stress is reduced notably in the crown of the excavation and increased in the floor. These results are consistent with the formal analysis. The evaluation of HONDO II code was not performed against this benchmark problem, since it did not satisfy the previous simpler static benchmark problem.

4.2.3 Slip in a Jointed Body Induced by a Harmonic Shear Wave

The dynamic behavior of a plane discontinuity loaded by a normally incident, plane harmonic shear wave presents a simple test of the dynamic performance of UDEC. The problem shown in Figure 4-1c consists of a normally incident plane harmonic shear wave and a plane discontinuity with limited shear strength separating two homogeneous, isotropic, semi-infinite elastic bodies. If the transient shear stress exceeds the shear strength of the joint, slip will occur at the interface. As a result, energy is partitioned between reflected and transmitted waves and absorption at the interface. In an analysis of this problem by Miller (1978), closed-form solutions were derived for the transmission, reflection, and absorption coefficients.

Comparison of the acoustic coefficients for the wave propagation is conducted in terms of the dimensionless stress. Good correspondence is observed between the UDEC results and closed-form solutions over a wide range of dimensionless stresses. The UDEC analysis also confirmed that when the joint has a limited shear strength or cohesion, the shear wave transmitted across the interface has the peak amplitude of shear stress. The way in which boundary tractions can be specified in the HONDO II code prevented the comparison of acoustic coefficients at the interface for the HONDO II and closed-form solutions. The particular problem with HONDO II is that it is not possible to apply a static normal traction on one boundary and an independent, time-varying traction, either normal or shear, to another. This prevented application of a static normal stress to the joint, which is required to mobilize the joint shear strength and thus support wave propagation across it. The joint interface model incorporated in the HONDO II code does not include the component for cohesion. Examining the nature of the motion associated with shear-wave interaction with a joint of zero shear strength, the joint reflected the wave almost completely.

4.2.4 Line Source in an Elastic Medium with a Slip-Prone Joint

The problem shown in Figure 4-1d consists of a plane joint of infinite lateral extent in an elastic medium and a dynamic load at some distance from the discontinuity. The closed-form solution to this problem was derived by Day (1985) as a special symmetric condition for the general problem of slip of an interface due to a dynamic point source (Salvado and Minster, 1980). The problem was solved in terms of the magnitude of slip induced on the joint by the explosive-induced local load.

The result of the UDEC analysis provided satisfactory correspondence with the closed-form solution, confirming that the distinct element scheme and the Mohr-Coulomb rock-joint model provided a coherent basis for dynamic analysis of jointed rock. This exercise and that involving harmonic loading of a jointed medium as illustrated in Section 4.2.3 also confirmed the satisfactory performance of the viscous (nonreflecting) boundaries for the UDEC problem domain.

The qualification study on HONDO II against the problem was not performed, since HONDO II did not satisfactorily reproduce the response of the previous simpler problem involving harmonic loading of a jointed medium.

4.2.5 Summary of Results

Performance of UDEC on the suite of benchmark problems indicates that the code is a valid simulation of jointed rock, to the extent that the mechanics of these media may be represented by the conceptual models expressed in the various problems. However, whether UDEC is a valid simulation of the engineering behavior of jointed rock requires laboratory studies to verify the Continuously-Yielding and Barton-Bandis joint formulations, and field studies to evaluate the behavior in a proper engineering setting.

In its current formulation, HONDO II is not capable of simulating the mechanics of jointed rock in a way suitable for repository design and performance assessment. Some of its deficiencies in this respect are related to the application of static and dynamic boundary loads in the analysis.

4.3 LABORATORY INVESTIGATION OF ROCK-JOINT BEHAVIOR

4.3.1 Development of Laboratory Test Apparatus

Task 2 of the Seismic Rock Mechanics Project includes various activities whose objective is the laboratory characterization of the static and dynamic behavior of jointed rock specimens. Task 2 has two major pre-program activities: one is the design, development, installation, and operation of a rock-joint dynamic shear test apparatus; and the other is sample collection and preparation. The latter is discussed in the following subsection. The apparatus will be used to measure responses that will quantify the properties of rock joints when subject to various prescribed static and dynamic conditions. Both full-scale specimens extracted from field site and later scale-model specimens are to be accommodated by the apparatus. The development of the rock-joint dynamic shear test apparatus has been reported by Kana et al. (1990).

Figure 4-2 shows the assembly of a servocontrolled rock-joint dynamic shear test apparatus, designed, fabricated, and assembled at Southwest Research Institute. The apparatus consists of vertical and horizontal servocontrolled loading actuators, reaction frames, and shear box fixtures. The maximum loading capacity for each of the three vertical actuators is 30,000 lb and 20,000 lb for the horizontal actuator. The horizontal actuator can be operated in either a load or displacement control mode. Several loading patterns such as harmonic load and displacement, groundshock, and earthquake time histories can be generated through the use of a function generator. Each actuator is equipped with a 25,000-lb capacity load cell for monitoring the applied forces. A second horizontal actuator with a maximum loading capacity of 50,000 lb equipped with a 50,000-lb capacity load cell is in the process of being installed to apply higher amplitude static and dynamic loads. The instrumentation for monitoring the applied normal load is arranged to provide an analog output for the sum of the three load cells, as well as for the individual signals.

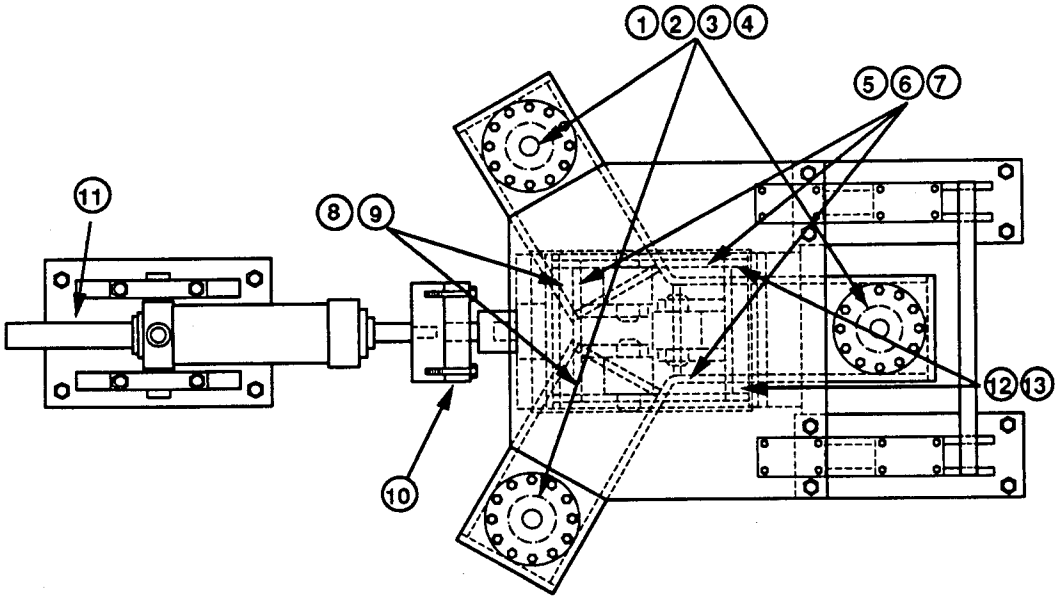

Note: Numbers refer to channels identified in Table 1

TOP VIEW

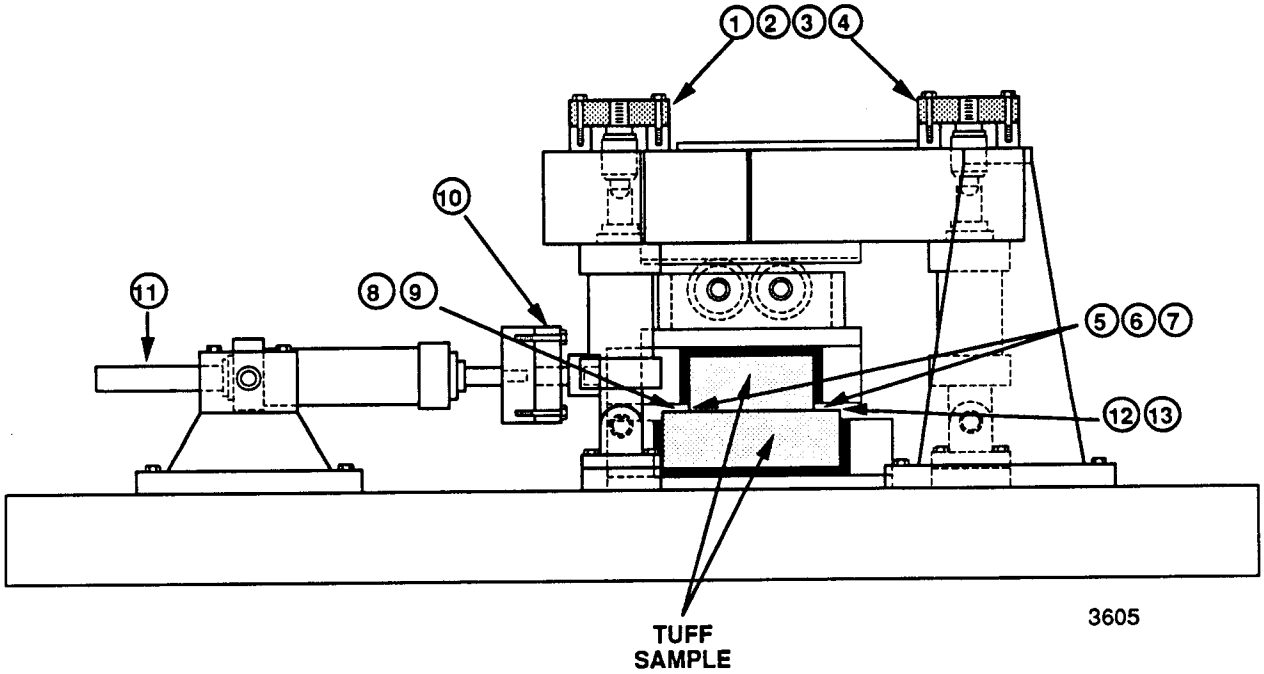

SIDE VIEW

Figure 4-2. Assembly and instrumentation of the dynamic shear apparatus

The bottom shear box was designed to house a specimen with maximum dimensions of 12 x 8 x 4 in. The top shear box houses a specimen with maximum dimensions of 8 x 8 x 4 in. Both are grouted in their respective specimen boxes. A 1-inch gap between the top and bottom box edges of the assembled specimen unit is allowed. The bottom shear box and other fixed devices are bolted to a 4 ft x 7 ft x 6 in. thick steel base plate for rigidity. The horizontal translation of the top shear box along the direction of shearing is guided through three rollers between the top shear box and normal load frame. It is also guided through side rollers not shown in Figure 4-2. Thus, the normal load frame and the side rollers prevent rotation of the vertical actuators (and therefore the top specimen block also) about a vertical axis perpendicular to the direction of shearing.

4.3.1.1 Normal Load System

Normal compression is applied to the specimen by three vertical actuators set at 120-degree angles about the specimen's vertical centerline. These actuators act through individual load cells whose output is summed and used as the control signal. The total normal load is controlled at a preselected static or slowly ramped value. This total resultant load is ultimately applied to the specimen via the normal load frame which acts on the three normal load rollers (see top view of Figure 4-2), and thereby on the top specimen box. The line of action for this normal load is through the null position of the top specimen box. The normal load frame is constrained to three degrees of freedom--vertical translation, rotation about the horizontal axis in line with the shear, and rotation about the horizontal axis transverse to the shear. These constraints are assured by two double flexures which connect the normal load frame to a fixed reaction brace, and by the two side roller assemblies, which act on the top specimen box. Thus, the top specimen block is constrained to these same three degrees of freedom, plus a fourth, which is translation in the direction of shear.

4.3.1.2 Horizontal Load System

The horizontal actuator produces direct shear to the top specimen box via the horizontal load cell, which acts through a spherical coupling. This coupling accommodates slight misalignment in the horizontal shearing motion. It also allows for elevation changes of the top specimen due to vertical load, joint surface roughness, and progressive wear. Control of the horizontal actuator load is based on the horizontal relative shear displacement, described in the next subsection.

4.3.1.3 Instrumentation and Control

Instrumentation channels are identified in Figure 4-2 and Table 4-1. All load cells are typical commercial strain-gauge units with dominant sensitivity to tension and compression along one axis. Reaction to the applied static normal load is measured in terms of vertical displacements of the two blocks at three locations of the interface near the interface. (For detail discussion, see the report by Kana et al., 1990.) The transducers used for measurements are of proximity (noncontacting) eddy-current sensing type, since horizontal movement of the two surfaces must be allowed, but only vertical displacement changes must be sensed.

The horizontal transducers, mounted by bonding onto the top specimen block, provide one measure of top block absolute motion at the near end of the block. All horizontal displacement transducers are Linear Variable Differential Transformers (LVDTs), and any one can be used for horizontal displacement control. One device is located on the horizontal actuator ram. However, to account for potential slack in the linkages and grout, two of the devices are located on the far side of the specimen blocks and are installed so as to measure horizontal displacement of the top block relative to the bottom block. An average of these two represents a measure of the fourth and final degree of freedom of the top block, and can be compared with a preselected input source, which depends on the dynamic motion desired.

TABLE 4-1 INSTRUMENTATION CHANNEL IDENTIFICATION

1	-	Vertical Load Cell No. 1
2	-	Vertical Load Cell No. 2
3	-	Vertical Load Cell No. 3
4	-	Analog Summation of Total Vertical Normal Load
5	-	Vertical Relative Specimen Displacement at Right of Bottom Specimen Block
6	-	Vertical Relative Specimen Displacement at Near Left of Bottom Specimen Block
7	-	Vertical Relative Specimen Displacement at Far Left of Bottom Specimen Block
8	-	Horizontal Acceleration at Near Left of Top Specimen Block
9	-	Horizontal Acceleration at Near Right of Top Specimen Block
10	-	Horizontal Load Cell
11	-	Horizontal Actuator Displacement
12	-	Horizontal Displacement of Top Block Relative to Bottom Block at Far Right Corner
13	-	Horizontal Displacement of Top Block Relative to Bottom Block at Far Left Corner

4.3.1.4 Data Acquisition and Processing

The thirteen channels of data identified in Table 4-1 are sampled and recorded directly on the hard disk of a 640K memory personal computer with a 40-megabyte hard disk and diskette option. The computer also contains a special math coprocessor and high-speed card option. The software allows sampling of data at preselected rates and times required by the various types of dynamic tests described above. Data are ultimately transferred to a diskette for further processing and plotting on other digital computers.

4.3.1.5 Demonstration Tests

A demonstration test series with an artificial specimen (concrete block) was conducted to demonstrate the capability of the apparatus. The general conclusion was that when allowance is made for the artificial composition of the host specimen, the direct shear apparatus returns results consistent with shear tests on natural joints. With the unique capabilities of this machine, the results from the demonstration provided a basis for proceeding to determine the static and dynamic properties of natural joints in tuff. (For a detail illustration and discussion of the demonstration, see the report by Kana et al., 1990.) As a result of the demonstration, the following three conclusions were considered essential to future dynamic tests of natural rock-joint specimens.

(1) The currently used 1-inch range LVDT's will need to be replaced with 2-inch range LVDT's to provide better linearity over a greater range.

(2) The effect of controlling the horizontal displacement at the specimen, rather than at the actuator ram, needs to be evaluated.

(3) The grinding action, which induces higher acceleration-frequency measurements than the required acceleration frequency during joint shear, will have a substantial impact on specifications for some of the dynamic tests required by this project. Preliminary earthquake-type data indicate that matching a filtered acceleration-response spectrum will be required for a valid simulation. Procedures and hardware necessary for performing such tests have been shown to be adequate. The exact details will have to be adjusted somewhat, however, depending on the nature of site data from which a required response spectrum will be generated. In particular, a relationship between filter cut-off frequency and measured distance from a source must be established. Use of this filter process will probably be required on all dynamic tests to be conducted. These details must be resolved by the time the schedule requires tests of this type.

4.3.2 Sample Collection and Preparation Activities

Task 2 includes a variety of testing activities for the determination of basic material properties of tuff, tuff joint interface properties, and rock-joint responses under pseudo-static and various dynamic loading conditions with special interest in repeated dynamic loadings arising from earthquakes and groundshocks. To carry out the testing activities, a considerable number of specimens with a naturally occurring joint are needed; a current estimation suggested a minimum of 45 jointed tuff specimens. This number may vary as the experiments proceed and a better understanding on tuff joint behavior is obtained.

To acquire such a large number of jointed tuff specimens requires considerable effort. The following sections discuss some technical aspects regarding the activity for jointed tuff specimen collection.

4.3.2.1 Site Selection for Sample Collection

One of the primary goals of the Seismic Rock Mechanics Project is to develop methodologies to evaluate, validate, and reduce uncertainties in the prediction models which eventually will be used to assess the effects of possible occurrences of earthquake as well as groundshock events on the short-term and long-term performance of a proposed underground repository at Yucca Mountain. The results of this study are expected to be used by the NRC staff and its contractors as a basis to determine the adequacy of DOE's repository design relevant to seismic activities during the process of License Application. To better serve the purpose, one would expect that the rock specimens to be tested in the laboratory come directly from the site to be evaluated or studied; that is, from the proposed Yucca Mountain repository site. However, the collection of tuff rock-joint specimens from the Yucca Mountain site is not currently feasible because the site characterization program proposed by the DOE has been delayed substantially. It is the understanding that the site characterization program will not be started until the end of 1991 while Task 2 of the Seismic Rock Mechanics Project is to be completed in August 1991 to ensure that the overall objective of the project can be achieved in a timely fashion. In light of the

complications, selection of an alternative site for sample collection to perform the studies proposed in Task 2 is justified.

Three criteria have been established to facilitate the process of site selection. The first is that the rock type at the site selected should be similar (e.g., welded and jointed) to the tuff material at the proposed repository horizon at the Yucca Mountain site so that the experimental results and the conclusions reached may be directly applicable. The second criterion is that the site to be selected should contain sufficient favorable locations for a collection of at least 50 rock-joint specimens. This criterion is important because of the relatively large dimension for the rock-joint specimens required to perform the proposed experiments in Task 2. The required dimension is 12 x 8 x 4 inches for the bottom portion and 8 x 8 x 4 inches for the top portion of a prepared rock-joint specimen, and a natural joint interface is in between these two portions. The third criterion is that the site selected should be easily accessible. The activity for specimen collection involves not only collection itself but also transporting heavy equipment and specimens collected from the site.

Based on the three criteria, two alternative sites were evaluated, one in the southern part of Texas and the other at Apache Leap, Arizona. Field observation shows that the rock at the southern Texas site is a nonwelded tuff, which is different from that at the proposed repository horizon at Yucca Mountain. The southern Texas tuff also is considerably weaker. Thus, the tuff at the southern Texas site does not satisfy the first siting criterion; and so the site is not suitable for sample collection.

On the other hand, the Apache Leap site in Arizona is suitable for specimen collection. Its rock is a vitrified and densely welded tuff, which is similar to the tuff at the proposed repository horizon. Field observation indicates that Apache Leap tuff is moderately to heavily jointed. The tuff at the proposed repository horizon is also heavily jointed. While some differences in physical properties between the tuffs at these two sites do exist, these differences may be quantified so that validation of corresponding rock joint models will still be achieved, provided that account is taken of differences in corresponding parameters.

The Apache Leap welded tuff has two predominant vertical joint sets, one minor subvertical joint set and one horizontal joint set with joint spacing ranging from 2 inches to a few feet. The joint spacing is crucial to the success of the sample collection activity. For the purpose of this study, the joint spacing should be at least 4 inches to be collectable. However, field experience indicates that it will be much easier to collect specimens at areas with larger joint spacing. This restraint limits the usable areas for sample collection at the Apache Leap site. (Discussion for other restraints is provided in a later subsection.) The area of interest for sample collection at the Apache Leap site is located around an abandoned highway tunnel, so it is accessible in terms of transportation. There is a distinct advantage in selecting this area. Since this section of the highway has been abandoned for quite some time, potential interference is minimized. This greatly facilitates the collection activity.

The Apache Leap site is a private property belonging to the Magma Mine Company. The Apache Leap Tuff Site Overview Committee (ALTSOC) is responsible for reviewing the application to access the Apache Leap site and making recommendations to the Magma Mine Company. Our request was approved on November 1989.

4.3.2.2 Important Considerations for Sample Collection

Several important factors need to be considered regarding whether a local area at the site is suitable for sample collection, and whether the rock joints collected are acceptable for the project experiments. As stated previously, the objective of Task 2 is to determine tuff-joint behavior subjected to pseudostatic and dynamic loadings. The tuff at the proposed

repository horizon at Yucca Mountain is about 800 ft below the surface, and the weathering condition on the tuff joints should be relatively minor. Therefore, collecting and testing tuff joints that are highly weathered must be avoided. Because almost all the vertical joints seen on the ground at the site were believed to be highly weathered, they were not suitable for samples. This condition led to a decision to focus sample collection on the horizontal and vertical joints from inside the abandoned highway tunnel which is approximately 50 to 60 ft below the surface. This decision considerably reduced the potential area usable for sample collection at the selected site.

As discussed in Section 4.3.1, the rock-joint dynamic shear test apparatus was designed and fabricated to have a 1-inch gap between the top and bottom specimen-box edges of the assembled specimen unit. To prevent potential interference of the top box edge with the specimen joint interface of the bottom specimen half, not only must the specimen joint interface fall within the 1-inch gap, but also its apparent relief has to be smaller than 1/2 inch. This restraint was applied in the field to determine the acceptability of a collected joint interface.

4.3.2.3 Techniques for Sample Collection

Several techniques are available for sample collection of rock joints. Among them are chain saw, or wire saw cutting; high-pressure water-jet cutting; hydraulic fracturing; and large-diameter core drilling.

For the first three, chain sawing has been used successfully in nonwelded tuff but not as successfully in welded tuff because of the frequent breakdown of the equipment. The high-pressure water-jet technique has demonstrated its effectiveness in cutting welded tuff. However, this technique is still state-of-the-art; and the cost for a high pressure water jet is high. In addition, considerable amount of water would be required for the process of cutting; and the ability to maintain a constant water supply in the field is questionable and expensive. The third technique, hydraulic fracturing, requires considerable small-diameter drilling around the boundary of a rock block to be collected. This drilling serves two purposes: (1) it allows hydraulic pressure to be applied on the walls of the boreholes drilled, and (2) a preferential fracture path is created along the direction of the boreholes. However, because a considerable number of holes needs to be drilled for each sample to be collected, the process for collection is slow.

Another concern, and perhaps the most important one for the three techniques (chain saw, hydraulic fracturing, and high-pressure water jet), is that they can be used effectively only for shallow cutting. Difficulty arises as the cutting goes deeper. Given the large number of specimens needed for testing and relatively less amount of area usable for sample collection, obtaining an adequate number of specimens using these techniques would be difficult.

Large-diameter core drilling, on the other hand, is relatively favorable. Its advantages are that it is reasonably fast and less expensive, and has less machine maintenance problems. Considerable experience has been accumulated over the years in core drilling in the welded tuff at the Apache Leap site. To take advantage of this experience and also take into consideration other favorable factors, large-diameter core drilling was selected for the sample collection.

4.3.2.4 Discussion for Sample Collection

Because of the large dimension needed for testing, it was determined that 18-inch diameter core would be collected and 18-inch diameter, thin-wall core barrels would be used for the drilling.

When performing large-diameter core drilling, two basic methods for obtaining a rock-joint feature are used. One is drilling to intersect a joint feature, and the other

is drilling parallel to the joint feature with the joint surface (interface) coinciding with the central plane of the core. The first method is preferred and usually allows sufficient dimension for joint specimen preparation, but often takes a longer time to obtain a rock joint than the second method does. This is especially true when the joint spacing is several feet wide. Although the second method has its advantages, two problems are associated with it. It is extremely difficult (1) to align the axis of drilling with the strike/dip of a joint interface and (2) to make the joint interface to be collected coincide with the central plane of the core. Very often, under-sized core pieces are obtained, which are not suitable for rock-joint specimen preparation. The first method, therefore, was used for most of the drilling in this sample-collection activity except for three holes. Among the three, one was a vertical hole and the other two were angle holes. Only one potentially useful joint specimen was obtained as a result of these three drillings.

Drilling for sample collection was performed by the Boyles Brothers Drilling Company. The company has a few thousand feet of drilling experience directly related to the Apache Leap site and of obtaining core samples with a diameter up to 6 inches. This experience was considered helpful to this project. Through the entire period of sample collection, a Center representative was on site to provide technical decisions concerning location, direction (angle), and depth of drilling and to be responsible for technical aspects regarding packing and transporting core pieces collected. The entire activity for collecting tuff specimens was conducted following the Center Technical Operating Procedure TOP-006, "Procedure for Obtaining Seismic Rock Mechanics Test Specimens from the Field." The drilling project was initiated on December 10, 1989, and completed on February 9, 1990. A Joy 22 drill rig (Figure 4-3) was used. A borehole was usually started using a 1.5- or 2.5-ft long core barrel (18 inches in diameter). If a joint interface were not intersected after a depth equal to the barrel length was drilled, this core barrel was replaced with a 4-ft long barrel for continuing drilling. A core breaker was used to break the core in the event that no joint was intersected after 4 ft of drilling.

A total of 29 boreholes were drilled. Figure 4-4 presents a schematic drawing showing the locations of the boreholes drilled for sample collection at the Apache Leap site. Of these, 8 were vertical holes, and 21 were angle or near-horizontal holes. Except hole No. 14, all the angle holes were inside the highway tunnel, and most were on the north wall. The depth of drilling for the holes ranged from 5 to 11 ft. The hole numbers not indicated in the figure are those with drilled depth less than 2 ft and from which no potentially usable joint specimens were produced.

The vertical drilling produced only three potentially usable joint specimens. The reason is simply because most of the intersected horizontal-joint interfaces were too rough and their apparent relief exceeded the maximum 1-inch gap value set by the design of the test apparatus as well as the 1/2-inch value for the purpose of avoiding interference. Even for those three joint specimens which were considered potentially usable, their joint interfaces barely satisfy the 1/2-inch requirement. This finding caused a major shift of drilling from the originally planned vertical direction to angle drilling. Although this shift substantially slowed down the drilling program, it was nevertheless necessary.

The program was also considerably impacted by two other problems. The first one was due to the abrasiveness of the Apache Leap welded tuff. The so-called diamond bits installed at the bottom end of a core barrel for cutting purpose consist of industrial diamond particles in an alloy matrix. During cutting, the alloy matrix is supposed to be eroded to expose fresh diamond particles; and these diamonds cut the rock. If the rock is relatively soft, the diamonds will last a long time. Since the Apache Leap welded tuff is a hard rock, the diamonds wear out very quickly. However, cutting can still proceed smoothly if fresh diamonds can be exposed fairly quickly through erosion of the alloy matrix. The bits first selected for this sample

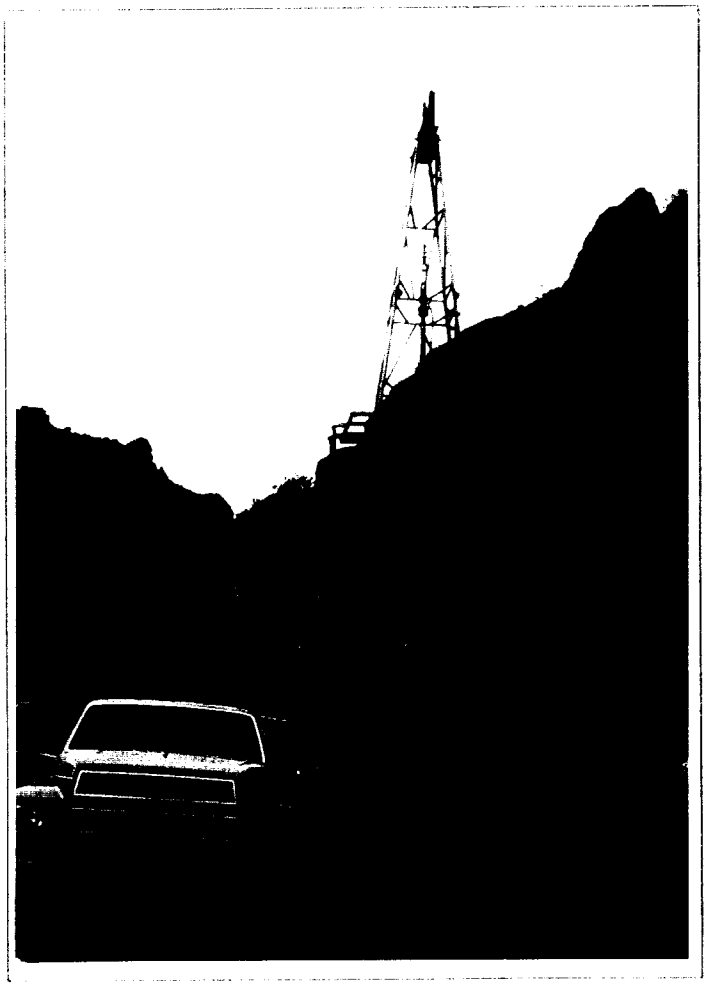

Figure 4-3. Truck-mounted Joy 22 drill rig

collection program had a matrix material that was very hard and difficult to erode away. As a result, drilling was slowed down substantially. This problem was mitigated by using diamond bits with relatively soft matrix material.

The second problem was associated with core breaking. The longest core barrel used in the program was 4 ft. If a joint interface were not intersected after 4 ft of drilling, the core needed to be broken and taken out of the hole for subsequent drilling; but breaking an 18-inch diameter core was difficult in the hard rock. A pair of wedges was used for this purpose at a shallow depth; at greater depths, a steel bar containing a wedge on one end was used. The force was applied by striking a 6- or 10-lb hammer to the end of the wedge. Experience indicated that 20 to 30 minutes were needed to break a shallow core loose; at relatively greater depths, even longer time and greater effort were required. Sometimes severe damage to an otherwise perfect joint interface was incurred because of this breaking process.

At the completion of this collection activity, a total of 50 potentially usable joint specimens was obtained; 44 of them were from the central north wall of the abandoned highway tunnel and had relatively smooth joint interfaces. Figure 4-5 shows a typical 18-inch diameter core with a smooth joint interface. Several attempts were made to locate other favorable areas for drilling in light of potential safety concerns of a large number of boreholes in one small area, but these attempts failed.

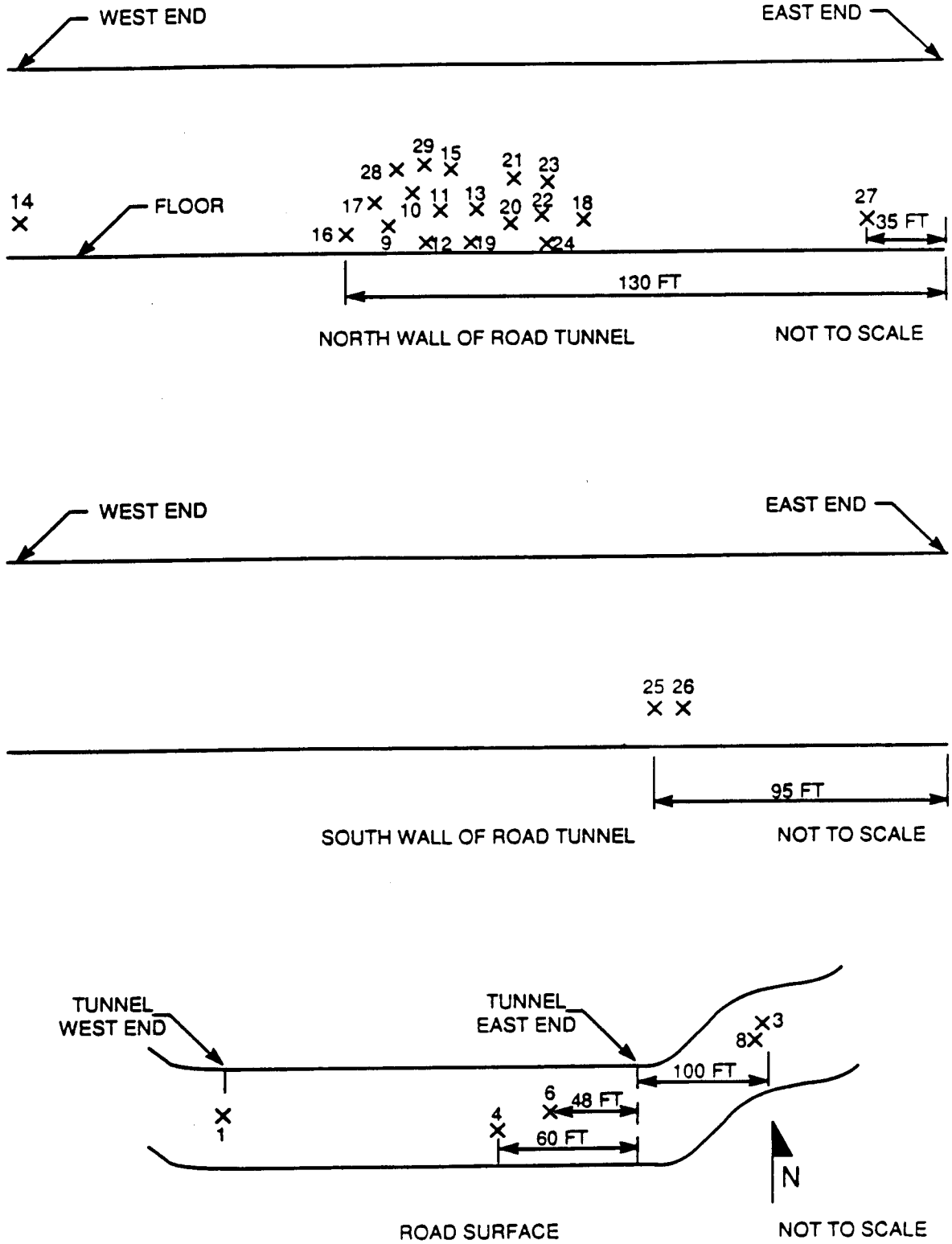

Figure 4-4. Location of drilled holes for sample collection at the Apache Leap site

Figure 4-5. An 18-inch diameter core with a smooth joint interface

4.3.2.5 Summary of Results

The difficulties notwithstanding, the sample collection was a success. Fifty potentially usable joint specimens were obtained, which is 10 percent more than needed according to the current experimental plan. This surplus is necessary to ensure that an adequate number of joint specimens will survive the preparation procedure, or these additional specimens may be used for other types of experiments if required.

Drilling in welded tuff is a slow process. However, the rate of drilling may be improved by careful selection of matrix material used for diamond bits. Experience indicates that a relatively soft matrix material facilitates drilling in the tuff rock.

Breaking a large-diameter core (e.g., 18 inches in diameter) from a borehole is a difficult task. It was a constant problem during sample collection, and some potential specimens were lost because of it. A new design for a core breaker is required if a similar drilling activity is implemented.

It was also found that drilling to intersect the joint has a better chance for obtaining usable jointed specimens than drilling parallel to the joint.

4.4 FIELD SITE EVALUATION AND SELECTION

The three purposes for conducting field studies of seismic effects on the mechanical response of underground mine facilities and geohydrologic response of jointed and fractured rock are (1) to clarify and quantify the relation among seismically induced ground motion and mechanical response and changes in groundwater conditions, (2) to generate a reliable data set for

a particular site, and (3) to evaluate rock-joint models and computer codes for simulation of the effect of seismic activities.

Seismic events in mines (called rockbursts when they result in excavation damage) are by far the most prolific source of information on the response of underground excavations and potentially on the geohydrologic response to seismic loading. Studies have shown that no systematic differences have been observed between these mine seismic events and natural earthquakes. Thus, most of the physical and geomechanical principles established for natural earthquakes also apply to mine seismic events (McGarr, 1984). This important observation indicates that mine seismic events may be a natural analog to natural earthquakes and that observed underground mine response (including groundwater) to mine seismic events may be applied in predicting repository response to natural earthquakes. Since there appears to be little data available to subsurface motion generation from natural earthquakes for the study of rock structural and geohydrologic responses nor will these data be accumulated quantitatively in the near future, study of mine seismic events offers an attractive alternative.

Three important factors need to be considered in the selection of a mine site for the study of seismic events. The first is that the host rock mass for mining should be well characterized geologically and structurally. Naturally jointed rock mass is a must. The second is that the recurrence time for seismic events and/or rockbursts needs to be small. These conditions provide the capacity (1) to measure, over a reasonable time span, deformation of excavations and groundwater responses in jointed rock subject to repetitive seismic loadings and (2) to relate the observations to the rock-mass structural conditions. From these data, it is possible to evaluate the various models of joint deformation, and, in particular, to assess their capacity to simulate accumulation of jointed surface damage under progressive shear deformation and cyclic loading. Both these matters are a central concern in the Seismic Rock Mechanics Project. Another governing factor in the selection of a mine site is that mechanical response and groundwater hydrology studies can be performed at the same mine.

Several potential sites for study are located in the U.S. and Canada; among them, the Lucky Friday Mine is technically attractive and was selected for our instrumented field studies. The Lucky Friday mine (a lead-silver mine) is in the Coeur d'Alene region of Mullan, Idaho.

The Lucky Friday Mine has been very well-characterized geologically. Extensive publications concerning geology in the Coeur d'Alene region are readily available. The primary orebody for the Lucky Friday Mine is a near-vertical silver and lead vein with nearly 1500 ft of minable strike length. The orebody is bounded on its north and south extents by faults and is cut by several major fault structures which strike in a roughly NW-SE direction. Several minor faults or fracture zones are also found in the mine.

The mine experiences a significant problem in mining-induced seismicity. The seismicity (or rockburst) is the result of either violent failure of the intact rock through propagation of new shear fractures, or slip on existing fault or bedding surfaces. These events can be quite large in magnitude, with the largest measured to date at 4.0 Richter magnitude. The Lucky Friday Mine experiences over fifty +1.0 Richter events per year, and on the order of ten to twenty +2.0 magnitude events. Thousands of smaller(<1.0) events occur in a typical year.

The mine has performed extensive studies into the location, nature, and causes of the seismic events. Currently a microseismic system with more than 30 channels is installed that continuously monitors the microevents and locates their coordinates. Historical data are available from this system dating back to the early 1970s. The U.S. Bureau of Mines also has installed a macro-seismic monitoring system, which has the ability to support full waveform analysis. The data storage system includes time of arrival and frequency-duration data.

The mine is among several other mines in the region which have had extensive rock mechanics studies in the past. A substantial data base presently exists on the rock mechanics of the Lucky Friday Mine.

Another favorable factor leading to the selection of the Lucky Friday Mine is that the mine management is cooperative, and the technical staff of the mine showed genuine interest in execution of the project.

The Nos. 5,200 and 5,700 stations of the Lucky Friday Mine have been selected for instrumented field studies for (1) dynamic effects on underground openings and (2) seismic effects on the hydrologic regime, respectively. Design of instrumented field experiments and the preparation of a technical operating procedure for drilling, instrumentation, and data collection are in progress.

4.5 REFERENCES

Banerjee, P. K., and S. Ahmad. 1985. Advanced three-dimensional dynamic analysis by boundary element methods. *Advanced Topics in Boundary Element Analysis*. Cruse, T. A., et al., eds. New York: American Society of Mechanical Engineers (ASME) 72:65-81.

Brady, B. H. G., and E. T. Brown. 1985. *Rock Mechanics for Underground Mining*. London: George Allen and Unwin:527.

Brady, B. H. G., M. L. Cramer, and R. D. Hart. 1985. Preliminary analysis of a loading test on a large basalt block. Technical Note. *Int. J. Rock Mech. Min. Sci. & Geomech. Abstr.* 22:345-348.

Brady, B. H. G., S. M. Hsiung, and A. H. Chowdhury. 1990. *Qualification Studies on the Distinct Element Code UDEC Against Some Benchmark Analytical Problems*. NRC Contract NRC-02-88-005. CNWRA 90-004. San Antonio, Texas: Center for Nuclear Waste Regulatory Analyses (CNWRA):1-148.

Brandshaug, T., B. Dasgupta, B. H. G. Brady, S. M. Hsiung, and A. H. Chowdhury. 1990. *Qualification Studies on the Finite Element Code HONDO II Against Some Benchmark Analytical Problems*. NRC Contract NRC-02-88-005. CNWRA 90-006. San Antonio, Texas: CNWRA:1-39.

Cundall, P. A. 1988. Formulation of a three-dimensional distinct element model: Part I--A scheme to detect and represent contacts in a system composed of many polyhedral blocks. *Int. J. Rock Mech. Min. Sci. & Geomech. Abst.* 25(3)107-116.

Day, S. M. 1985. Test problem for plane strain block motion code. S-Cubed, Inc., Memorandum to Itasca, Inc., Minneapolis, Minnesota.

Kana, D. D., D.C. Scheidt, B. H. G. Brady, A. H. Chowdhury, S. M. Hsiung, and B. W. Vanzant. 1990. *Development of a Rock Joint Dynamic Shear Test Apparatus*. NRC Contract NRC-02-88-005. CNWRA 90-005. San Antonio, Texas: CNWRA:1-27.

Key, S. W. 1986. A data structure for three-dimensional sliding interface. *Int. Conf. on Computational Mechanics*. Tokyo, Japan:1-29.

McGarr, A. 1984. Scaling of ground motion parameters, state of stress, and total depth. *J. Geophys. Res.* 89(B8):6969-6979.

Miller, P. K. 1978. The effects of boundary friction on the propagation of elastic waves. *Bull. Seis. Soc. America* 68:987-998.

Olsson, W. A. 1982. Experiments on a slipping crack. *Geophys. Res. Letters* 9(8):797-800.

Salvado, C., and J. B. Minster. 1980. Slipping interfaces: A possible source of radiation from explosive sources. *Bull. Seis. Soc. America* 70:659-670.

Williams, J. R., G. Hocking, and G. G. W. Mustoe. 1985. The theoretical basis of the discrete element method. *Proceedings of the International Conference on Advances in the Numerical Mathematics in Engineering*. United Kingdom: University of Swansea:897-906.

5. INTEGRATED WASTE PACKAGE EXPERIMENTS

by Gustavo Cragnolino, Hersh Manaktala, and Narasi Sridhar

5.1 TECHNICAL OBJECTIVES

The overall technical objectives of the Integrated Waste Package Experiments (IWPE) Project are:

(1) To develop a good understanding of the information currently available on metal corrosion and on other metal degradation processes.

(2) To assess the current status of Yucca Mountain Project (YMP) Waste Package Programs.

(3) To conduct waste package experiments to scope and study the key parameters affecting long-term material performance.

(4) To assess experimentally YMP selected waste package materials and designs and provide independent evaluation for reasonable assurance of long-term performance.

(5) To facilitate a continuous technical integration support to NRC and the Center in the area of waste package performance.

The objectives of the IWPE are planned to be accomplished by the following tasks listed in accordance with Revision 1 of the program plan:

(1) Task 1 - Collection and Review of Information for Assessment of Current Status of YMP Corrosion and Materials Program for Waste Package Containers

(2) Task 2 - Waste Package Experimental Programs

(3) Task 3 - General Support and Reporting

The current quarterly report follows the task classification given above. A second revision of the IWPE program plan was submitted to NRC on May 23, 1990. Following the approval of this plan, future quarterly reports will reflect the Revision 2 task classification.

5.2 COLLECTION AND REVIEW OF INFORMATION ON CORROSION OF WASTE PACKAGE CONTAINERS

As one of the activities in this task, a literature review was initiated, covering initially work conducted by Cortest Columbus under NRC sponsorship. The experimental work conducted by Cortest Columbus has been published in five reports (Beavers, 1988a, 1988b, 1989a, 1989b, 1990a). In addition to this report, Cortest Columbus prepared a review of the literature (Beavers, Feb. 1990b).

The literature review covers the influence of environmental variables on the corrosion behavior of candidate container materials for the tuff repository. The review is a good summary of the literature available for the specific case of the tuff repository and contains updated information on the more common forms of localized corrosion and stress corrosion cracking (SCC) for the austenitic and Cu-base alloys. The effects of heat decay and radiation on corrosion are included, as well as a brief discussion of the possible impact of microbiologically induced corrosion on the performance of the container alloys. However, it would be highly desirable to have a critical

assessment of other possible failures modes, even though some of them may be not anticipated according to our current experience or knowledge. It should be emphasized that an adequate characterization of the tuff repository, and in particular its evolution with time, does not exist. A complete description in terms of such variables as water chemistry, pH, Eh, and trapped and dissolved gases is not yet available. Most of the corrosion studies have been carried out using natural or simulated J-13 well water, solutions concentrated by evaporation from J-13 well water, or solutions based on J-13 water containing increasing concentrations of aggressive species (e.g., 100X in Cl^- concentration).

The purpose of the Cortest experimental work on cyclic potentiodynamic polarization (CPP) was to examine the effects of environmental and metallurgical variables on the electrochemical behavior of candidate canister materials. The approach was based on the use of potentiodynamic polarization curves with a forward potential scanning from a cathodic potential towards anodic potentials, followed by a reverse scanning when the current density reached $1x10^{-3}$ A/cm2. Using this method the pitting potential and the repassivation potential as well the corrosion, passivation (maximum current), and passive currents were determined. Apparently, the corrosion potential was measured initially, before the potential scan was started and after the specimen was exposed to the solution overnight. A second aspect of their approach is that they used a statistical experimental matrix for the evaluation of the effect of many environmental variables including pH and temperature.

Four of the six materials initially selected by DOE (LLNL) as candidate alloys were used by Cortest. They are: AISI 304L SS, Incoloy Alloy 825, CDA 102 (Copper) and CDA 715 (Cu-30Ni).

In the Appendix of the First Semi-Annual Report (Beavers, 1988a), the laboratory procedure adopted for running polarization curves was described as well as the procedure used for the preparation of a simulated tuff groundwater with a chemical composition similar to that of J-13 well water. It should be noted that the composition of the simulated J-13 well water prepared according to this procedure differs slightly from that reported in Table 1 of the same report (no reference given).

It is worthwhile to note that the composition of J-13 well water reported by various authors varies according to different sources. Only recently (Glassley, 1990), the range of concentrations apparently found by different authors for all the species of interest has been reported. Although the variations are not significant, it is convenient to recognize that the range of concentrations measured makes unjustifiable many efforts to prepare simulated J-13 well water according to the values reported by a given author. The main effort should be directed to identify the role of the different anionic species in the acceleration or inhibition of localized corrosion and to evaluate whether the different cations play a distinctive role.

The approach adopted by Cortest for the statistically designed experiment depended heavily on the criteria used in the selection of the independent variables of interest and the dependent variables. Fifteen variables were chosen by selecting the concentration of thirteen different species in addition to pH and temperature. Nine of these species are present in J-13 well water; three species (NO_2^-, H_2O_2 and oxalic acid) are considered to be formed by radiolysis, and the remaining one (O_2) is present in the undersaturated zone from air and also is formed by radiolysis of water.

Several problems arise from this particular selection of species and concentration values studied. They are as follows:

(1) The concentration of HCO_3^- is dependent on pH. This means, for example, that for an initial concentration of HCO_3^- equal to 2000 mg/l or 32 mmoles/l the actual concentration will be significantly lower at pH 5 than at pH 10, since at the lowest

pH HCO_3 has been mostly transformed in CO_2 which has evolved from the solution. Therefore, the effect of HCO_3- concentration on the dependent parameters cannot be assessed independently of the effect of pH.

(2) The concentrations of Si and Al are dependent of the concentration of F, which acts as a complexing agent. In the case of Al, which is added to the solution as a cation [presumably in the form of a salt like $Al_2(SO_4)_3$], the stable complex is AlF_6^-. The formation of this complex reduces the concentration of Al^{3+} well below the initial concentration, mainly when the F^- concentration is 200 mg/l, equivalent to 10.5 mmoles/l, and represents a concentration that is more than 10 times higher than the highest Al^{+3} concentration used in the test matrix [20 mg/l or 0.74 mmoles/l]. Si is added in the form of $SiO_2.xH_20$, but it can be easily converted to SiF_6^-. This is particularly true at the lowest concentration included in the test matrix, which is 0.035 mmoles/l. Even at the highest initial concentration, 3.5 mmoles/l, the concentration of noncomplexed Si is significantly reduced, making invalid the adoption of the initial concentration as representative of the particular environment.

(3) Several species were included in the test matrix as a result of radiolysis. They are NO_2^-, H_2O_2, $H_2C_2O_4$ (oxalic acid) and also O_2, although O_2 is also included as a consequence of the aerobic nature of the repository. The reasons for the inclusion of oxalic acid in favor of other organic species is not clear. Although it can be argued that in the repository the presence of organic compounds can be expected, by no means can it be assumed that oxalic acid is the prevailing species. Acetic acid is stable up to 300 C, while oxalic decomposes above 150 to 170 C. The additional fact that oxalic acid is a good complexing agent for iron may complicate even further the interpretation of the results.

Regarding the other species, due to the nature of the experimental method adopted, which is the measurement of anodic polarization curves under potentiostatic control, interference occurs between the reducible/oxidizable species in the environment and the true anodic behavior of the material. The ideal situation is to remove all the electrochemically active species that may participate in charge transfer reactions at the metal surface (i.e., species such as oxygen and H_2O_2) and study precisely the anodic behavior of such a surface by applying controlled potentials. The role of the radiolytically generated species should be studied under open-circuit conditions to interpret their effect on the redox potential of the environment and the corrosion potential of the metal. The role of species of anionic species that can act as both as reducible species (e.g., nitrate, nitrite) and as inhibitors can, however, be studied using potentiodynamic/potentiostatic methods.

Despite the above mentioned criticisms, the approach used by Beavers and Thompson is an important attempt at defining the quantitative effects of relevant environmental variables on localized corrosion. By conducting studies in solutions containing anionic and cationic species found in J-13 well water, but covering a wide range of concentrations, they are able to identify regions of the environmental space where additional research is needed.

5.3 WASTE PACKAGE EXPERIMENTAL PROGRAMS

5.3.1 Corrosion of Container Materials in the Tuff Repository Environment

As a requirement for most of the tasks in the IWPE project, it is essential that the initial condition of the candidate container materials be characterized fully. This characterization will (1) result in a better understanding of differences in corrosion data among various laboratories, (2) ensure that testing is performed on sound materials, and (3) enable quantification

of any microstructural changes due to long-time exposure to temperatures in the range of 200 - 300 C. The material characterization work project consists of optical metallography, SEM-EDX analysis of various microstructural features, and corrosion studies in standard solutions designed to test the intergranular corrosion susceptibility. The following tasks were performed under the sub-task heading of Electrochemical Characterization of Materials.

5.3.1.1 Optical Metallography

The candidate container materials are in the form of 0.5 in. thick plates. The list of materials received along with their heat numbers and chemical compositions is shown in Table 5-1. Samples for metallographic studies were cut from these plates such that cross-sections parallel and perpendicular to the rolling direction were both examined. The results to date from the metallographic examination are reported below.

Incoloy Alloy 825: The microstructures at two magnifications are shown in Figures 5-1a and 5-1b. The 500X micrograph indicates that the grain boundaries are free of precipitates (at least at this magnification). The cuboidal precipitate appears orange in color and is most probably a titanium nitride. Titanium is added in this alloy to stabilize the alloy against grain-boundary carbide precipitation. The low-magnification micrograph shows that there is great variation in grain size in this plate with large grains being surrounded by small grains. The cause of the dual grain size distribution is not clear. It can be due to too short a time at annealing temperature which resulted in insufficient grain growth or it can be due to inhomogeneity in prior hot work. Further investigation is necessary to ascertain whether this microstructure is untypical and whether further annealing can eliminate this problem.

It is felt that since the grain boundaries are clean, localized corrosion behavior is most probably independent of grain size. Hence, localized corrosion studies are proceeding with this material. However, there is a potential concern for stress corrosion cracking and thermal stability studies because these phenomena may be affected significantly by differences in grain size. Hence further studies will be conducted to resolve this issue.

304L Stainless Steel: The microstructures are shown in Figures 5-2a and 5-2b. The grain boundaries appear to be free of precipitation. The dark, elongated particles within the grains are most probably sulfide inclusions. This will be verified by SEM-EDX analysis.

316L Stainless Steel: The microstructure of 316L stainless steel was found to be similar to that of 304L stainless steel. The grain boundaries appeared to be free of precipitates. As in the case of the 304L stainless steel, sulfide inclusions were seen as elongated particles.

Hastelloy Alloy C-22: The microstructure of Hastelloy Alloy C-22 is shown in Figure 5-3. As in the other austenitic materials, the grain boundaries appear to be free of precipitates. The few dark particles in the form of bands are believed to originate from the solidification stage.

TABLE 5-1. HEAT NUMBERS AND CHEMICAL COMPOSITIONS OF THE CANDIDATE CONTAINER MATERIALS IN THE IWPE PROJECT.

Alloy	Heat No.	Composition (wt.%)							
	Ni	Fe	Cr	Mo	W	Cu	Al		Other
304L	T0954	9.14	Bal.	18.3	-	-	-	-	C - 0.022
316L	P80746	10.04	Bal.	16.4	2.1	-	0.3	-	C - 0.01
IN - 825	HH4371FC	41.1	30.4	22.1	3.2	-	1.8	- Ti- 0.82	C - 0.01
HA-C-22	8-3175	Bal.	3.8	21.4	13.6 3.0	-	-	C - 0.004	
CDA - 102	6681	-	-	-	-	-	99.95	-	-
CDA - 613	M5459	-	2.5	-	-	-	90.54	6.65	-
CDA - 715	7037/6132a	29.6	0.5	-	-	-	69.1	-	C - 0.13

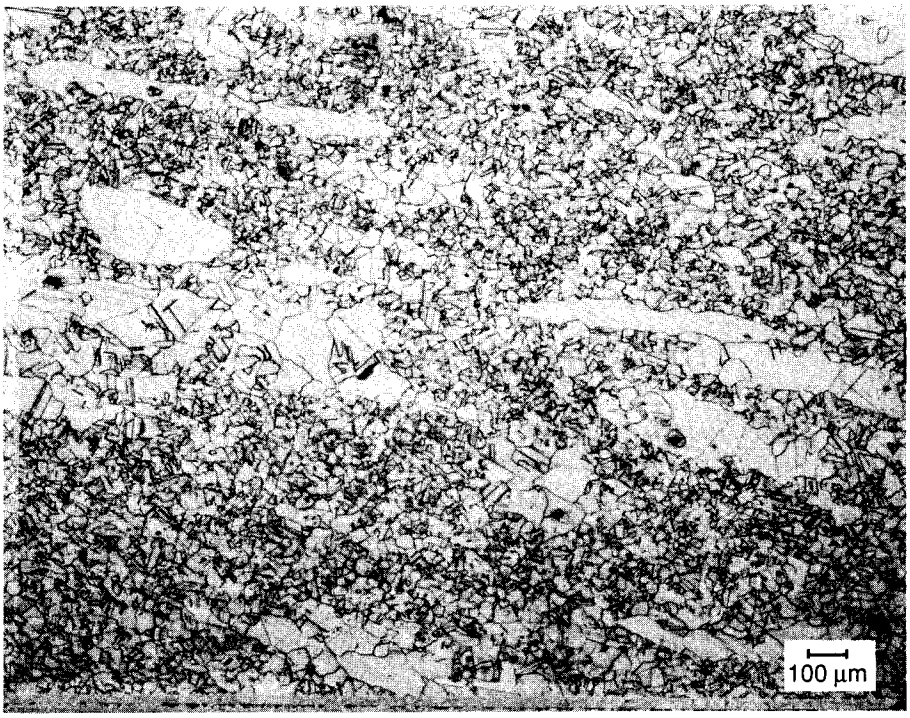

Figure 5-1a. Microstructure of Incoloy alloy 825, transverse cross-section (50X magnification)

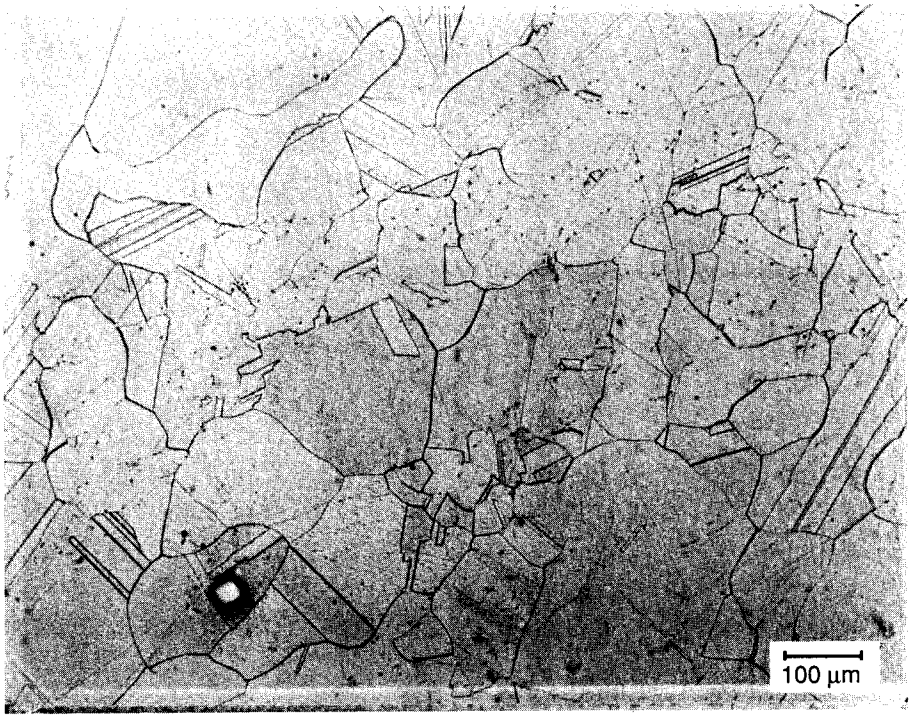

Figure 5-1b. Microstructure of Incoloy alloy 825, transverse cross-section (500X magnification)

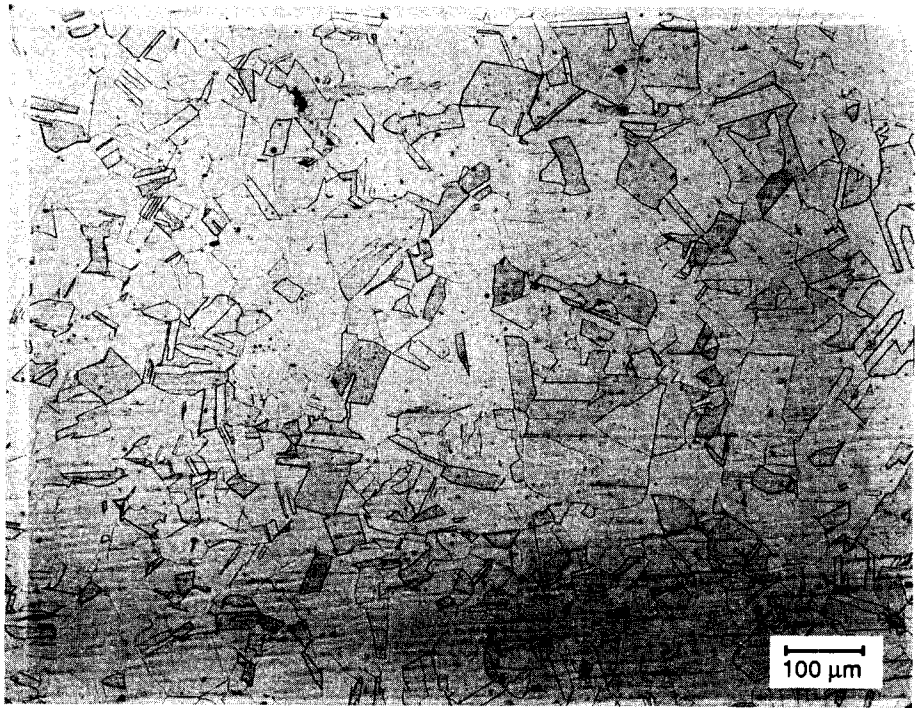

Figure 5-2a. Microstructure of 304L stainless steel, transverse cross-section (100X magnification)

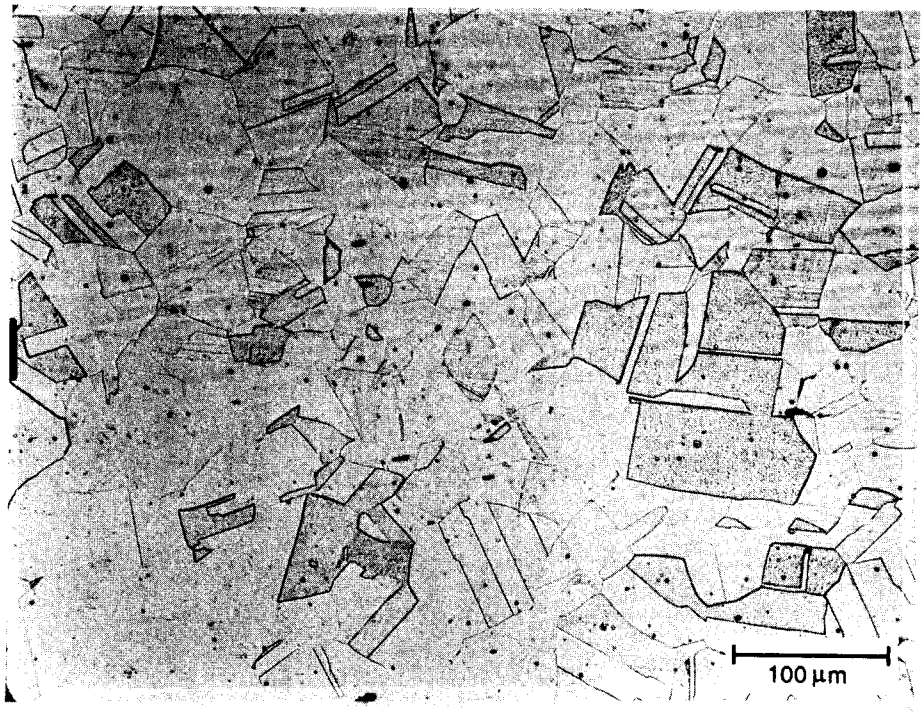

Figure 5-2b. Microstructure of 304L stainless steel, transverse cross-section (200X magnification)

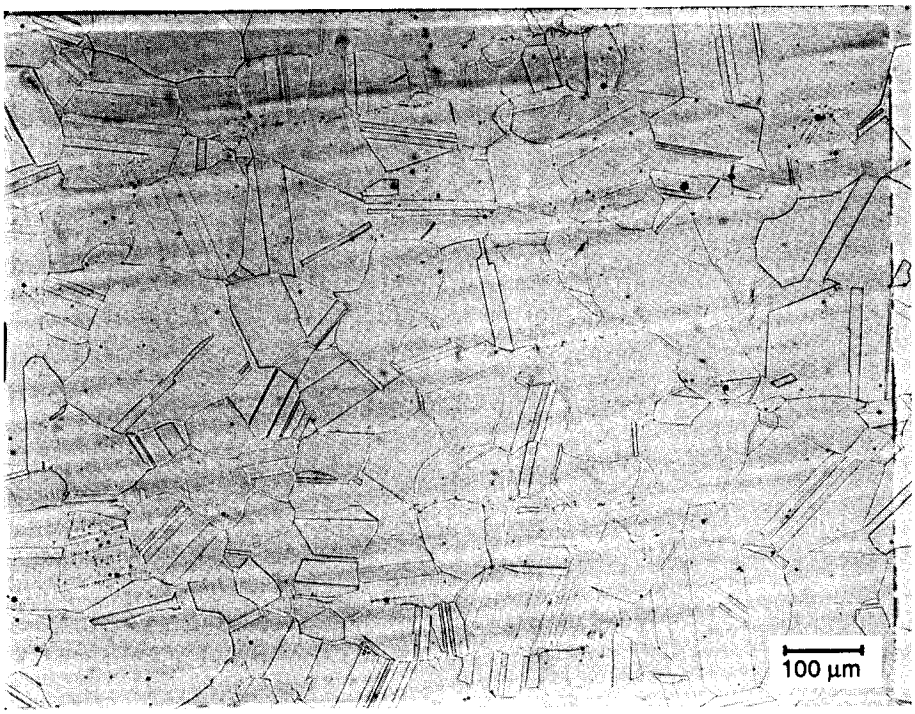

Figure 5-3. Microstructure of Hastelloy alloy C-22 (100X magnification)

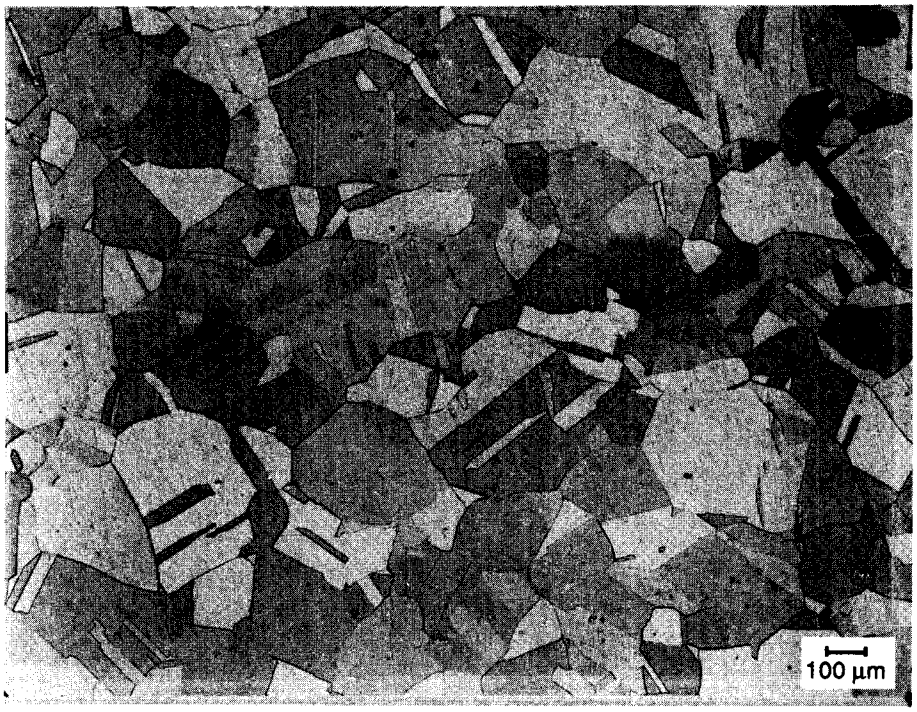

Figure 5-4. Microstructure of OFH copper (CDA-102), longitudinal cross-section (50X magnification)

CDA-102 (OFH Copper): The microstructure of CDA 613 is shown in Figure 5-4. The relatively equiaxial grains are typical of this material. The inclusion content is relatively low.

CDA 613 (Cu-Al Alloy): The microstructure is shown in Figures 5-5a and 5-5b. It is uncertain at this time whether this is a typical microstructure for this alloy and whether some of the features of the microstructure shown are metallographic artifacts. The tentative conclusion from the micrographs is that the material is in the as-hot worked condition and that the precipitates (dark particles) are probably Cu-Fe-Al intermetallics. However, further investigation is needed to verify these conclusions.

A survey of metallographic information for all the alloys under study is also being conducted to identify typical microstructures and possible deviations related to thermo-mechanical treatments.

5.3.1.2 SEM-EDX Analysis

SEM-EDX analysis was performed specifically to identify compositional differences between the bulk and surface of materials. Identification is especially important to the chromium-containing alloys that are in the annealed condition. Hence SEM-EDX analysis was conducted only on these materials. Analyses were performed on the mill-surface (as-descaled surface) and the mid-section of the plates. The results, given in Table 5-2, show significant depletion of chromium at the surface of both Hastelloy Alloy C-22 and Incoloy Alloy 825. The mid-section analysis, which should reflect the expected composition of the material, matches the certified chemical composition of the alloy (Table 5-1), thus verifying the accuracy of the SEM-EDX analysis for chromium. It must be noted that the SEM analysis for heavy elements such as tungsten can differ from other spectroscopic analyses. Table 5-2 also shows no significant chromium depletion for the two stainless steels.

In laboratory tests, the surface layer is machined off; and hence chromium depletion is generally not of concern. The surface composition is of importance in the actual field performance of the container material where the surface is not machined. The origin of the depletion is speculative at this time. It is hypothesized that chromium depletion occurs during the annealing stage when the surface chromium is converted to an oxide which then is removed by descaling operation (also called pickling operation) in the mill.

5.3.1.3 Corrosion Tests In Standard Solutions

Intergranular corrosion tests according to ASTM A-262, Practice B, have been initiated on the austenitic alloys. Results of these tests will be described in the next reporting period.

5.3.2 Metallurgical Stability of Container Materials in Tuff Repository Environment

The technical objectives of experimental work being conducted on Materials Stability are to identify the key parameters that control the long-term materials stability of the candidate high-level radioactive waste container materials and to obtain quantitative data via laboratory experiments. Included under this task are studies of the stability of protective surface films formed on copper-based alloys. The experimental work is both of confirmatory and exploratory nature. The information generated under this task is anticipated to be used for verifying the validity of models and data that DOE might generate for predicting the performance of the HLW container under repository environment.

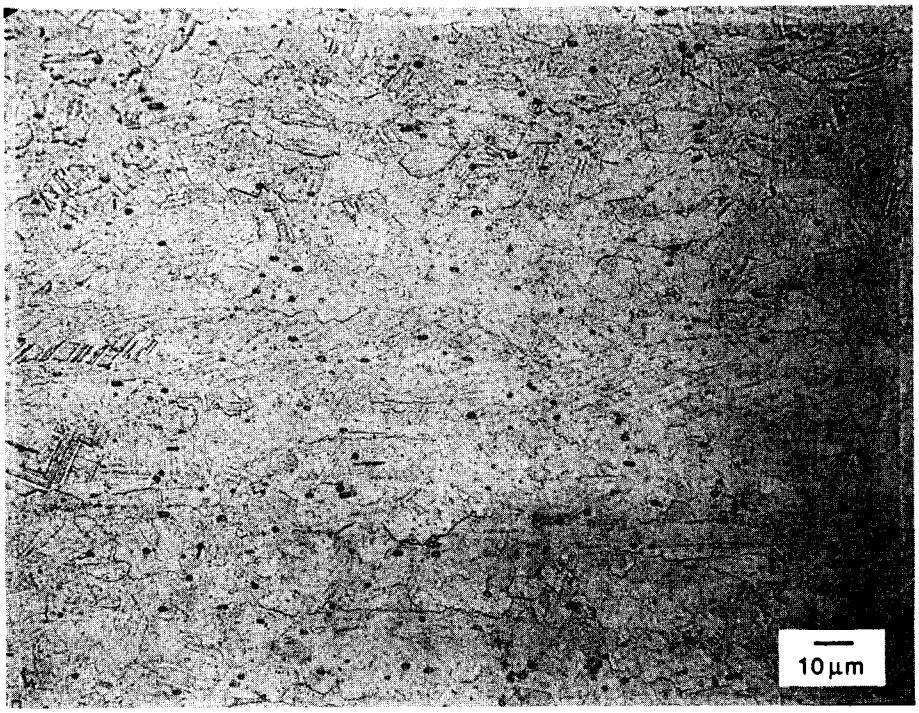

Figure 5-5a. Microstructure of CDA-613 (Aluminum Bronze), transverse cross-section (500X magnification)

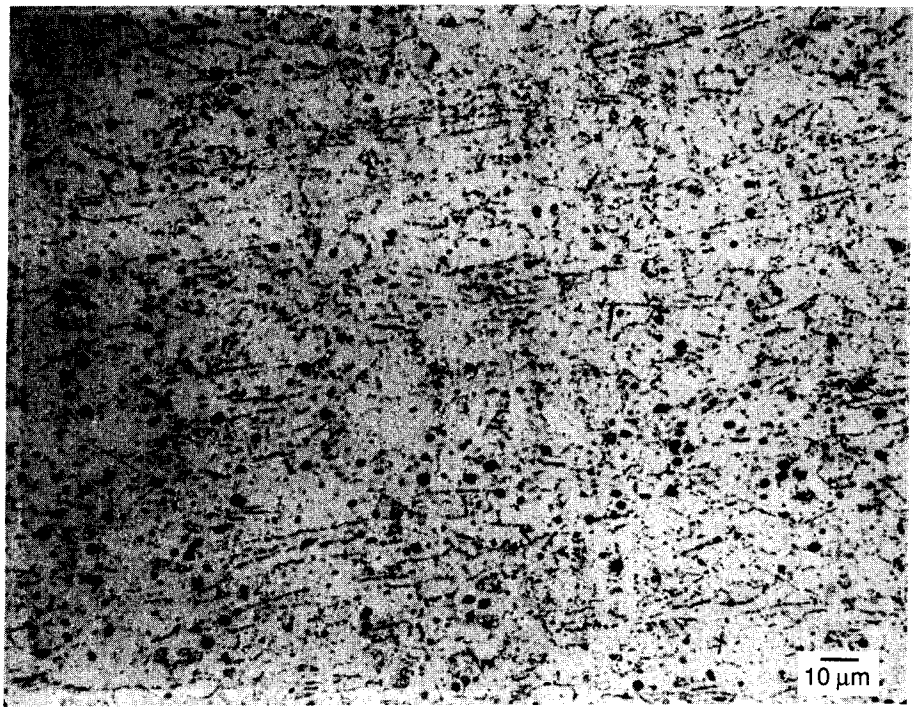

Figure 5-5b. Microstructure of CDA-613, longitudinal cross-section (500X magnification)

TABLE 5-2. SURFACE AND BULK ANALYSES OF CHROMIUM CONTAINING ALLOYS BY SEM-EDX.

Alloy	Element Analyzed	Weight Percent Mill Surface	Weight Percent Bulk
304L	Fe	68.7	69.2
	Ni	8.9	8.9
	Cr	18.99	18.59
	Si	1.2	1.5
	Al	0.4	0.2
	Mn	1.6	1.4
	Cu	0.3	0.3
316L	Fe	68.5	68.5
	Ni	9.4	9.4
	Cr	16.9	16.9
	Si	0.9	0.9
	Al	0.3	0.3
	Mn	2.0	2.0
	Cu	0.3	0.3
	Mo	1.7	1.7
IN-825	Fe	43.5	29.0
	Ni	35.3	42.0
	Cr	15.8	22.7
	Si	0.9	0.5
	Al	0.5	0.2
	Ti	0.4	0.9
	Cu	1.6	1.5
	Mo	2.1	3.2
HA-C-22	Fe	4.0	4.2
	Ni	62.1	57.7
	Cr	13.6	21.4
	Al	1.5	0.7
	Mo	13.0	11.3
	W	4.6	4.2

In the first part of the project under Task 3, Materials Stability of Candidate HLW Container Materials, four priority subtasks have been identified covering both surface and bulk materials properties alteration/degradation phenomena.

5.3.2.1 Low-Temperature Sensitization (LTS) of Austenitic Materials

Objective. The objective of this subtask is to study the long-term thermal and thermodynamic stability of the metallurgical phases present in the candidate austenitic HLW container materials, and relate the meta-stability and slow transformations processes to likely failure in a geologic repository during the containment period.

Introduction. A major concern in using austenitic stainless steels for structural applications is their susceptibility to develop a sensitized microstructure when exposed in the 500°C to 800°C temperature range (Povich et al. Aug. 1978, Povich, Feb. 1978). Such temperature-range exposures could occur during sheet metal production, and container fabrication and welding processes (Solomon, June 1978). In the case of HLW containers, high-temperature exposure in the range indicated above would occur during welding closure and possibly during heat treatments that might be used during fabrication of the waste package.

It is well-known that microstructural alterations, as a result of the sensitization phenomena, can lead to less desirable or even unacceptable properties (mechanical, corrosion, etc.) of the fabricated component. Since the LTS is a very slow process, it may not lead to a readily observable sensitized microstructure in the short period of time between container fabrication and emplacement in the repository. Although some information is available in the literature on the conditions that could lead to LTS in austenitic materials, no direct relationship has been established among various processing parameters and service conditions that could be present in a repository. The kinetics of the LTS phenomena may depend on parameters such as fabrication (residual) stresses, welding, alloying and impurity elements, grain size, prior thermo-mechanical treatments, amount of cold work, microstructure and morphology, and size of second-phase or impurity particles. In addition, gamma radiation, radiolytic products, and chemistry and oxygen content of the environment may affect substantially the corrosion resistance.

Accomplishments. During FY89-90, a literature survey was conducted on Incoloy alloy-825 and Types 304, 304L, and 316L austenitic stainless steels, to understand the effects of residual stresses, amount of cold work, grain size, welding, post-weld heat treatments, and chemical nature and oxygen content of the test environment, on the activation energy of the LTS phenomena. The results of the literature information were presented at the IWPE Peer Review at Center in July 1989. Based on the existing information and recommendations of the peer review committee members, a test matrix is being prepared to conduct experiments principally on Incoloy alloy-825. However, specimens of Types 304, 304L and 316L will also be included in the tests as reference specimens and for validating/calibrating the Center test procedure with DOE and literature published information.

Additional tests to study the effects of alloying elements; heat-to-heat variations; amount and morphology of second-phase particles and impurities; gamma radiation; and radiolytic products of air, moisture, and liquids on the LTS phenomena will be considered after analyzing the effects of the parameters being studied in the FY90 and FY91 test matrix.

5.3.2.2 Stability of Thick-Oxide Film Formation in Copper and Copper-Based Alloys

Objective. The objective of this subtask is to study the kinetics of thick-oxide film formation, spallation, and regeneration in copper and copper-based alloys.

Introduction. The behavior of copper and its alloys depends to a large extent on the properties and maintenance of a protective surface film. The oxide films that form on copper-based alloys in gaseous or aqueous environments are generally adherent and follow a parabolic growth kinetics when the oxide thickness is small. However, much less is known about thick films, which are likely to be generated in a repository over the long service-life of the HLW container (spanning hundreds to thousands of years). There is already some evidence that thick oxide films formed on some of the candidate copper-based alloys for the HLW container are susceptible to spallation (Yunker et al., Dec. 1986, Yunker, June 1986). The mechanism of spallation and regeneration of thick surface films under extended exposures to varying gaseous, vapor, and liquid environments, is not very well understood. However, such information is necessary in order to evaluate the ability of the surface films to provide protection for the base metal. This would be accomplished through understanding the kinetics of formation, spallation, and the regeneration of thick surface films under repository conditions. It is presently assumed that the repository environment will be dry, followed by the presence of vapor phase, and finally there is a possibility of water intrusion. It is also essential that the investigations cover the much less studied and understood phenomenon of aqueous corrosion of copper and copper-based alloys with pre-film of oxide(s) formed in gaseous and/or vapor phases.

Accomplishments. A review of the literature information (primarily DOE-generated reports) was conducted to understand the performance of the three candidate copper-based alloys in anticipated Yucca Mountain environment (both in the presence of gamma radiation and in an environment without radiation). The results indicate that the vapor phase is more aggressive than the liquid phase in a gamma radiation environment. The data also indicates that alloy CDA-715 (cupro-nickel) has the lowest rate of corrosion of the three candidate copper-based alloys in a radiation free environment; while it is the highest under radiation environment (Manaktala, Apr. 1990). It is believed that spallation of the thick surface oxide film observed on alloy CDA-715 is related to, at least in part, to the mechanical stresses built up at the interface between the oxide and the metal. Verification of this hypothesis is important, as it provides indication of the stability of the protective oxides. A test matrix is being developed to validate this hypothesis, and to study the kinetics of thick oxide film formation, spallation, and regeneration. The emphasis would be on developing kinetics (rate) equations which would take into account factors such as the alloy composition, temperature of exposure, environment (gaseous, vapor, or liquid), and sequence in which the oxide-film is formed in varying environment.

5.4 REFERENCES

Beavers, J. A., and N. G. Thompson. 1988. *Container Corrosion in High Level Nuclear Waste Repositories*. NRC Contract No. NRC-04-87-009. Year 1, First Semi-Annual Report. Columbus, Ohio: Cortest Columbus, Inc.

Beavers, J. A., and N. G. Thompson. 1988. *Container Corrosion in High Level Nuclear Waste Repositories*. NRC Contract No. NRC-04-87-009. Year 1, Second Semi-Annual Report. Columbus, Ohio: Cortest Columbus, Inc.

Beavers, J. A., and N. G. Thompson. 1989. *Container Corrosion in High Level Nuclear Waste Repositories*. NRC Contract No. NRC-04-87-009. Year 2, First Semi-Annual Report. Columbus, Ohio: Cortest Columbus, Inc.

Beavers, J. A., and N. G. Thompson. 1989. *Container Corrosion in High Level Nuclear Waste Repositories*. NRC Contract No. NRC-04-87-009. Year 2, Second Semi-Annual Report. Columbus, Ohio: Cortest Columbus, Inc.

Beavers, J. A., and N. G. Thompson. 1990. *Container Corrosion in High Level Nuclear Waste Repositories*. NRC Contract No. NRC-04-87-009. Year 3, First Semi-Annual Report. Columbus, Ohio: Cortest Columbus, Inc.

Beavers, J. A., and N. G. Thompson. 1990. *Environmental Effects on Corrosion in the Tuff Repository*. NUREG/CR-5435. Washington, D.C.: NRC.

Glassley, W. E. 1990. *Geochemical Interactions*. Presentation to the Nuclear Waste Technical Review Board, January 18-19, 1990, Pleasanton, California. Livermore, California: Lawrence Livermore National Laboratory (LLNL).

Manaktala, H. K. 1990. Degradation modes in candidate copper-based materials for high-level radwaste canisters. Paper No. 512. *Proceeding of Corrosion '90 Conference*. Houston, Texas: National Association of Corrosion Engineers (NACE).

Povich, M. J., and P. Rao. 1978. Low temperature sensitization of welded type 304 stainless steel. *Corrosion* 34(8):269.

Povich, M. J. 1978. Low temperature sensitization of type 304 stainless steel. *Corrosion* 34(2):60.

Solomon, H. D. Continuous cooling sensitization of type 304 stainless steel. *Corrosion* 34(6):183.

Yunker, W. H., and R. S. Glass. 1986. *Long-Term Corrosion Behavior of Copper-Base Materials in a Gamma-Irradiated Environment*. Report No. UCRL-94500, DE87-007098. Livermore, California: LLNL. Also published in *Scientific Basis for Nuclear Waste Management* 84. Boston, Massachusetts: Material Research Society:579.

Yunker, W. H. 1986. *Corrosion of Copper-Based Materials in Gamma Radiation*. Report No. HEDL-7612, DE87-005594. Richland, Washington: Westinghouse Hanford Company.

6. STOCHASTIC ANALYSIS OF UNSATURATED FLOW AND TRANSPORT

by Rachid Ababou

6.1 TECHNICAL OBJECTIVES

A quantitative characterization of large-scale flow and radionuclide transport through the heterogeneous unsaturated fractured rock of Yucca Mountain will be necessary to evaluate compliance with the siting criteria and performance objectives associated with the proposed Yucca Mountain HLW repository 10CFR Parts 60.122 and 60.113. The pertinent technical issues concerning radionuclide migration at Yucca Mountain will need to be understood so as to demonstrate that the hydrogeologic conditions at the repository site strongly inhibits radionuclide transport to the accessible environment and meets performance criteria. Realistic modeling of the complex, heterogeneous flow and transport processes at Yucca Mountain will require incorporating the effects of relatively small-scale space-time variability in modeling large-scale unsaturated flow and radionuclide transport.

The specific objectives of the Stochastic Analysis of Unsaturated Flow and Transport Project are as follows:

(1) To perform a review of the literature and assess available models and data relevant to the subject site.

(2) To select a global approach to model large-scale flow and transport in unsaturated fractured rock.

(3) To develop submodels for incorporation into the global model.

(4) To perform large-scale simulations and participate in the validation of flow/transport models for the Yucca Mountain repository.

The effective starting date of the project was February 2, 1990. The project is divided in three tasks to accomplish the objectives.

(1) Task 1 - Review, Analysis, and Development of Modeling Approach

(2) Task 2 - Stochastic Submodel Development and Implementation

(3) Task 3 - Large-Scale Flow/Transport Simulation and Data Analysis

The complete results of literature review, initial data assessment, model selection, and first stages of model development will be presented in an integrated fashion in the next quarterly report. Preliminary aspects of the work accomplished so far are described in the following subsections.

6.2 PRELIMINARY RESEARCH AND ACCOMPLISHMENTS

In the screening phase of the project (part of Task 1), an adequate modeling approach is to be selected. It will be concerned with the perceived difficulty in obtaining site-specific hydrodynamic data and the anticipated complexity of modeling three-dimensional processes with stratification, fracturing, and other geologic heterogenities occurring over a broad spectrum of length scales. Preliminary efforts focused on four main areas of research listed as follows, with a brief discussion of each presented in the rest of this section.

(1) Continuation of a literature review and assessment of previously developed models of flow and solute transport in heterogeneous and fractured porous media (including fracture-network models and some single-fracture models).

(2) Data-oriented review and research focusing on the correlation among different types of hydrodynamic parameters as well as the development of a framework for future use of existing databases towards model validation.

(3) Determination of adequate computational means (supercomputer access) and establishment of an efficient computer graphics laboratory at the Center to visualize large computer-generated or field-measured datasets such as heterogeneous moisture patterns, flow pathways, fracture networks, geological strata and topography (all in three spatial dimensions).

(4) Continued development of previously initiated work on key numerical issues in nonlinear and spatially random models of subsurface flow and transport processes (to be expanded during Task 2, once the precise modeling approach has been selected).

The first ongoing activity, literature review of modeling approaches, is being used to guide and justify the subsequent choice of a strategy for modeling Yucca Mountain (on scales of hundreds of meters to kilometers). Some of the key questions to be answered are: (1) whether a detailed three-dimensional simulation approach will be computationally feasible given the required large space-time scales of simulation; (2) which simplifications are reasonable and which ones are not for modeling unsaturated flow and transport in spatially distributed geologic systems, particularly in the presence of porous matrix/fracture interactions; and (3) what are the criteria and tests required to ensure the adequacy ("validity") of the mathematical/numerical model, what are the outputs of interest, and how should the model quantify the uncertainty of its own outputs. These questions will be addressed when the review is completed.

For the second activity, an interaction with other research groups has been pursued to integrate measured hydrodynamic parameters and flow data from controlled, unsaturated flow-transport experiments (INTRAVAL Test Cases of the Jornada Trench Site, University of New Mexico in Las Cruces, and the Apache Leap Site, University of Arizona in Tucson) into the database to be used in this project. To initiate the Center's participation to INTRAVAL, R. Ababou presented a paper on "High-Resolution Modeling of Three-Dimensional Flow Fields" at the 4th INTRAVAL workshop (Las Vegas, Nevada, Feb. 5-10, 1990). Along these lines, R. Ababou will contribute a chapter devoted to the modeling of the Las Cruces trench experiment to the final INTRAVAL report (Phase I, in preparation). Similarly, dialogue and exchange of information are continuing with the University of Arizona group, with a view to utilizing their isothermal experiments in unsaturated fractured tuff for testing and validating this project's model and sub-models. This was the object of an NRC/Center/University of Arizona meeting in Tucson. Recent advances on the stochastic approach were also discussed at the same meeting, and R. Ababou gave a seminar on the "Spatial and Statistical Structure of 3D Groundwater Flow in Random Porous Media" (Department of Hydrology and Water Resources, University of Arizona, Tucson, February 28, 1990).

It is emphasized that the two sets of experiments (Las Cruces and Apache Leap site) are different in many respects, except perhaps for their field scales. Each has its advantages and drawbacks. The Las Cruces strip-source trench experiments occur in nonfractured unconsolidated soil and are relatively easy to interpret. The more complex Apache Leap borehole experiments (currently being redesigned) will be conducted in fractured tuff. The results from the Apache Leap site will perhaps be more difficult to integrate into a model-validation exercise. They will provide, however, a wealth of in-situ data, including currently available fracture trace exposures and

core data as well as laboratory flow-transport experiments on cores and fractured blocks that may possibly be used for sub-model validation. Apart from these two experimental sites, hydraulic data from the G-Tunnel experimental facility near Yucca Mountain are also available. Since site-specific data will necessarily be scarce, there is a great need for correlating various experimental results obtained at different sites, including other sites than the few mentioned above.

The rationale for exploiting data that are only indirectly relevant to the specific site will be to rely on qualitatively reasonable hydrogeologic analogies (by proxy) and to utilize physical models whereby statistical correlations among easily measurable parameters and less accessible parameters can be explicitly identified. Along these lines, a model is presently being developed that clearly indicates the effects of certain cross correlations in the general case of randomly heterogeneous, and possibly fractured, porous formations. The significance of this work is, first, that correlations among spatially variable parameters may help reduce the uncertainty of model outputs and, second, that the simulated flow and transport patterns will be more realistic if the correct correlations are taken into account. A more detailed summary of this research will be appended to the next quarterly report.

The third activity mentioned earlier was to resolve some concrete technical issues to ensure the computational feasibility of the project. It is anticipated that the stochastic flow and transport models will be computationally intensive and that large three-dimensional datasets will need to be processed. For these reasons, a NASA grant was proposed for Cray-2 supercomputer time on November 1, 1989, and it has recently been accepted. A total of 150 equivalent CPU hours of Cray-2 has been made available for a period of one year. The *Stochastic Flow and Transport Project Plan* is being revised accordingly to reflect the additional resources provided by the NASA grant. In addition, the Center is also developing computer-graphics capabilities. The Dynamic Graphics Interactive Volumetric Modeling software running on a Silicone Graphics workstation was used to visualize large three-dimensional pressure and moisture data from Cray-2 simulations of stochastic unsaturated flow, as previously generated by the saturated/unsaturated BIGFLOW code (1).

For example, the attached color plates (Figure 6-1 and Figure 6-2) depict three-dimensional views of transient moisture plumes after ten days of strip-source infiltration. The particular flow conditions were originally selected to mimic the first Las Cruces trench experiment. Another goal was to test theoretical predictions concerning the pressure-dependent anisotropy of the effective hydraulic conductivity for an imperfectly stratified, three-dimensional random porous matrix. The random stratification leads to horizontal spreading of the marginally wet moisture front, as can be seen on the color plates, in full three-dimensional space. The amount of detail in this simulation helps capture the heterogeneity of the moisture pattern over a wide range of scales. The horizontal spread is not uniform; layers have holes, and wet lenses or horizontal "tongues" tend to remain suspended over dryer lenses of soil. These results are encouraging, and suggest the feasibility of developing similar computer simulations and data processing techniques for studying the Yucca Mountain unsaturated flow system.

The fourth and last activity listed concerned numerical analyses. The key numerical difficulties to be expected in a project of this nature are (1) the highly nonlinear nature of the unsaturated flow problem; (2) the highly heterogeneous, discontinuous nature of the geologic formation; and (3) the complex nonlinear interactions that occur among the various components of the heterogeneous system. The nonlinearly coupled processes are typically characterized by distinct space-time scales, e.g., matrix flow and fracture flow. A paper focusing on the numerical difficulty of the unsaturated flow equation will be presented by R. Ababou at the VIIIth International Conference on Computational Methods in Water Resources, Venice, Italy, June 1990, under the title "Numerical Analysis of Nonlinear Unsaturated Flow Equations." The paper focuses on nonlinearity and the competition between capillary diffusion and gravity-driven flow. Future work will likely focus on efficient ways to include fractures and to improve the time-stepping and nonlinear solution algorithms by taking into account certain specific features of unsaturated flow.

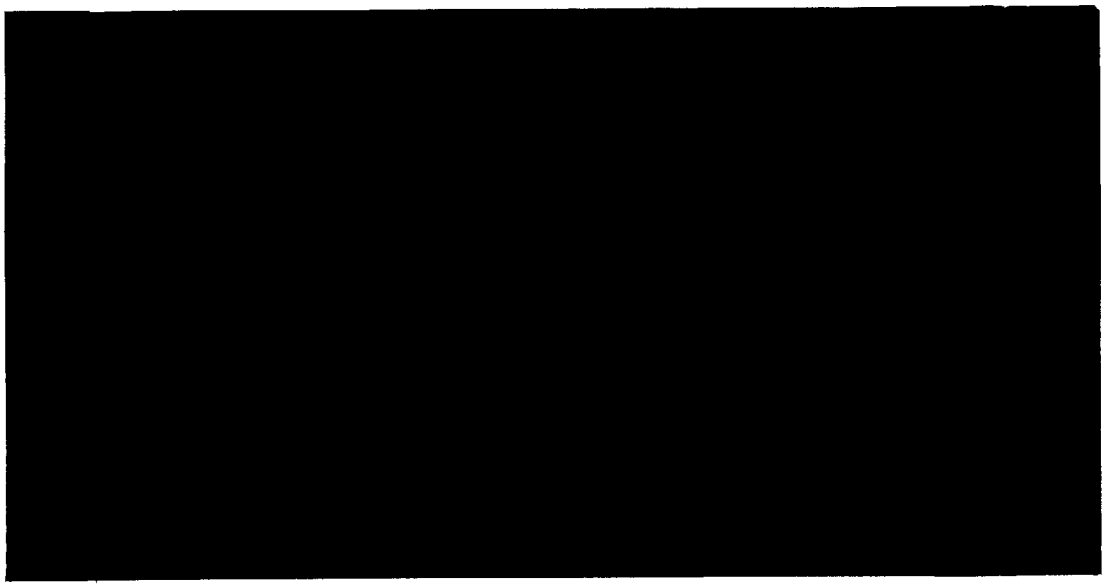

Figure 6-1. Front view of three-dimensional moisture plume from stochastic flow simulations of Ababou (1988)

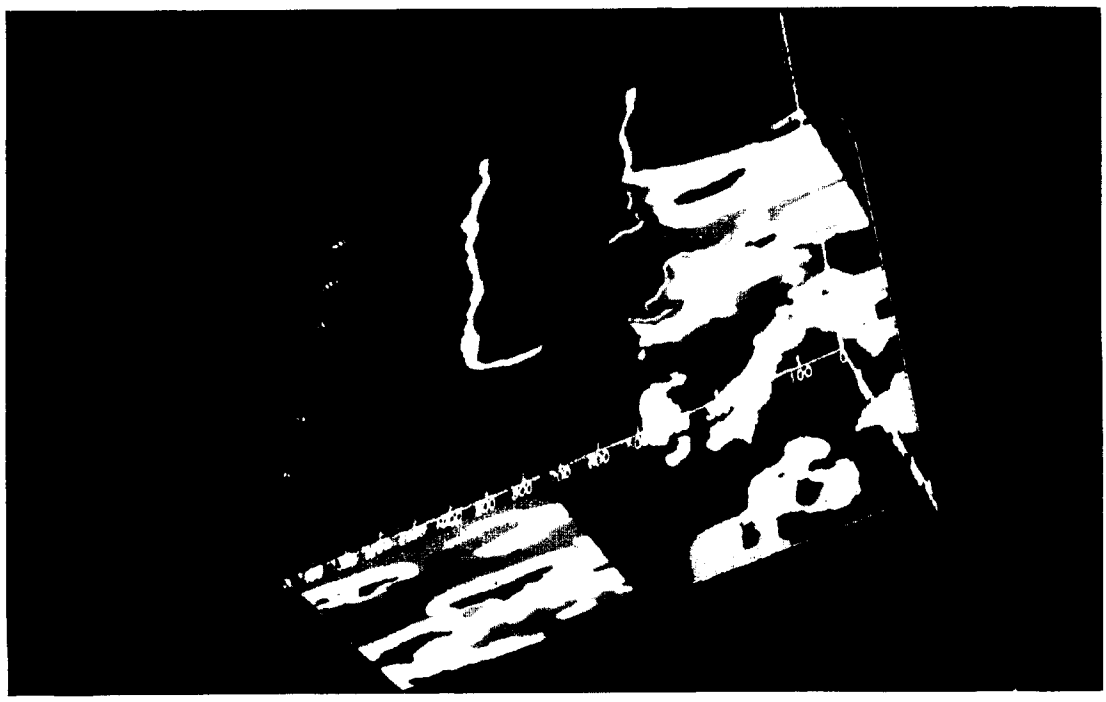

Figure 6-2. Back view of three-dimensional moisture pattern, with moisture plume visible in purple and blue (simulations from Ababou, 1988)

Robustness and adaptivity will be needed for these algorithms to be efficient in the case of highly contrasted or nearly discontinuous hydrodynamic coefficients, as occurs in fractured porous media.

The research and its by-products are to be integrated with and utilized in performance assessment activities. Indications of future work along these lines were presented by R. Ababou under the title "Large-Scale Unsaturated Flow and Groundwater Travel Times: Synthetic and Conditional Experiments" at the First Performance Assessment NRC Workshop, Washington, D.C., February 15-16, 1990. The level of effort and integration are being defined, in part, based on the MOU Phase I results obtained by the NRC staff.

6.3 REFERENCE

Ababou, R. 1988. *Three-Dimensional Flow in Random Porous Media*. Ph.D. Dissertation, 2 vols. Boston, Massachusetts: Massachusetts Institute of Technology:1-833.

7. GEOCHEMICAL NATURAL ANALOGS

by English C. Pearcy and William M. Murphy

Investigators: English C. Pearcy and William M. Murphy

7.1 TECHNICAL OBJECTIVES

The objectives of the Geochemical Analog of Contaminant Transport in Unsaturated Rock Project are:

(1) To obtain a knowledge of the state of the art in natural analog studies applied to contaminant transport and to participate in a workshop on the use of natural analogs for identification of significant processes and events and for validation of performance-assessment modeling. The literature review and workshop will permit identification of principles for the effective application of geochemical natural analog studies to the HLW repository problem at Yucca Mountain. Conclusions are to be reached through the literature review and workshop to guide research on a natural analog system in the latter stages of the project.

(2) To design and undertake a geochemical natural analog study of contaminant transport relevant to the proposed repository in the unsaturated zone at Yucca Mountain. Fundamental new data will be obtained to improve the understanding of particular processes and events affecting contaminant transport in unsaturated media. The research also will demonstrate a methodology in which data from nature are used to guide site-characterization activities and to validate predictive models for geochemical transport, particularly at time and space scales generally inaccessible in laboratory studies.

The specific tasks to be performed in the Geological Analog of Contaminant Transport in Unsaturated Rock Project are:

(1) Task 1 - Literature Review and Workshop

(2) Task 2 - Identification of Site and Development of a Work Plan

(3) Task 3 - Development of Methodology and Data Acquisition

(4) Task 4 - Interpretation of Data and Modeling

7.2 ASSESSMENT OF THE LITERATURE

In the second quarter of FY90, literature was examined for references on geochemical natural analogs using criteria to determine pertinent publications. These criteria (posed as questions) included: (1) What sites have been the subjects of previous study? (2) What methods have been used and with what success? (3) What geochemical processes are amenable to natural analog study and with what degree of resolution? and (4) What sites would constitute good analogs of conditions at Yucca Mountain?

Progress in Task 1 includes searches of the electronic databases GEOREF, GEOARCHIVE, GEOBASE, CHEM ABSTRACTS, and NTIS using keywords which delimit many investigations of natural analogs. Bibliographies from volumes of the *CEC Natural Analog Working Group Proceedings* recently published have also provided many pertinent references. References also have been obtained from journal articles and books. A total of 223 germane references have been identified. Of these 223, hard copies of 109 have been obtained, and 35 have been reviewed by W. Murphy and E. Pearcy. Appendix A lists the references identified to date with those reviewed marked with an asterisk.

APPENDIX A

ASSESSMENT OF THE LITERATURE FOR GEOCHEMICAL NATURAL ANALOGS

ASSESSMENT OF THE LITERATURE FOR GEOCHEMICAL NATURAL ANALOGS

Australian Atomic Energy Commission (AAEC). 1986. The Alligator Rivers analogue project: Proposed international project on analogues of radioactive waste repositories. Lucas Heights, Australia: AAEC.

Airey, P. L. 1986. Radionuclide migration around uranium ore bodies in the Alligator Rivers region of the Northern Territory of Australia: Analogue of radioactive waste repositories, a review. *Chemical Geology* 55(3-4):255-268.

Airey, P. L. 1987. Application of natural analogue studies to the long-term prediction of far-field migration at repository sites. *Commission of the European Communities (CEC) Natural Analogues in Radioactive Waste Disposal: A Symposium*. Come, B., and N. Chapman, eds. Brussels: CEC:32-41.

Airey, P. L., P. Duerden, D. Roman, C. Golian, T. Nightingale, T. Payne, B. Davey, and D. Gray. 1987. The Koongarra ore body: A natural analogue of radionuclide migration in the far field of HLW repositories. *Commission of the European Communities Natural Analogues in Radioactive Waste Disposal: A Symposium*. Come, B., and N. Chapman, eds. Brussels: CEC:175-215.

Airey, P. L., P. Duerden, D. Roman, C. Golian, T. Nightingale, T. Payne, B. G. Davey, D. Gray, A. Snelling, and D. Lever. 1987. The prediction of the long-term migration of radionuclides in the far field of high level waste repositories: Results from the Alligator Rivers natural analogue study. *The Geological Disposal of High Level Radioactive Wastes*. Greece: Theophrastus:507-524.

Airey, P. L., P. Duerden, D. Roman, G. Golian, T. Nightingale, T. Payne, B. G. Davey, D. Gray, J. Fabryka-Martin, D. B. Curtis, A. Snelling, D. A. Lever, and P. J. Shirvington. 1987. Radionuclide migration around uranium ore bodies: Analogue of radioactive waste repositories. NUREG/CR-5040, AAEC/C55. Lucas Heights, Australia: AAEC.

Airey, P. L., C. Golian, and D. A. Lever. 1987. An approach to the mathematical modelling of the uranium series redistribution within ore bodies. NUREG/CR-5060, AAEC/C49. Lucas Heights, Australia: AAEC.

Airey*, P. L. 1985. The role of natural analogs in modelling for field transport of radionuclides. *Commission of the European Communities Natural Analog Working Group, First Meeting*. Come, B., and N. Chapman, eds. Brussels: CEC.

Airey*, P. L., and M. Ivanovich. 1985. Geochemical analogs of high level radioactive waste repositories. B. Come and N. Chapman, eds. *Commission of the European Communities Natural Analog Working Group, First Meeting*. Brussels: CEC.

Alexander, W. R., R. D. Scott, A. B. MacKenzie, and I. G. McKinley. 1988. A natural analog study of radionuclide migration in a water-conducting fracture in crystalline rock. *Radiochimica Acta* 44-45:283-289.

Alexander*, W. R., R. D. Scott, A. B. MacKenzie, and I. G. McKinley. 1987. Natural analog studies at Grimsel, southern Switzerland. *Commission of the European Communities Natural Analogues in Radioactive Waste Disposal: A Symposium*. Come, B., and N. Chapman, eds. Brussels: CEC:473-484.

Alterescu, S. 1987. Leaching of natural and nuclear waste glasses in sea water: Progress report. CY 85, 86, and 87. DOE/ET/47927-T2. Greenville, Maryland: NASA Goddard Space Flight Center/Dept. of Energy.

Ames, L. L., J. E. McGarrah, and B. A. Walker. 1983. Sorption of trace constituents from aqueous solutions onto secondary minerals: I. Uranium. *Clays and Clay Mineralogy* 31:321-334.

Ames, L. L., J. E. McGarrah, and B. A. Walker. 1983. Sorption of trace constituents from aqueous solutions onto secondary minerals: II. Radium. *Clays and Clay Mineralogy* 31:335-342.

**Amter, S. 1989. Natural analogues. *Engineering Geology* 26(4):431-440.

Andrews, R. W., and F. J. Pearson, Jr. 1984. Transport of 14C and uranium in the Carrizo Aquifer of South Texas: A natural analog of radionuclide migration. G. L. McVay, ed. *Materials Research Society Symposia Proceedings* 26. Boston, Massachusetts: Mat. Res. Soc.:1085-1092.

Apt, K. E., J. P. Balagna, E. A. Bryant, G. A. Cowan, W. R. Daniels, R. J. Vidale, and D. G. Brookins. 1978. Search for other natural fission reactors. Vienna: International Atomic Energy Agency (IAEA):677.

Astudillo, J. 1988. Spanish activities in the field of natural analogues. *Commission of the European Communities Natural Analogue Working Group, Third Meeting*. Come, B., and N. Chapman, eds. Snowbird, Utah: CEC:119-125.

Barretto, P. M., and K. Fujimori. 1986. Natural analogue studies: Geology and mineralogy of Morro do Ferro, Brazil. *Chemical Geology* 55(3-4):297-312.

Birchard, G. F., and D. H. Alexander. 1983. Natural analogues: A way to increase confidence in predictions of long-term performance of radioactive waste disposal. *Scientific Basis for Nuclear Waste Management VI*. Brookins, D. G., ed. Boston, Massachusetts: Elsevier:323-329.

Bouska, V. 1978. An ancient natural uranium reactor. *Geol. Pruzkum.* 20(4):121.

Bowie, S. H. U. 1970. World uranium deposits. *Uranium Exploration Geology: Proceedings of a Panel on Uranium Exploration Geology*. Vienna: IAEA:23-33.

Brondi, A. 1985. Italian activity in the field of natural analogues and natural evidence. *Commission of the European Communities Natural Analogue Working Group, First Meeting*. Come, B., and N. Chapman, eds. Brussels: CEC:112-128.

Brookins, D. G. 1976. Oklo phenomenon: Geological and nuclear aspects. *American Association of Petroleum Geologists (AAPG) Bulletin* 60(8):1391. Tulsa, Oklahoma: AAPG.

Brookins, D. G. 1976. Shale as a repository for radioactive waste: The evidence from Oklo. *Environmental Geology* 1:255-259.

Brookins, D. G. 1978. In Paris: Oklo reactor re-analyzed. *Geotimes* 23(3):27-28.

Brookins, D. G. 1979. Thermodynamic considerations underlying the migration of radionuclides in geomedia: Oklo and other examples. *Scientific Basis for Nuclear Waste Management*. New York: Plenum Press:355.

Brookins, D. G. 1983. Migration and retention of elements at the Oklo natural reactor. *Environmental Geology* 4:201-208.

Brookins, D. G. 1984. *Geochemical Aspects of Radioactive Waste Disposal.* New York: Springer-Verlag:1-347.

Brookins, D. G. 1984. Natural analogs. *Geochemical Aspects of Radioactive Waste Disposal.* New York: Springer-Verlag:197-231.

Brookins, D. G. 1986. Natural analogues for radwaste disposal: Elemental migration in igneous contact zones. *Chemical Geology* 55(3-4):337-344.

Brookins, D. G. 1987. Igneous contact zones: Natural analogs for high level radwaste disposal. *The Geological Disposal of High Level Radioactive Wastes.* Greece: Theophrastus:545-553.

Brookins, D. G. 1988. Radionuclide behavior at the Oklo natural reactor. Oak Ridge National Laboratory (ORNL) Technical Report, Vol. 10501. Oak Ridge, Tennessee: ORNL:1-178.

Brookins, D. G. 1988. Some natural analog studies for radioactive waste disposal in sedimentary rocks. Oak Ridge National Laboratory Technical Report, Vol. 72. Oak Ridge, Tennessee: ORNL1-72.

Brookins, D. G., M. S. Abashian, L. H. Cohen, and A. Williams. 1983. Natural analogues: Alamosa River monzonite intrusive into tuffaceous and andesitic rocks. *Scientific Basis for Nuclear Waste Management VI.* Brookins, D. G., ed. Boston, Massachusetts: Elsevier:299-306.

Brookins, D. G., M. S. Abashian, L. H. Cohen, and H. A. Wollenberg. 1982. Radwaste storage in crystalline rocks: A natural analog. *Proceedings of International Symposium on Migration in the Terrestrial Environment of Long-Lived Radionuclides from the Nuclear Fuel Cycle.* Organized by the International Atomic Energy Agency (IAEA), the Commission of the European Communities, and the OECD Nuclear Energy Agency. Conference held in Knoxville, Tennessee. Vienna: IAEA:775-782.

Brookins*, D. G. 1987. Natural and archeological analogs: A review. *Commission of the European Communities Natural Analogues in Radioactive Waste Disposal: A Symposium.* Come, B., and N. Chapman, eds. Brussels: CEC.

Brookins*, D. G. 1987. Sandstone uranium deposits: Analogs for SURF disposal in some sedimentary rocks. *Commission of the European Communities Natural Analogues in Radioactive Waste Disposal: A Symposium.* Come, B., and N. Chapman, eds. Brussels: CEC.

Cadelli, N. 1987. Natural analogues and performance assessments: A point of view based on the PAGIS experience. *Commission of the European Communities Natural Analogues in Radioactive Waste Disposal: A Symposium.* Come, B., and N. Chapman, eds. Brussels: CEC:3-11.

Cathles, L. M. 1988. Modeling the fluid flow responsible for primary mineralization at Pocos de Caldas, Osamu Utsumi uranium mine, Brazil. *Commission of the European Communities Natural Analogue Working Group, Third Meeting.* Come, B., and N. Chapman, eds. Snowbird, Utah: CEC:190-192.

Cathles, L. M. 1988. Perspectives from industrial scale natural analogues. *Commission of the European Communities Natural Analogue Working Group, Third Meeting.* Come, B., and N. Chapman, eds. Snowbird, Utah: CEC:220-226.

Chapman, N. 1985. Analogue of elemental diffusion over 5000 years in sediments: Close but not close enough? *Commission of the European Communities Natural Analogue Working Group, First Meeting.* Come, B., and N. Chapman, eds. Brussels: CEC:157-159.

Chapman, N. A., ed. 1985. Mass transport to deep environments: Radioactive waste burial and its natural analogues. *3rd Deep Geology Natural Workshop*. Durham, U.K.: Environmental Resource Council.

Chapman, N. A., I. G. McKinley, and J. A. T. Smellie. 1984. *The Potential of Natural Analogues in Assessing Systems for Deep Disposal of High-Level Radioactive Waste*. NTB 84-41, KBS 84-16, Eir Ber 545. Swedish Nuclear Fuel and Waste Management Co. (SKB) and the Swiss Radioactive Waste Cooperative (NAGRA).

Chapman, N. A., and J. A. T. Smellie. 1986. Natural analogues to the conditions around a final repository for high-level radioactive waste. *Chemical Geology*:1-55.

Chapman*, N. A. 1988. Natural analogue studies in the CEC MIRAGE-2 programme (1985-1989): A review of progress to January 1988. *Commission of the European Communities Natural Analogue Working Group, Third Meeting*. Come, B., and N. Chapman, eds. Snowbird, Utah: CEC:26-42.

Cohen, J. J., and C. F. Smith. 1982. Validation of predictive models for geologic disposal of radioactive waste via natural analogs. *Proceedings of the Symposium on Uncertainties Associated with the Regulation of the Geologic Disposal of High-Level Radioactive Waste*. Kocher, D. C., ed. NUREG/CP-OO22; CONF-810372. Washington, D.C.: NRC:215-221.

Cowan, G. A., ed. 1976. A natural fission reactor. *Scientific American* 235(1):36-47.

Cowan, G. A. 1978. Migration paths for Oklo reactor products and applications to the problem of geological storage of nuclear waste. *Les Reacteurs de Fission Naturels*. Vienna: IAEA:693.

Cowan, R., and R. C. Ewing. 1989. Freshwater alteration of basaltic glass, Hanauma Bay, Oahu, Hawaii: A natural analogue for the alteration of borosilicate glass in fresh water. *Materials Research Society Symposium Proceedings*. Boston, Massachusetts: Mat. Res. Soc. 127:49-56.

Cramer, J. J. 1986. A natural analog for a fuel waste disposal vault. *Second International Conference on Radioactive Waste Management*. Rosinger, E. L., ed. Winnipeg, Canada: Canadian Nuclear Society:697-702.

Cramer, J. J. 1986. Sandstone-hosted uranium deposits in northern Saskatchewan as natural analogs to nuclear fuel waste disposal vaults. *Chemical Geology* 55(3-4):269-279.

Cramer*, J. J. 1985. Cigar Lake project: A U-deposit natural analog. *Commission of the European Communities Natural Analog Working Group, First Meeting*. Come, B., and N. Chapman, eds. Brussels: CEC.

Cramer*, J. J. 1988. Natural analogue studies on the Cigar Lake uranium deposit: An update. *Commission of the European Communities Natural Analogue Working Group, Third Meeting*. Come, B., and N. Chapman, eds. Snowbird, Utah: CEC:50-56.

Cramer*, J. J., P. Vilks, and J. P. A. Larocque. 1987. Near-field analog features from the Cigar Lake uranium deposit. *Commission of the European Communities Natural Analogues in Radioactive Waste Disposal: A Symposium*. Come, B., and N. Chapman, eds. Brussels: CEC:59-72.

Crisman, D. P., and G. K. Jacobs. After 1982. Native copper deposits of the Portage Lake Volcanics, Michigan: Their implications with respect to canister stability for nuclear waste isolation in the Columbia River Basalts beneath the Hanford Site, Washington. RHO-BW-ST-26 P, Contract DE-AMO6-76-RLO2225. Washington, D.C.: Department of Energy (DOE).

Cross, J. E., A. Haworth, I. Neretnieks, S. M. Sharland, and C. J. Tweed, eds. 1989. Modelling of redox front and uranium movement in a uranium mine at Pocos de Caldas. *Migration '89*. Monterey, California:21.

Curtis, D. B. 1986. Geochemical controls on 99Tc transport and retention. *Chemical Geology* 55(3-4):227-231.

Curtis, D. B., T. M. Benjamin, and A. J. Gancarz. 1981. The Oklo reactors: Natural analogs to nuclear waste repositories. *The Technology of High-Level Nuclear Waste Disposal; Advances in the Science and Engineering of the Management of High-Level Nuclear Wastes*. DOE/TIC-4621, DE82009594:255-283. Washington, D.C.: DOE.

Curtis, D. B., T. M. Benjamin, A. J. Gancarz, R. Loss, K. Rosman, J. Delaeter, J. E. Delmore, and W. Maeck. 1987. Geochemical controls on the retention of fission products at the Oklo natural fission reactors. *Commission of the European Communities Natural Analogues in Radioactive Waste Disposal: A Symposium*. Come, B., and N. Chapman, eds. Brussels: CEC:140-141.

Curtis, D. B., J. H. Cappis, R. E. Perrin, D. J. Rokop, and J. T. Fabryka-Martin. 1987. The geochemistry of natural technetioum and plutonium. *Commission of the European Communities Natural Analogues in Radioactive Waste Disposal: A Symposium*. Come, B., and N. Chapman, eds. Brussels: CEC:354-355.

De Laeter, J. R. 1985. The Oklo reactors: Natural analogues to nuclear waste repositories. *Search* 16(7-8):193-196.

De Laeter, J. R., K. J. R. Rosman, and C. L. Smith. 1980. The Oklo natural reactor: Cumulative fission yields and retentivity of the symmetric mass region fission products. *Earth and Planetary Science Letters* 50:238-246.

de Marsily, G. 1985. A modeller's viewpoint on the possible use of analogues for flow and transport. *Commission of the European Communities Natural Analogue Working Group, First Meeting*. Come, B., and N. Chapman, eds. Brussels: CEC:1-39.

Degueldre, C. A. 1987. In-laboratory, on-site, in-situ sampling and characterization of Grimsel colloids: Phase I. *Commission of the European Communities Natural Analogues in Radioactive Waste Disposal: A Symposium*. Come, B., and N. Chapman, eds. Brussels: CEC:409-419.

DOE. 1989. Geological systems as natural analogs for radioactive waste repositories. January 1976-May 1989 (Citations from the Energy Database):1-68.

Doi, K., S. Hirono, and Y. Sakamaki. 1975. Uranium mineralization by ground water in sedimentary rocks. *Japan. Economic Geology* 70:628-646.

Dongarra, G. 1984. Geochemical behaviour of uranium in the supergene environment. *Uranium Geochemistry, Mineralogy, Geology, Exploration and Resources*. England: The Institution of Mining and Metallurgy:18-22.

Doumas, C., and L. Papazoglou. 1980. Santorini tephra from Rhodes. *Nature* 287:322-324.

Dran, J. C. 1975. A multidisciplinary analysis of the Oklo uranium ores. *The Oklo Phenomenon*. Vienna: IAEA:223-234.

Duerden, P., ed. 1988. Alligator Rivers Analogue Project - Progress Report: May 1988 - August 1988. Australia: Australian Nuclear Science and Technology Organization (ANSTO):1-270.

Duerden, P., C. Golian, C. J. Hardy, T. Nightengale, and T. Payne. 1987. Alligator Rivers analogue project: Review of research and its implication for model validation. *Commission of the European Communities Natural Analogues in Radioactive Waste Disposal: A Symposium*. Come, B., and N. Chapman, eds. Brussels: CEC:82-91.

Duffield, J. R., L. Xu, and D. R. Williams. 1988. Chemical speciation modeling of the South Terras and Madeira Abyssal Plain natural analogue sites. DOE-RW-87.128, APCM-56. United Kingdom: Department of the Environment.

Duffy, C. J., ed. 1978. Uranium solubilities in the Oklo reactor zones. *Les Reacteurs de Fission Naturels*. Vienna: IAEA:229.

Dunn, C. 1980. The biochemical expression of deeply buried uranium mineralization in Saskatchewan, Canada. *Developments in Economic Geology - Geochemical Exploration 1980*:437-452.

Durrand, C., D. Le Gressus, and D. Massignon. 1975. A multidisciplinary analysis of the Oklo uranium ores. *The Oklo Phenomenon*. Vienna: IAEA:223.

Durrani, S. A., K. A. R. Khazal, S. R. Malik, J. H. Fremlin, and G. Hendry. 1975. Thermoluminescence and fission-track studies of the Oklo fossil reactor materials. *The Oklo Phenomenon*. Vienna: IAEA:207-222.

Dymkov, Y. M., Y. G. Pavlov, and Y. N. Zav'yalov. 1979. Phase composition and morphogenetic features of uraninite from the Oklo reactor, Gabon. *Geochemistry International* 16(1):113-124.

Edghill, R. 1988. Colloids in Koongarra groundwater. ANSTO Alligator Rivers Analogue Project - Progress Report, May 1988-August 1988. Australia: ANSTO:245-252.

Edghill, R., and B. G. Davey. 1988. Alpha activity and mineralogy associations. ANSTO Alligator Rivers Analogue Project - Progress Report, May 1988-August 1988. Australia: ANSTO:147-156.

Eisenberg, N. A. 1986. Natural analogues and validation of performance assessment models. *Chemical Geology* 55(3-4):189-201.

Eisenbud, M., K. Krauskopf, E. P. Franca, W. Lei, R. Ballad, and P. Linsalata. 1984. Natural analogs for the transuranic actinide elements: An investigation in Minas Gerais, Brazil. *Environmental Geology and Water Science* 6(1):1-9.

Elders*, W. A. 1987. A natural analog for near-field behaviour in a high level radioactive waste repository in salt: The Salton Sea geothermal field, California, USA. *Commission of the European Communities Natural Analogues in Radioactive Waste Disposal: A Symposium*. Come, B., and N. Chapman, eds. Brussels: CEC.

Escalier, P. 1988. French radioactive wastes performance assessment and the natural analogues approach: An overview. *Commission of the European Communities Natural Analogue Working Group, Third Meeting, Snowbird, Utah*. Come, B., and N. Chapman, eds. Brussels: CEC:193-202.

Ewing, R. C., and M. J. Jercinovic. 1987. Natural analogues: Their application to the prediction of the long-term behavior of nuclear waste forms. *Materials Research Society Symposia Proceedings*. Boston, Massachusetts: Mat. Res. Soc. 84:67-83.

Fabryka-Martin, J. T., D. Roman, P. L. Airey, D. Elmore, and P. W. Kubik. 1987. Redistribution of natural iodine 129 among mineral phases and groundwaters in the Koongarra uranium ore deposit, N.T., Australia. *Commission of the European Communities Natural Analogues in Radioactive Waste Disposal: A Symposium*. Come, B., and N. Chapman, eds. Brussels: CEC:374-385.

Frejacques, C., and R. Hageman, eds. 1976. Conclusions from studies of Oklo natural reactors. *International Symposium on the Management of Wastes from the LWR fuel Cycle*. Washington, D.C.: Energy Research Development Administration:68-69.

Gancarz, A. J., ed. 1978. U-Pb age (2.05e+9) of the Oklo uranium deposit. *Natural Fission Reactors, Paris, 1977, Panel Proceedings Series*. Vienna: IAEA:513-520.

Gancarz, A., G. Cowan, D. Curtis, and W. Maeck. 1980. 99Tc, Pb and Ru migration around the Oklo natural fission reactors. *Scientific Basis for Nuclear Waste Management*. New York: Plenum Press:601-608.

Gascoyne*, M. 1987. The use of uranium-series disequilibrium for site characterization and as an analog for actinide migration. *Commission of the European Communities Natural Analogues in Radioactive Waste Disposal: A Symposium*. Come, B., and N. Chapman, eds. Brussels: CEC.

Giblin, A. M., ed. 1980. The role of clay adsorption in genesis of uranium ores. *Proceedings of the International Symposium on the Pine Creek Geosyncline, Panel Proceedings Series III*. Vienna: IAEA:521-529.

Girardi, F., and M. D'Alessandro. 1988. Applicability and perspectives of natural analogues as demonstration of Pagis models. *Commission of the European Communities Natural Analogue Working Group, Third Meeting, Snowbird, Utah*. Come, B., and N. Chapman, eds. Brussels: CEC:145-158.

Glasbergen, P. 1987. Hydrological studies and natural isotope data as indication for ground-water flow in deep sedimentary basins. *Commission of the European Communities Natural Analogues in Radioactive Waste Disposal: A Symposium*. Come, B., and N. Chapman, eds. Brussels: CEC:420-435.

Golian, C., and P. Duerden. 1987. Application of open-system modelling to studies of secondary mineralization (Koongarra) and rock matrix diffusion (Krakemala). *Commission of the European Communities Natural Analogues in Radioactive Waste Disposal: A Symposium*. Come, B., and N. Chapman, eds. Brussels: CEC:328-341.

Golian, C., M. Ivanovich, D. A. Lever, and G. Longworth. 1988. Modelling radionuclide migration in the Koongarra ore deposit. ANSTO Alligator Rivers Analogue Project - Progress Report, May 1988 - August 1988. Australia: ANSTO:65-68.

Goodell, P. C. 1981. Geology of the Pena Blanca uranium deposits, Chihuahua, Mexico. *American Association of Petroleum Geologists - Studies in Geology* 3. Mexico: AAPG:275-292.

Goodwin, B. W., J. J. Cramer, and D. B. McConnell. 1988. The Cigar Lake uranium deposit: An analogue for nuclear fuel waste disposal. *Commission of the European Communities Natural Analogue Working Group, Third Meeting, Snowbird, Utah*. Come, B., and N. Chapman, eds. Brussels: CEC:180-189.

Grambow, B., M. J. Jercinovic, R. C. Ewing, and C. D. Byers. 1985. Weathered basalt glass: A natural analogue for the effects of reaction progress on nuclear waste glass alteration. *Materials Research Society Symposia Proceedings*. Boston, Massachusetts: Mat. Res.Soc. 50:263-272.

Grandstaff, D. E. 1976. A kinetic study of the dissolution of uraninite. *Economic Geology* 71:1493-1506.

Green, D. C., and V. A. Guthrie. 1987. Natural mineral analogues from a hydrothermally altered granite. *Commission of the European Communities Natural Analogues in Radioactive Waste Disposal: A Symposium*. Come, B., and N. Chapman, eds. Brussels: CEC:436-441.

Griffault, L., M. Iebrak, B. Lemiere, P. Piantone, and J. F. Sureau. 1987. Hydrothermal alteration systems as analogues of nuclear waste repositories in granitic rocks. *Commission of the European Communities Natural Analogues in Radioactive Waste Disposal: A Symposium*. Come, B., and N. Chapman, eds. Brussels: CEC:191-204.

Haaker, R. F., and R. C. Ewing. 1981. Natural analogues for crystalline radioactive waste forms, Part II: Non-Actinide Phases. *Proceedings of the Third International Symposium on the Scientific Basis for Nuclear Waste Management*. Moore, J. G., ed. Boston, Massachusetts: Plenum Press:299-306.

Hallberg*, R. O., P. Ostlund, and T. Wadsten. 1987. A 17th century bronze cannon as analogue for radioactive waste disposal. *Commission of the European Communities Natural Analogues in Radioactive Waste Disposal: A Symposium*. Come, B., and N. Chapman, eds. Brussels: CEC.

Hammer, C. U., H. B. Clausen, W. L. Friedrich, and H. Tauber. 1987. The Minoan eruption of Santorini in Greece dated to 1645 BC? *Nature* 328(6):517-519.

Hardy*, C. J., and P. Duerden. 1988. Progress in the Alligator Rivers analogue project. *Commission of the European Communities Natural Analogue Working Group, Third Meeting, Snowbird, Utah*. Come, B., and N. Chapman, eds. Brussels: CEC:43-49.

Haverslew, B., and H. Y. Tammemagi. 1985. Geochemical analysis of core from a geothermal anomaly. INFO-0155. Ottawa: Atomic Energy Control Board.

Heiken, G., and F. McCoy, Jr. 1984. Caldera development during the Minoan eruption, Thira, Cyclades, Greece. *Journal of Geophysical Research* 89(B10):8441-8462.

Herzog, F. 1987. Modelling isotope distributions in borecores. *Commission of the European Communities Natural Analogues in Radioactive Waste Disposal: A Symposium*. Come, B., and N. Chapman, eds. Brussels: CEC:239-248.

Hodgkinson, D., and D. Lever. 1985. Natural analogues for radioactive waste burial: A modelling perspective. *Commission of the European Communities Natural Analogue Working Group, First Meeting*. Brussels: CEC:15-31.

Hofman, B., J. P. Dearlove, M. Ivanovich, D. A. Lever, D. C. Green, P. Baertschi, and T. Peters. 1987. Evidence of fossil and recent diffusive element migration in reduction haloes from Permian red-beds of nothern Switzerland. *Commission of the European Communities Natural Analogues in Radioactive Waste Disposal: A Symposium*. Come, B., and N. Chapman, eds. Brussels: CEC:217-238.

Hooker, P. J. 1988. The U.K. natural analogues programme. *Commission of the European Communities Natural Analogue Working Group, Third Meeting, Snowbird, Utah*. Come, B., and N. Chapman, eds. Brussels: CEC:88-95.

Hooker, P. J., and N. A. Chapman. 1987. UK (United Kingdom) natural analogue co-ordinating group: First annual report. DOE-RW-88.036. United Kingdom: Department of the Environment.

Hooker, P. J., A. B. MacKenzie, R. D. Scott, M. Ivanovich, T. K. Ball, I. R. Basham, A. J. Bloodworth, and P. D. Roberts. 1986. Natural analogues of radionuclide migration: Reconnaissance study of sites. FLPU 86-6. British Geological Survey.

Hooker*, P. J., N. A. Chapman, A. B. MacKenzie, R. D. Scott, and M. Ivanovich. 1987. Natural analogues of radionuclide migration in sediments in Britain. *Commission of the European Communities Natural Analogues in Radioactive Waste Disposal: A Symposium*. Come, B., and N. Chapman, eds. Brussels: CEC.

Ildefonse*, P., J. P. Muller, B. Clozel, and G. Calas. 1989. A natural analogue of waste repository in tuff: Evaluation of radionuclide migration by secondary alteration minerals, radiation induced defects and dose rate estimation. *Geological Society of America Abstracts with Programs* 21(6):A20.

Ivanovich, M. 1985. Evidence for field measurements of retardation factors for U/Th/Ra radionuclides. *Commission of the European Communities Natural Analogue Working Group, First Meeting*. Come, B., and N. Chapman, eds. Brussels: CEC:129-132.

Ivanovich*, M., P. Duerden, T. Payne, T. Nightingale, G. Longworth, M. A. Wilkins, R. B. Edghill, D. J. Cockayne, and B. G. Davey. 1987. Natural analog study of the distribution of uranium series radionuclides between the colloid and solute phases in the hydrogeological system of the Koongarra uranium deposit N.T., Australia. *Commission of the European Communities Natural Analogues in Radioactive Waste Disposal: A Symposium*. Come, B., and N. Chapman, eds. Brussels: CEC:300-313.

Jakubick*, A. T., and W. Church. 1986. Oklo natural reactors: Geological and geochemical conditions - A review. Research Report. Ottawa: Atomic Energy Control Board (Canada):1-53.

Jantzen, C. M. 1986. Prediction of nuclear waste glass durability from natural analogs. *Advances in Ceramics* 20:703-712.

Jercinovic, M. J., R. C. Ewing, and N. S. Criepi. 1987. Basaltic glasses from Iceland and the deep sea: Natural analogues to borosilicate nuclear waste-form glass. SKB-JSSP-TR-88-01. Svensk Kaernbraenslefoersoerjning A.B., Stockholm.

Johnson, A. B., Jr. 1988. Metal durability from the ancient metals. *Commission of the European Communities Natural Analogue Working Group, Third Meeting, Snowbird, Utah*. Come, B., and N. Chapman, eds. Brussels: CEC:227-230.

Kamineni, D. C. 1986. Distribution of uranium, thorium and rare-earth elements in the Eye-Dashwa Lakes Pluton: A study of some analogue elements. *Chemical Geology* 55(3-4):361-373.

Katayama, N., K. Kubo, and S. Hirono. 1974. Genesis of uranium deposits of the Tono Mine, Japan. IAEA-SM-183/11. Vienna: IAEA:437-452.

Kim*, J. I., G. Buckau, and R. Klenze. 1987. Natural colloids and generation of actinide pseudocolloids in groundwater. *Commission of the European Communities Natural Analogues in Radioactive Waste Disposal: A Symposium*. Come, B., and N. Chapman, eds. Brussels: CEC.

Krauskopf, K. B. 1986. Thorium and rare-earth metals as analogs for actinide elements. *Chemical Geology* 55(3-4):323-335.

Krauskopf, K. B. 1988. Geology of high-level nuclear waste disposal. *Annual Review of Earth and Planetary Sciences* 16:173-200.

Krishnaswami, S., W. C. Graustein, and K. K. Turekian. 1982. Radium, thorium and radioactive lead isotopes in groundwaters: Application to the in situ determination of adsorption-desorption rate constants and retardation factors. *Water Resources Research* 18(6):1633-1675.

Kuroda, P. K. 1975. Fossil nuclear reactor and plutonium-244 in the early history of the solar system. *The Oklo Phenomenon*. Vienna: IAEA:479.

Lancelot, J. R., A. Vitrac, and C. J. Allegre. 1975. The Oklo natural reactor: Age and evolution studies by U-Pb and Rb-Sr systematics. *Earth and Planetary Science Letters* 25:189.

Langmuir, D. 1978. Uranium solution-mineral equilibria at low temperatures with applications to sedimentary ore deposits. *Geochimica et Cosmochimica Acta* 42:547-569.

Laul, J. C., and T. C. Maiti, eds. 1990. Natural radionuclides in groundwater. *High Level Radioactive Waste Management*. Las Vegas, Nevada: American Nuclear Society and American Society of Civil Engineers:137-142.

Laul, J. C., and M. R. Smith. 1988. Disequilibrium study of natural radionuclides of uranium and thorium series in cores and briny groundwaters from Palo Duro Basin, Texas. PNL/SRP-5783. Battelle Pacific Northwest/DOE.

Laul, J. C., R. J. Walker, C. K. Shearer, J. J. Papike, and S. B. Simon. 1984. Chemical migration by contact metamorphism between pegmatite and country rocks: Natural analogs for radionuclide migration. *Materials Research Society Symposium Proceedings*. Boston, Massachusetts: Mat. Res. Soc. 26:951-958.

Lei, W., P. Linsalata, E. Penna Franca, and M. Eisenbud. 1986. Distribution and mobilization of cerium, lanthanum and neodymium in the Morro do Ferro Basin, Brazil. *Chemical Geology* 55(3-4):313-322.

Lemire, R. J., and F. Garisto. 1989. The solubility of U, Np, Pu, Th, and Tc in a geological disposal vault used for nuclear fuel. Pinawa, Manitoba, Canada: Atomic Energy of Canada Limited (AECL):123.

Lever, D. A. 1988. Some comments on the application of natural analogues in support of performance assessments in the U.K. *Commission of the European Communities Natural Analogue Working Group, Third Meeting, Snowbird, Utah*. Come, B., and N. Chapman, eds. Brussels: CEC:203-208.

Lever*, D. A. 1987. Natural analogues and radionuclide transport model validation. *Commission of the European Communities Natural Analogues in Radioactive Waste Disposal: A Symposium*. Come, B., and N. Chapman, eds. Brussels: CEC.

Linsalata, P., M. Eisenbud, and E. Penna Franca. 1987. Biogeochemical studies of the Ra, U, Th, and REE deposit at Morro do Ferro: A qualitative application to improve confidence in radionuclide immobilization processes. *Commission of the European Communities Natural Analogues in Radioactive Waste Disposal: A Symposium*. Come, B., and N. Chapman, eds. Brussels: CEC:116-118.

Loss, R. D., K. J. R. Rosman, and J. R. De Laeter. 1984. Transport of symmetric mass region fission products at the Oklo natural reactors. *Earth and Planetary Science Letters* 68:240-248.

Lutze*, W., and B. Grambow. 1987. The use of natural analogs in the long-term extrapolation of glass corrosion processes. *Commission of the European Communities Natural Analogues in Radioactive Waste Disposal: A Symposium*. Come, B., and N. Chapman, eds. Brussels: CEC.

Maas, R. 1989. Nd-Sr isotope constraints on the age and origin of unconformity-type uranium deposits in the Alligator Rivers Uranium Field, Northern Territory, Australia. *Economic Geology* 84:64-90.

Marinos, G. P., and P. G. Marinos. 1978. The groundwater potential of Santorini Island. *Thera and the Aegean World*. London: Thera and the Aegean World, Inc.: 297-305.

McConnell*, D. B., and J. J. Cramer. 1987. Simulating the movement of radium and lead away from the Cigar Lake uranium deposit. *Commission of the European Communities Natural Analogues in Radioactive Waste Disposal: A Symposium*. Come, B., and N. Chapman, eds. Brussels: CEC.

McKinley, I. G., and U. Frick. 1988. Swiss natural analogue research. *Commission of the European Communities Natural Analogue Working Group, Third Meeting, Snowbird, Utah*. Come, B., and N. Chapman, eds. Brussels: CEC:104-109.

McKinley, I. G., A. B. MacKenzie, J. M. West, and R. D. Scott. 1984. A natural analogue study of radionuclide migration in clays. *Materials Research Society Symposia Proceeding* 26. G. L. McVay, ed. Boston, Massachusetts: Mat. Res. Soc.:851-857.

McKinley, I. G., C. McCombie, and P. Zuidema. 1988. Applications of natural analogues in Swiss safety analysis. *Commission of the European Communities Natural Analogue Working Group, Third Meeting, Snowbird, Utah*. Come, B., and N. Chapman, eds. Brussels: CEC:173-179.

McKinley*, I. G. 1985. Applications of analogs in near-field geochemistry. *Commission of the European Communities Natural Analog Working Group, First Meeting*. Come, B., and N. Chapman, eds. Brussels: CEC.

McLaren, K. G. 1978. The Oklo phenomenon-natural nuclear reactors. *Search* 9(8-9):301.

Miekeley, N., H. C. Jesus, C. L. P. Silveira, and I. L. Kuechler. 1989. Colloid investigations in the Pocos de Caldas natural analog project. *Material Resources Society Symposium Proceedings - Scientific Basis for Nuclear Waste Management 12* 127:831-842.

Nakashima, S. and H. Nakamura. 1987. Mechanisms and quantitative evaluations of radionuclide fixation in rocks and sediments. *Commission of the European Communities Natural Analogues in Radioactive Waste Disposal: A Symposium*. Come, B., and N. Chapman, eds. Brussels: CEC:386-396.

Nash*, J. T., H. C. Granger, and S. S. Adams. 1981. Geology and concepts of genesis of important types of uranium deposits. *Economic Geology 75th Anniversary Volume*. New Haven, Connecticut: Economic Geology Publishing Company:63-116.

Naudet, R. 1976. The Oklo nuclear reactors: 1800 million years ago. *Interdisciplinary Science Reviews* 1(1):72-84.

Needham, R. S., and P. G. Stuart-Smith, eds. 1980. Geology of the Alligator Rivers uranium field. *Proceedings of the International Symposium on the Pine Creek Geosyncline, Panel Proceedings Series III*. Vienna: IAEA:233-258.

Neretnieks, I. 1986. Some uses for natural analogues in assessing the function of a HLW repository. *Chemical Geology* 55(3-4):175-188.

Neretnieks*, I. 1985. The need for geologic evidence for radionuclide migration in the geosphere. *Commission of the European Communities Natural Analog Working Group, First Meeting*. Come, B., and N. Chapman, eds. Brussels: CEC.

Ochiai, Y., M. Yamakawa, S. Takeda, and F. Harashima. 1988. Natural analogue study on Tono Uranium Deposit in Japan. *Commission of the European Communities Natural Analogue Working Group, Third Meeting, Snowbird, Utah*. Come, B., and N. Chapman, eds. Brussels: CEC.126-139.

Page, R. W., W. Compston, and R. S. Needham, eds. 1980. Geochronology and evolution of the late-Archean basement and Proterozoic rocks in the Alligator Rivers uranium field, Northern Territory, Australia. *Proceedings of the International Symposium on the Pine Creek Geosyncline, Panel Proceedings Series III*. Vienna: IAEA:39-68.

Papike, J. J. 1986. Thermally induced chemical migration: A natural analog approach. (Technical Progress Report). DOE/ER/13259-T2. Washington, D.C.: DOE.

Papike, J. J., J. C. Laul, and P. Nabelek. 1982. Contact metamorphism between quartz monzonite and limestone/argillite: A natural analog study for radionuclide migration. *Geological Society of America Abstracts with Programs* 14(7):583.

Papp, T. 1988. Natural analogues in SKB safety assessments. *Commission of the European Communities Natural Analogue Working Group, Third Meeting, Snowbird, Utah*. Come, B., and N. Chapman, eds. Brussels: CEC:162-170.

Papp, T. 1988. The PAAG group and natural analogues. *Commission of the European Communities Natural Analogue Working Group, Third Meeting, Snowbird, Utah*. Come, B., and N. Chapman, eds. Brussels: CEC:159-161.

Papp*, T. 1987. The role of natural analogues in safety assessment and acceptability. *Commission of the European Communities Natural Analogues in Radioactive Waste Disposal: A Symposium*. Come, B., and N. Chapman, eds. Brussels: CEC.

Parneix, J. C., M. T. Menager, L. Trotignon, and J. C. Petit. 1987. Hydrothermal alteration in Auriat Granite (Massif Central, France): Analogy with a radwaste disposal. *Commission of the European Communities Natural Analogues in Radioactive Waste Disposal: A Symposium*. Come, B., and N. Chapman, eds. Brussels: CEC:449-461.

Patyn*, J., P. Del Marmol, and M. Monsecour. 1987. Environmental tracers for validating predictive models. *Commission of the European Communities Natural Analogues in Radioactive Waste Disposal: A Symposium*. Come, B., and N. Chapman, eds. Brussels: CEC:444-448.

Penrose, W. R., W. L. Polzer, E. H. Essington, D. M. Nelson, and K. A. Orlandini. 1990. Mobility of plutonium and americium through a shallow aquifer in a semiarid region. *Environmental Science and Technology* 24(2):228-234.

Petit, J. C. 1988. Analogue studies at the French Atomic Energy Commission during the period 1986-1988. *Commission of the European Communities Natural Analogue Working Group, Third Meeting, Snowbird, Utah*. Come, B., and N. Chapman, eds. Brussels: CEC:75-87.

Petruso, K. M. 1978. Lead weights from Akrotiri: Preliminary observations. *Thera and the Aegean World*. London: Thera and the Aegean World, Inc.: 547-553.

Pichler, H., and W. Schiering. 1977. The Thera eruption and Late Minoan-IB destructions on Crete. *Nature* 267:819-822.

Pirc, S., and A. W. Rose. 1980. Uranium anomalies in paleo-aquifers near sandstone-type uranium deposits in the Devonian Catskill Formation of Pennsylvania. *Developments in Economic Geology - Geochemical Exploration 1980*. New York: Elsevier: 219-231.

Rae, J., and J. H. Black. 1986. Modelling of migration of leached radionuclides by groundwater. *Philosophical Transactions of the Royal Society of London* A319(1545):97-108.

Read, D., and P. J. Hooker. 1989. The speciation of uranium and thorium at the Broubster natural analog site, Caithness, Scotland. *Materials Research Society Symposium Proceedings*. Boston, Massachusetts: Mat. Res. Soc. 127:763-770.

Robbins, G. A. 1981. Use of natural analogs to assess high-level radioactive waste repository performance. M. Kent, ed. *New Horizons in Engineering Geology*. Association of Engineering Geologists 24th Annual Meeting. Portland, Oregon: Ass. Eng. Geol.:51.

Roberts, P. D., T. K. Ball, P. J. Hooker, and A. E. Milodowski. 1989. A uranium geochemical study at the natural analog site of Needle's Eye, SW Scotland. *Materials Research Society Symposium Proceedings*. Boston, Massachusetts: Mat. Res. Soc. 127:933-940.

Ross*, C. A. M., C. Degueldre, M. Ivanovich, and G. Longworth. 1987. Colloid benchmark exercise: An interlaboratory study of sampling and characterization techniques for natural colloids in oxic groundwater. *Commission of the European Communities Natural Analogues in Radioactive Waste Disposal: A Symposium*. Come, B., and N. Chapman, eds. Brussels: CEC.

Ruskeeniemi, T., H. Niini, B. Sodernolm, and M. Versterinen. 1989. The Palmottu U-Th deposit in SW Finland as a natural analogue to the behaviour of spent nuclear fuel in bedrock: A preliminary report. *Water-Rock Interaction*. Rotterdam: Balkema:601-604.

Saager, R., K. Thiel, G. J. Hennig, and U. Bangert. 1980. Uranium redistribution in weathered conglomerates of the early PreCambrian Pongola Supergroup, South Africa: Inferences from a study by alpha spectrometry and fission track micromapping. Developments in Economic Geology - Geochemical Exploration 1980. New York: Elsevier:233-249.

Sargent, F. P. 1985. What can the earth scientists provide? *Commission of the European Communities Natural Analogue Working Group, First Meeting*. Come, B., and N. Chapman, eds. Brussels: CEC:105-111.

Sato, C., Y. Ochiai, and S. Takeda. 1987. Natural analog study of Tono Sandstone type uranium deposit in Japan. *Commission of the European Communities Natural Analogues in Radioactive Waste Disposal: A Symposium*. Come, B., and N. Chapman, eds. Brussels: CEC:462-472.

Sekine, K., T. Murakami, N. Yanase, T. Ohnuki, H. Isobe, and A. Kasai. 1988. Migration behaviour of uranium and thorium series nuclides: Relevant to alteration. ANSTO Alligator Rivers Analogue Project - Progress Report, May 1988 - August 1988. Australia: ANSTO:157-186.

Shade, J. W. 1981. Comparison of glass and ceramic leaching behaviour by natural analogs. *Nuclear and Chemical Waste Management* 2(3):219-228.

Shea, M. 1984. Uranium migration at some hydrothermal veins near Marysvale, Utah: A natural analog for waste isolation. *Material Resources Society Symposium Proceedings - Scientific Basis for Nuclear Waste Management*. Boston, Massachusetts: Mat. Res. Soc. 26:227-238.

Shea, M. 1985. Performance assessment input: Marysvale natural analog study. *Commission of the European Communities Natural Analogue Working Group, First Meeting*. Come, B., and N. Chapman, eds. Brussels: CEC:160-163.

Shea, M. 1987. Marysvale natural analogue study: Feasibility phase results. *Commission of the European Communities Natural Analogues in Radioactive Waste Disposal: A Symposium*. Come, B., and N. Chapman, eds. Brussels: CEC:275-286.

Shea*, M. 1988. Marysvale fracture controlled mass transport study. *Commission of the European Communities Natural Analogue Working Group, Third Meeting, Snowbird, Utah*. Come, B., and N. Chapman, eds. Brussels: CEC:11-25.

Sidle, W. C., D. Sayala, and T. Steinborn. 1985. Natural analogues in evaporites for the interpretation of mineralogic and geochemical variations in a nuclear waste repository system. *EOS, Transactions, American Geophysical Union* 66(46):1153.

Skytte-Jensen, B. 1985. Geochemical model needs. *Commission of the European Communities Natural Analogue Working Group, First Meeting*. Come, B., and N. Chapman, eds. Brussels: CEC:43-54.

Slater*, E. A. 1980. Late Bronze Age Aegean metallurgy in the light of the Thera analyses. *Thera and the Aegean World*. London: Thera and the Aegean World, Inc.:197-215.

Smellie, J. 1985. Proposed programme of investigation at Pocos de Caldas, Minas Gerais, Brazil. *Commission of the European Communities Natural Analogue Working Group, First Meeting*. Come, B., and N. Chapman, eds. Brussels: CEC:171-174.

Smellie, J. A. T. 1988. Some Swedish natural analogue studies: A review. *Commission of the European Communities Natural Analogue Working Group, Third Meeting, Snowbird, Utah*. Come, B., and N. Chapman, eds. Brussels: CEC:96-103.

Smellie, J., N. Chapman, I. McKinley, E. P. Franca, and M. Shea. 1989. Testing safety assessment models using natural analogs in high natural series groundwaters. The second year of the Pocos de Caldas Project. *Materials Research Society Symposium Proceedings*. Boston, Massachusetts: Mat. Res. Soc. 127:863-870.

Smellie*, J. 1988. Pocos de Caldas, Minas Gerais, Brazil: A natural analogue study. *Commission of the European Communities Natural Analogue Working Group, Third Meeting, Snowbird, Utah*. Come, B., and N. Chapman, eds. Brussels: CEC:57-73.

Smellie*, J. A. T., A. B. MacKenzie, and R. D. Scott. 1985. An analogue validation study of natural radionuclide migration in crystalline rocks using uranium-series disequilibrium studies. *Commission of the European Communities Natural Analog Working Group, First Meeting*. Come, B., and N. Chapman, eds. Brussels: CEC.

Smellie*, J. A. T., L. B. Magno Jr., N. A. Chapman, I. G. McKinley, and E. P. Franca. 1987. The Pocos de Caldas project feasibility study: 1986-7. *Commission of the European Communities Natural Analogues in Radioactive Waste Disposal: A Symposium*. Come, B., and N. Chapman, eds. Brussels: CEC.

Snelling, A. A., and B. L. Dickson. 1988. A study of the weathering history at Koongarra. ANSTO Alligator Rivers Analogue Project - Progress Report, May 1988 - August 1988. Australia: ANSTO:13-20.

Soreau, S., and P. Glasbergen. 1988. Preliminary indications from natural isotopes on the dissolution of rocksalt in deep circulating groundwater of the Netherlands. *Commission of the European Communities Natural Analogue Working Group, Third Meeting, Snowbird, Utah*. Come, B., and N. Chapman, eds. Brussels: CEC:209-219.

Soyer, B. 1984. Geochemistry of uranium in the hydrographic network. *Uranium Geochemistry, Mineralogy, Geology, Exploration and Resources*. England: The Institution of Mining and Metallurgy:109-116.

Stuckless, J. S. 1986. Applications of U-Th-Pb isotope systematics to the problems of radioactive waste disposal. *Chemical Geology* 55(3-4):215-225.

Sunder, S., P. Taylor, and J. J. Cramer. 1988. XPS and XRD studies of uranium rich minerals from Cigar Lake, Saskatchewan. *Material Resources Society Symposium Proceedings - Scientific Basis for Nuclear Waste Management 11*. Boston, Machusetts: Mat. Res. Soc. 112:465-472.

Sverjensky, D. A. 1988. Geochemical modelling of the Koongarra uranium deposit. ANSTO Alligator Rivers Analogue Project - Progress Report, May 1988 - August 1988. Australia: ANSTO:21-64.

Tammemagi, H. Y., B. Haverslew, and N. C. Sturchio. 1986. Investigations of the Empire Creek Stock, Montana, as an analogue to a nuclear waste repository. *Chemical Geology* 55(3-4):375-385.

Thomas, G. F., and G. Till. 1984. The dissolution of unirradiated UO2 fuel pellets under simulated disposal conditions. *Nuclear and Chemical Waste Management* 5:141-147.

Ulmer, G. C., G. H. Kacandes, and D. E. Grandstaff. 1986. Icelandic geothermal fields as an analog for nuclear waste disposal in basalt. *Advances in Ceramics* 20:755-764.

Valkiainen, M. 1988. Finnish natural analogue research. *Commission of the European Communities Natural Analogue Working Group, Third Meeting, Snowbird, Utah*. Come, B., and N. Chapman, eds. Brussels: CEC:110-118.

Van Luik, A. E. 1987. Uranium in selected endorheic basins as partial analogue for spent fuel disposal in salt. *Commission of the European Communities Natural Analogues in Radioactive Waste Disposal: A Symposium*. Come, B., and N. Chapman, eds. Brussels: CEC:92-103.

Van Luik*, A. E. 1985. The use of natural analogs in the process of building confidence in performance assessment models. *Commission of the European Communities Natural Analog Working Group, First Meeting*. Come, B., and N. Chapman, eds. Brussels: CEC.

Vidale, R. J., ed. 1978. The highest temperatures recorded by the Oklo mineral phase assemblages and rock textures. *Natural Fission Reactors, Proceedings of the Technical Committee Meetings 1977, Paris. Panel Proceedings Series*. Vienna: IAEA:235-242.

Vilks, P., J. J. Cramer, T. A. Shewchuk, and J. P. A. Larocque. 1988. Colloid and particulate matter studies in the Cigar Lake natural analog program. *Radiochimica Acta* 44-45:305-310.

Vovk, I. F. 1987. Some geochemical and mineralogical peculiarities of deposits of radioactive material as evidence for radiolysis in nature. *Commission of the European Communities Natural Analogues in Radioactive Waste Disposal: A Symposium*. Come, B., and N. Chapman, eds. Brussels: CEC:205-216.

Vovk, I. F. 1988. The IAEA report of the role of natural analogues in performance assessment. *Commission of the European Communities Natural Analogue Working Group, Third Meeting, Snowbird, Utah*. Come, B., and N. Chapman, eds. Brussels: CEC:140-144.

Waite, T. D. 1988. Radionuclide sorption processes in the weathered zone: Modelling and incorporation in the transport equation. ANSTO Alligator Rivers Analogue Project - Progress Report, May 1988 - August 1988. Australia: ANSTO:187-193.

Walton, R. D., and G. A. Cowan. 1975. Relevance of nuclide megration at Oklo to the problem of geologic storage of radioactive waste. *The Oklo Phenomenon*. Vienna: IAEA:499.

Warren, P. 1984. Absolute dating of the Bronze Age eruption of Thera (Santorini). *Nature* 308(5):492-493.

Watkins, N. D., R. S. J. Sparks, H. Sigurdsson, T. C. Huang, A. Federman, S. Carey, and D. Ninkovich. 1978. Volume and extent of the Minoan tephra from Santorini volcano: New evidence from deep-sea cores. *Nature* 271:122-126.

Wilde, A. R., T. P. Mernagh, M. S. Bloom, and C. F. Hoffman. 1989. Fluid inclusion evidence on the origin of some Australian unconformity-related uranium deposits. *Economic Geology* 84:1627-1642.

Wilpolt, R. H., and S. D. Simov. 1970. Uranium deposits in Africa. *Uranium Exploration Geology - Proceedings of a Panel on Uranium Exploration Geology, Vienna*. Vienna: IAEA:3-20.

Winograd, I. J. 1986. Archaeology and public perception of a trans-scientific problem: Disposal of toxic wastes in the unsaturated zone. U.S. Geological Survey. Open-file Report 86-136:1-31.

Wollenberg, H. A., and S. Flexser. 1986. Contact zones and hydrothermal systems as analogues to repository conditions. *Chemical Geology* 55(3-4):345-359.

Wright, R. J. 1970. Sandstone-type uranium deposits. *Uranium Exploration Geology - Proceedings of a Panel on Uranium Exploration Geology, Vienna*. Vienna: IAEA:219-237.

Wright, R. J. 1970. Unconformity uranium deposits. *Uranium Exploration Geology - Proceedings of a Panel on Uranium Exploration Geology, Vienna*. Vienna: IAEA:205-217.

Yanase, N. 1988. Distribution of uranium and actinium series radionuclides in rocks and groundwater. ANSTO Alligator Rivers Analogue Project - Progress Report, May 1988 - August 1988. Australia: ANSTO:123-146.

Young, R. G. 1984. Uranium deposits of the world, excluding Europe. *Uranium Geochemistry, Mineralogy, Geology, Exploration and Resources*. England: The Institution of Mining and Metallurgy:117-139.

Ziegler*, V., and J. Dardel. 1984. Uranium deposits in Europe. *Uranium Geochemistry, Mineralogy, Geology, Exploration and Resources*. England: The Institution of Mining and Metallurgy:140-161.

Zukin, J. G., D. E. Hammond, T. L. Ku, and W. A. Elders. 1987. Uranium - thorium series radionuclides in brines and reservoir rocks from two deep geothermal boreholes in the Salton Sea Geothermal Field, southeastern California. *Geochimica et Cosmochimica Acta* 51(10):2719-2731.